AURORAL EMISSIONS OF THE GIANT PLANETS

Anil Bhardwaj
Space Physics Laboratory
Vikram Sarabhai Space Centre
Trivandrum, India

G. Randall Gladstone
Southwest Research Institute
San Antonio, Texas

Abstract. Auroras are (generally) high-latitude atmospheric emissions that result from the precipitation of energetic charged particles from a planet's magnetosphere. Auroral emissions from the giant planets have been observed from ground-based observatories, Earth-orbiting satellites (e.g., International Ultraviolet Explorer (IUE), Hubble Space Telescope (HST), and Röentgensatellit (ROSAT)), flyby spacecraft (e.g., Voyager 1 and 2), and orbiting spacecraft platforms (e.g., Galileo) at X-ray, ultraviolet (UV), visible, infrared (IR), and radio wavelengths. UV, visible, and IR auroras are atmospheric emissions, produced or initiated when ambient atmospheric species are excited through collisions with the precipitating particles, while radio and X-ray auroras are beam emissions, produced by the precipitating species themselves. The emissions at different wavelengths provide unique and complementary information, accessible to remote sensing, about the key physical processes operating in the atmospheric and magnetospheric regions where they originate. This paper reviews the development of our current understanding of auroral emissions from Jupiter, Saturn, Uranus, and Neptune, as revealed through multispectral observations and supplemented by plasma measurements.

CONTENTS

1. INTRODUCTION

Electromagnetic radiation emanating from the high latitudes of a planet (also called auroral or polar latitudes) are generally referred to as "auroral emissions." They are generated through the excitation of upper atmospheric atoms and molecules by energetic electrons and ions precipitating down from the planet's magnetosphere along high-latitude magnetic field lines. Thus auroras are the observed signatures of electrodynamical coupling between a planet's magnetosphere and ionosphere. Auroral emissions can be produced at a wide range of wavelengths, from X-ray to radio wavelengths. Auroras play an important role in the energy balance between incoming solar radiation (both photons and solar wind particles) and outgoing planetary radiation and can have important chemical and dynamical consequences for the entire atmosphere-ionosphere-thermosphere system, globally and especially locally. By observing and modeling a planet's auroral emissions at different wavelengths, one can learn about composition, structure, temperature, energy budget, transport processes, and magnetospheric plasma properties all at once.

Since the discovery of ultraviolet auroral emissions from Jupiter in 1979 during the flyby of Voyager 1, there has been a great deal of research on the nature of giant planet auroras. (The planets Jupiter, Saturn, Uranus, and Neptune are often referred to as giant or outer planets.) The Voyager flybys of Jupiter (in March and July, 1979), Saturn (in November 1980 and August 1981), Uranus (in January 1986), and Neptune (in August 1989) provided the in situ measurements of magnetic field strength and morphology, magnetospheric plasma populations, and local remote sensing required to make an initial characterization of the relevant auroral physics at each planet. The Voyager results were generally supported by Earth-based observations (primarily far ultraviolet (FUV) observations made by the

Reviews of Geophysics, 38, 3 / *August 2000*
pages 295–353
8755-1209/00/1998RG000046*$15.00*
Paper number 1998RG000046

International Ultraviolet Explorer (IUE) satellite) until the Hubble Space Telescope (HST) era began, more specifically, the post-COSTAR (corrective optics space telescope axial replacement) (i.e., "repaired") HST era. The high spatial resolution of the FUV data from HST, supported by ground-based observations of H_3^+ emissions and Röentgensatellit (ROSAT) observations of X-ray emissions, has recently led to a significant modification in our understanding of Jupiter's aurora in particular. For example, Plate 1 shows the high spatial resolution possible with the space telescope imaging spectrograph (STIS) on HST for observing FUV auroral emissions from Jupiter and Saturn. The emissions at these different wavelengths provide unique and complementary information about the key processes at the auroral latitudes (and the magnetospheric regions) where they originate.

Until now, there have been few attempted reviews of giant planet auroral emissions. *Fox* [1986] provided an overview of models of auroras and airglow on all the planets, *Clarke et al*. [1989b] reviewed Jupiter's aurora and airglow in some detail, and *Prangé* [1992] reviewed Jovian ultraviolet (UV) and infrared (IR) auroras. More recently, *Prangé and Livengood* [1998] and *Ballester* [1998] have reviewed the IUE auroral observations on Jupiter and on Jupiter, Saturn, and Uranus, respectively. Very recently, *Kim et al*. [1998] reviewed the Jovian aurora, *Bhardwaj and Gladstone* [2000] summarized multispectral auroras on Saturn, Uranus, and Neptune, *Herbert and Sandel* [1999] reviewed the UV auroral and airglow observations on Uranus and Neptune, and *Bhardwaj* [1997a] reviewed experimental and theoretical studies of giant planet UV airglow emissions. Although auroral processes are not covered specifically, the book by *Atreya* [1986] provides an excellent source for understanding the upper atmospheres and ionospheres of the giant planets, the "fluorescent screen" of the aurora's "cathode ray tube" [*Akasofu*, 1980].

We recognize that many of the ideas presented here are rapidly becoming obsolete as more and better observational data are acquired. The excellent data available make it challenging for theorists and modelers to keep up with the often-changing paradigms in this field. Our review is intended to document a part of the large body of work that has been done in the last 20 or so years on giant planet auroras. Hopefully, our ideas on this subject will eventually stabilize, although there is no indication that this will happen any time soon.

Jupiter's aurora is the brightest and the most extensively studied (compared with the other giant planets) by virtue of its closer proximity to Earth. The Jovian aurora has been observed in X-ray, UV, visible, near and midinfrared, and radio wavelength ranges. Because of its closeness to the Earth, it was the first giant planet from which any kind of auroral emissions were observed. Auroras from Saturn and Uranus are observed at UV, IR, and radio wavelengths, but information about Neptune's aurora is currently only available at UV and radio wavelengths. The auroral emissions from the giant planets are generally believed to be produced by precipitating magnetospheric electrons, with some contribution from protons and/or heavy ions. Jupiter has the most spectacular auroral display, with an implied power input of $\sim 10^{14}$ W (about 1000 times more than in Earth's auroral regions), followed by Saturn and Uranus at $\sim 10^{11}$ W. Neptune has a relatively weak aurora, with an estimated input power of $\sim 10^9$ W.

In the next section we briefly define and review the primary processes that lead to auroral emissions from the giant planets and outline our current understanding of them. In the remaining sections we present an edited history of the relevant observations and theoretical work on the auroral emissions from Jupiter, Saturn, Uranus, and Neptune. Where possible, the emissions will be roughly grouped by energy, from X rays to thermal IR. We regret we are unable to review radio observations of giant planet auroras here. Readers are referred to several excellent reviews in this area [e.g., *Zarka*, 1992, 1998; *Carr et al*., 1983; *Kaiser*, 1993; *Kaiser et al*., 1984; *Desch et al*., 1991; *Zarka et al*., 1995; *Kaiser and Desch*, 1984]. We close by reviewing the most recent observations and speculating as to the future directions of the field.

2. AURORAL PROCESSES ON THE GIANT PLANETS

The atmospheric composition of the giant planets is close to solar, with hydrogen species and helium far outnumbering any C-, N-, or O-bearing species. In the upper atmospheres of these planets this dominance is generally greatly enhanced through the processes of condensation, photolysis, and diffusive separation. Thus it is not surprising that almost all auroral emissions observed on the giant planets result from particle impact excitation of hydrogen species. Some of the primary processes that occur during electron impact on molecular hydrogen are given in Table 1, where e_p represents a primary (or precipitating) energetic electron; $H_2(v)$ represents vibrationally excited molecular hydrogen; H_2^* represents energetic or fast (i.e., nonthermal) molecular hydrogen; $H_2(a)$ represents electronically excited molecular hydrogen in the $a\ ^3\Sigma_g^+$ state; $H_2(b)$ represents electronically excited molecular hydrogen in the $b\ ^3\Sigma_u^+$ (dissociative) state; $H_2(B, C)$ represents electronically excited molecular hydrogen in the $B\ ^1\Sigma_u^+$ state (the upper level of the Lyman band system) or $C\ ^1\Pi_u$ state (the upper level of the Werner band system), respectively; H(2p, 2s) represents electronically excited atomic hydrogen in either of the $n = 2$ states; H($3l$) represents electronically excited atomic hydrogen in any of the $n = 3$ states; $h\nu$ represents an emitted photon; and e_s represents a secondary electron.

All these processes yield atmospheric emissions. Other precipitating particles (e.g., protons and/or heavy

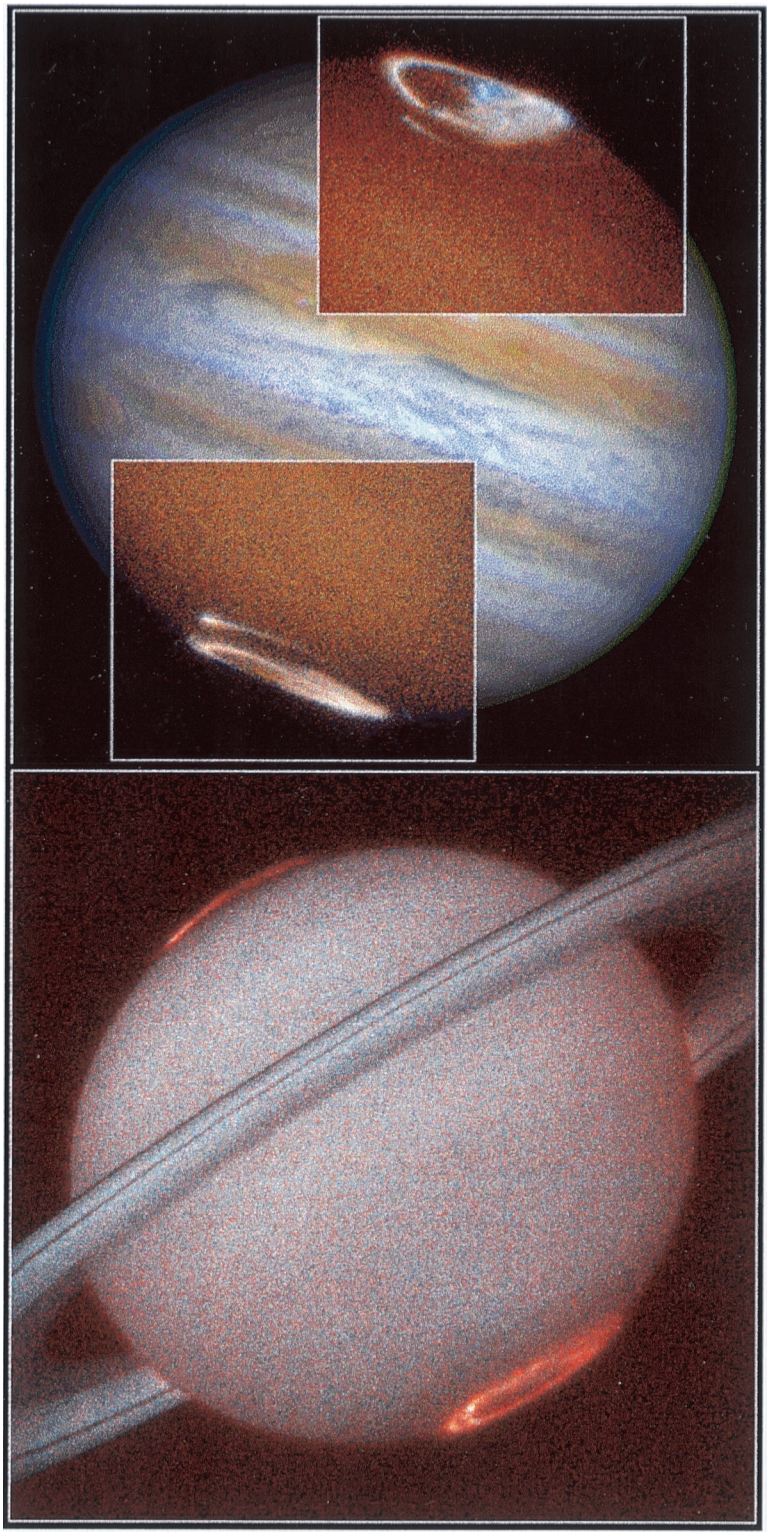

Plate 1. Hubble Space Telescope (HST) imaging spectrometer (STIS) false-color images showing the highly structured morphology of FUV auroral emissions from (top) Jupiter and (bottom) Saturn. The ~0.06″ spatial resolution and high sensitivity of STIS allow the study of auroral features as small as 180 km at Jupiter and as small as 380 km at Saturn. In the Jupiter image the bluish regions inside the northern auroral oval are regions in which H I Lyman α emissions are enhanced relative to the H_2 Lyman and Werner band emissions, and the "spot" emissions equatorward of the main oval are from the Io flux tube (IFT) footprint in both the north and south hemispheres. These images are taken from the Space Telescope Science Institute Web site (http://oposite.stsci.edu/pubinfo/1998.html), courtesy of J. Clarke (University of Michigan) and J. Trauger (NASA Jet Propulsion Laboratory).

TABLE 1. Primary Processes in the Impact of Electrons on H_2

Process	*Reaction Sequence*	*Result*
Vibrational excitation	$e_p + H_2 \rightarrow H_2(v) + e_p$; $H_2(v) + H_2 \rightarrow H_2^* + H_2$	heat, quadrupole emission (IR)
Electronic excitation	$e_p + H_2 \rightarrow H_2(b) + e_p$; $H_2(b) \rightarrow H_2(a) + h\nu$	$a - b$ continuum (MUV)
Electronic excitation	$e_p + H_2 \rightarrow H_2(B, C) + e_p$; $H_2(B, C) \rightarrow H_2 + h\nu$	Lyman and Werner bands (FUV)
Dissociative excitation	$e_p + H_2 \rightarrow H(2p, 2s) + H + e_p$; $H(2p, 2s) \rightarrow H + h\nu$	Lyman α (FUV)
Dissociative excitation	$e_p + H_2 \rightarrow H(3l) + H + e_p$; $H(3l) \rightarrow H(2l) + h\nu$	Balmer series (visible)
Ionization	$e_p + H_2 \rightarrow H_2^+ + e_s + e_p$; $H_2^+ + H_2 \rightarrow H_3^+ + H$	H_3^+ emission (IR)
Dissociative ionization and excitation	$e_p + H_2 \rightarrow H(2p, 2s) + H^+ + e_s + e_p$; $H(2p, 2s) \rightarrow H + h\nu$	Lyman α (FUV)

ions) would excite somewhat similar emissions, both directly and through the secondary electrons they produce. By contrast, X-ray (and radio) auroras are emitted by the precipitating particles themselves. For example, precipitating sulfur ions would emit X rays by first charge stripping to a highly ionized state, followed by charge exchange and excitation reactions as follows [cf. *Cravens et al*., 1995]:

Charge stripping $S^{(q-1)+} + H_2 \rightarrow S^{q+} + H_2 + e_s$

Charge transfer $S^{q+} + H_2 \rightarrow S^{(q-1)+*} + H_2^+$

X-ray emission $S^{(q-1)+*} \rightarrow S^{(q-1)+} + h\nu$,

where S^{q+} represents sulfur ions that are q electrons short of being neutral atoms and S^{q+*} represents such ions that are in an electronically excited state.

Many bright auroral emission features are expected at visible wavelengths (e.g., H I Balmer lines, He I 1083 nm), but these are difficult to detect against reflected sunlight when observing the giant planets from the vicinity of the Earth. For example, assuming a reflectivity of 30%, the backscattered sunlight at 656.3 nm (Hα) from Jupiter has a brightness of ~20 MR nm^{-1} (a rayleigh (R) is a unit of surface brightness equivalent to 10^6 photons cm^{-2} s^{-1} $4\pi sr^{-1}$), so that even a 0.01-nm-wide auroral emission line (e.g., the H I Lyman α line width is ~0.1 nm in the Jovian aurora, although most other emissions are expected to be much narrower) would have to compete with a reflected signal of 200 kR. Thus most of our remote sensing of giant planet auroral emissions has been accomplished at other than visible wavelengths. Important exceptions to this rule are the Voyager [e.g., *Cook et al*., 1981] and Galileo [e.g., *Ingersoll et al*., 1998] visible imagings of Jupiter's nightside aurora, which, because of their high spatial resolution, are providing strong new constraints on the width and altitude of the aurora.

3. JUPITER

The probable existence of auroras on Jupiter was predicted by *Schwitters* [1968] and *Hunter* [1969] when they detected Hα line (656.3 nm) emissions, with intensities of a few kilorayleighs, from ground-based telescopes (although the results were ambiguous). *Dulk et al*. [1970], using improved resolution, found no emissions with intensity greater than 10 kR from Jovian auroras. Further observations, with inconclusive evidence for auroras on Jupiter, were undertaken by *Rottman et al*. [1973], *Clary and Hunter* [1975], *Giles et al*. [1976], and *Holman and Hunter* [1977]. *Atreya et al*. [1977] presented evidence for the existence of auroral hot spots at the feet of the Io flux tube (IFT) using the Copernicus satellite spectrometer data. (The Io flux tube refers to a few million ampere current of ions and electrons on magnetic field lines that are short-circuited through the ionospheres of Io and Jupiter.) A Lyman α intensity exceeding 100 kR, in addition to about 1 kR of Lyman α airglow, was measured.

Taking analogy from the processes occurring in the upper atmosphere of the Earth, *Heaps et al*. [1973, 1975] suggested that electron and proton auroras should be present on Jupiter. These authors computed H, He, and H_2 emissions resulting from the precipitation of electrons and protons, degraded in energy by applying the continuous slowing down approximation (CSDA) method. Their results showed that for an electron aurora [*Heaps et al*., 1973], most of the Lyman α emission is due to dissociative excitation of H_2 rather than to direct excitation of H, while in the case of a proton aurora [*Heaps et al*., 1975], charge exchange and excitation of the precipitating H^+ provides the most important source of Lyman α. From the ground-based measurements of the 656.3-nm line of atomic hydrogen, *Heaps et al*. [1973] placed an upper limit of 10^{11} el cm^{-2} s^{-1} on an electron flux peaked in the sub-keV range and 10^{10} el cm^{-2} s^{-1} if the differential electron flux peaked near 10 keV. Assuming the auroral regions cover 1/50 of Jupiter's surface, this amounts to an input power of 200 GW, which is a very good upper limit considering that our current estimate of auroral input power is ~100 GW on Jupiter. *Heaps* [1976] explored the implications of electron precipitation for heating of the neutral atmosphere. *Cravens* [1975] considered the effect of precipitating 20-keV electrons on the atmosphere and ionosphere of Jupiter

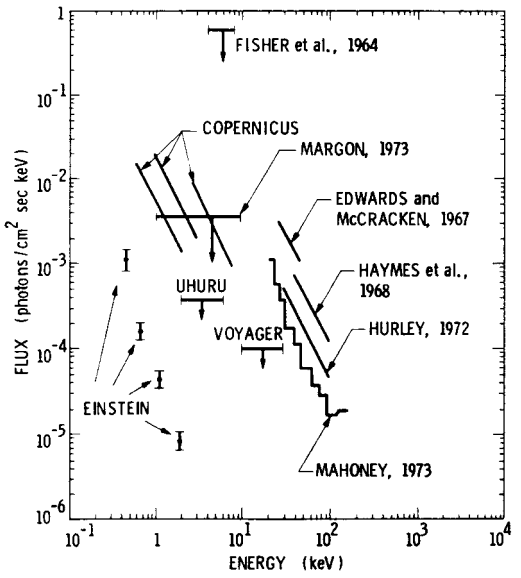

Figure 1. A comparison of the Einstein detection of Jovian X-ray emissions with previous upper limits [*Metzger et al*., 1983, Figure 3]. Voyager data are from *Kirsch et al*. [1981a], Copernicus data are from *Vesecky et al*. [1975], Uhuru data are from *Hurley* [1975], and all other data are from *Mahoney* [1973].

by calculating UV intensities, ionospheric densities, and neutral, electron, and vibrational temperatures. *Hunten and Dessler* [1977] suggested a mechanism for producing flux of soft electrons (50–300 eV), the precipitation of which was indicated by the Pioneer-observed high temperature of Jupiter's topside ionosphere [*Nagy et al*., 1976].

3.1. X-Ray Emissions

Following the discovery of a magnetosphere on Jupiter by the ground-based detection of nonthermal radio emissions [*Burke and Franklin*, 1955; *Bigg*, 1964; *Piddington and Drake*, 1968; cf. *Berge and Gulkis*, 1976], it was reasonable to expect, based on terrestrial analogy, that Jupiter should be a source of X-ray emissions produced via bremsstrahlung by the precipitation of energetic electrons from the magnetosphere into the upper atmosphere of the planet. In planetary atmospheres, bremsstrahlung X rays are produced when high-energy electrons are scattered by ambient atmospheric nuclei.

This expectation led to a series of searches, starting in 1962, to detect the X-ray emissions from Jupiter by rocket [*Fisher et al*., 1964], balloons [*Edwards and McCracken*, 1967; *Haymes et al*., 1968; *Hurley*, 1972; *Mahoney*, 1973], and satellites [*Vesecky et al*., 1975; *Hurley*, 1975]. In all these instances the results of attempts to detect X rays from Jupiter, at various energy ranges, were negative; these studies only provided upper limits to the X-ray fluxes in the energy range of their instruments (see Figure 1). There was also speculation that bombardment of the Galilean satellites by energetic particles within Jupiter's magnetosphere would produce substantial characteristic X-ray line emissions [*Mihalov*, 1973].

Although the Voyager spacecraft did not carry any X-ray detectors, the Low Energy Charged Particle (LECP) Experiment was somewhat sensitive to X rays in the 14- to 31-keV and 31- to 63-keV ranges. This allowed *Kirsch et al*. [1981a] to place an upper limit for Jovian X-ray emission, based on count rate enhancements observed in the direction of Jupiter when Voyager 1 was still approaching from 100–230 R_J away. Their upper limit corresponded to $<1.3 \times 10^{-4}$ photons cm^{-2} s^{-1} keV^{-1} at Earth in the 14- to 31-keV range. Since to produce this large an X-ray flux would require unrealistically large precipitating electron fluxes at Jupiter, and given the apparent hardness of the spectrum, Kirsch et al. concluded that the count rate enhancements were more likely due to energetic neutrals, possibly originating from the innermost Galilean satellite, Io, as a result of charge exchange between energetic ions and ambient neutrals.

The first positive detection of X-ray emissions from the polar regions of Jupiter was made by the imaging proportional counter (IPC) and high-resolution imaging (HRI) detectors on board the Einstein (High Energy Astronomical Observatory 2 (HEAO-2)) satellite [*Metzger et al*., 1983], finally ending a long frustrating search for them over a wide energy range. The emissions were detected in the 0.2- to 3.0-keV energy range (softer than the Voyager LECP range) from both auroral zones (north and south) of Jupiter. The observed energy spectrum of the X rays was soft and was characterized by a power law with an exponent of ~2.3 (see Figure 1 for flux versus energy spectrum). The total flux was found to be relatively constant in time, in contrast with the observations in the UV, where substantial long- and short-term variabilities had been observed. The measured X-ray flux at Earth of $\sim 6 \times 10^{-4}$ cm^{-2} s^{-1} corresponded to an X-ray luminosity of $\sim 4 \times 10^9$ W in the 0.2- to 3.0-keV energy band. *Metzger et al*. [1983] were not able to reconcile their data in terms of bremsstrahlung by precipitating electrons due to an unreasonably high input power requirement (10^{15}–10^{16} W) for this mechanism, about a factor of 100–1000 larger than the input power derived from Voyager and IUE observations as required for producing the UV aurora [*Broadfoot et al*., 1981a; *Durrance et al*., 1982; *Yung et al*., 1982]. Therefore Metzger et al. argued for K-shell line emissions from precipitating S and O ions, with energies of 0.3–4.0 MeV $nucleon^{-1}$, as the most plausible source of the Jovian auroral X rays. The X-ray line emissions (at ~0.53 nm for S ions and ~2.36 nm for O ions) arise as the energetic O and S ions are nearly stripped of electrons while precipitating, and then (through further collisions) are either directly excited or charge exchanged into an excited state, which emits an X-ray photon upon decay back to the ground state. The suggestion of energetic heavy ions as the source of auroral X-ray emissions from Jupiter was based in part on evidence from in situ

Voyager observations of a strong radial gradient in the energetic heavy ion flux [*Gehrels and Stone*, 1983], indicating a planetward ion flow from the outer magnetosphere [*Gehrels et al*., 1981]. The contrast between an approximately constant flux measured between 17 and 12 R_J and a sharp decrease between 12 and 6 R_J [*Gehrels and Stone*, 1983] suggested strong pitch angle scattering into the loss cone, and subsequent precipitation of these heavy ions into the auroral atmosphere, at a rate comparable to the strong pitch angle diffusion limit. However, the energy resolution of the IPC detector on the Einstein observatory was not sufficient to clearly distinguish a line spectrum (emissions from excited states of highly stripped S and O ions) from a continuum (electron bremsstrahlung).

The precipitating heavy ions should also produce line emissions at UV wavelengths during collisions with H_2. This was explored by *Waite et al*. [1988a] by observing Jovian auroras with IUE and also modeled by *Horanyi et al*. [1988]. These studies showed that the theoretically predicted intensities of ultraviolet O and S emissions were much larger than the upper limit values of intensities set by IUE. These authors suggested that the bulk of the auroral UV emissions are due to energetic (10–100 keV) electron precipitation which is deposited above the region of substantial methane absorption (i.e., at or above the homopause), while the X rays are due to line emissions produced by energetic (>300 keV nucleon^{-1}) heavy ion precipitation which is deposited considerably below the methane homopause level. (The homopause is the altitude level above which atmospheric gases have individual scale heights according to their molecular weights, rather than share a common scale height, as below this level. Generally, the homopause level occurs in the lower thermosphere.) As Jupiter's upper atmosphere is considerably more transparent to X rays than to FUV emissions, this scenario could satisfy both sets of observations since UV emissions associated with the heavy ion precipitation would be extinguished by the overlying hydrocarbons.

Barbosa [1990a] reexamined the question of electron bremsstrahlung as the mechanism for producing X-ray photons on Jupiter. He proposed that soft X rays observed by *Metzger et al*. [1983] are due to bremsstrahlung from the secondary electrons generated locally during ionization of H_2 by precipitating primary electrons. He showed that a good agreement with the Einstein X-ray measurements can be obtained (see Figure 2) with a beam of primary electrons (electrons assumed to be accelerated by a field-aligned potential drop and precipitated into the atmosphere) having a Maxwellian energy distribution with a characteristic energy of 30–100 keV, penetrating below the homopause with an energy flux of 10–20 ergs cm^{-2} s^{-1}, and ionization secondaries having a power law with spectral index ~2.

The model of *Barbosa* [1990a], however, does not comply with the theories of electron transport in the terrestrial auroral atmosphere [e.g., *Banks et al*., 1974; *Evans*, 1974; *Walt et al*., 1979; *Haider and Singhal*, 1983], since the secondary electron energy distribution parameters were chosen freely, independent of the primary electron beam parameters, to satisfy the observed X-ray spectrum of *Metzger et al*. [1983]. Essentially, in the model of *Barbosa* [1990a] the electron distribution used in the calculations consists of two components: (1) the primary electron part, which is assumed to have a Maxwellian distribution with energy flux and characteristic energy as the free parameters, and (2) the secondary electron part, which is assumed to have a power law distribution with spectral index and high-energy cutoff (together with the energy flux of secondary electrons) as the free parameters. No comparison between Barbosa's model and theoretical Jovian models was possible at that time since all the models focused on energies ≤10 keV [*Gérard and Singh*, 1982; *Waite et al*., 1983], whereas the calculations of Barbosa suggested electron energies in the range 30–100 keV.

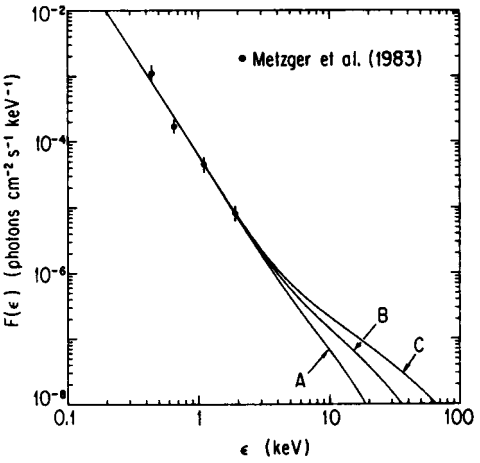

Figure 2. Electron bremsstrahlung photon flux $F(\varepsilon)$ for three auroral electron precipitation models [*Barbosa*, 1990a, Figure 3b]. In this model the secondary electron spectrum is unconstrained by the primary electron spectrum.

Following this, two independent theoretical models, one based on the two-stream method [*Waite*, 1991] and the other based on the continuous slowing down approximation (CSDA) [*Singhal et al*., 1992], performed self-consistent calculations of the electron energy flux distribution of the primary and secondary precipitating electrons in the atmosphere of Jupiter at energies of 10–100 keV. Both models showed that the expected X-ray photon flux is an order of magnitude or more smaller than both the observations and Barbosa's results in the spectral region sampled by Einstein (see Figure 3). This large discrepancy between the results of *Barbosa* [1990a] and those of *Waite* [1991] and *Singhal et al*. [1992] is due to the fact that the secondary electron distribution assumed by Barbosa is over 3 orders of magnitude larger at the altitude of peak auroral energy dissipation [cf. *Waite*, 1991, Figure 1; *Singhal et al*., 1992, Figure 4] than that predicted by the models. Thus the

most recent studies support the original work of *Metzger et al*. [1983] in suggesting that electron bremsstrahlung is unlikely to be the source of Jovian auroral X rays.

Around this time, two papers were also published [*Barbosa*, 1990b; *Waite et al*., 1992] predicting the X-ray intensity at Jupiter during future planetary missions. *Barbosa* [1990b] predicted the X-ray energy spectrum expected at observational distances of 10 and 100 R_J, based on his model of electron bremsstrahlung [*Barbosa*, 1990a], while *Waite et al*. [1992] predicted the intensity of electron bremsstrahlung–produced X rays using the two-stream method [*Waite et al*., 1983; *Waite*, 1991]. Calculations of *Waite et al*. [1992] predicted that precipitating auroral electrons consistent with the constraints from observed UV auroral emissions would produce bremsstrahlung X rays with sufficient energy and intensity to be detected by the Ulysses spacecraft at 10 R_J during its gravity-assisted flyby of Jupiter in February 1992. The model calculations [*Waite*, 1991; *Singhal et al*., 1992] predict a change in the slope of the X-ray emission spectrum at higher energies (≳5 keV), and this could provide an important discriminator between the heavy ion and bremsstrahlung models, if Jovian X rays could be measured at these high energies.

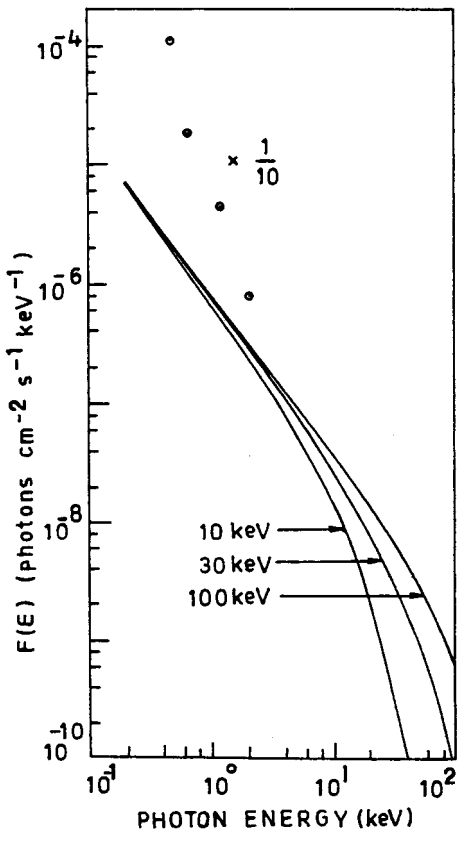

Figure 3. Electron bremsstrahlung photon flux $F(\varepsilon)$ for three similar auroral electron precipitation models [*Singhal et al*., 1992, Figure 5]. In this model the secondary electron spectrum is derived from the primary by the continuous slowing down approximation method.

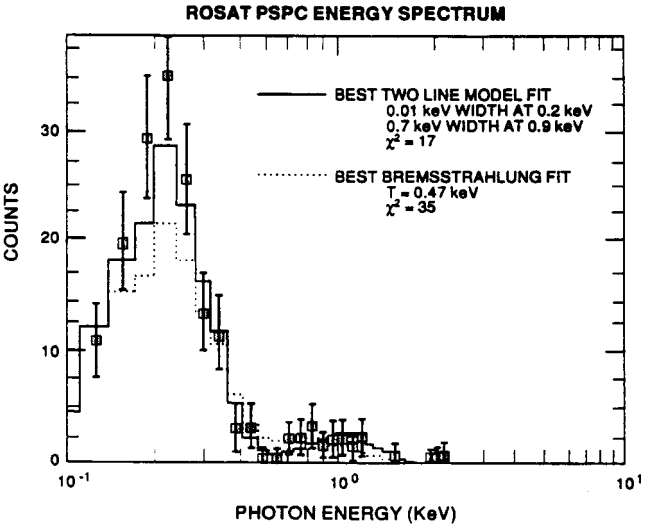

Figure 4. Jovian X-ray spectrum obtained by the Röentgen-satellit (ROSAT) position-sensitive proportional counter (PSPC) instrument, with the best fitting two-line and bremsstrahlung models overplotted [*Waite et al*., 1994, Figure 5].

The ambiguity about the source of X-ray radiation from Jupiter's auroral latitudes, with arguments and counterarguments for and against the electron bremsstrahlung and K shell ion emissions, was resolved to a certain extent by the Ulysses Gamma Ray Burst (GRB) experiment observations made from a distance of 163–110 R_J, which detected no significant emissions in the 27- to 48-keV energy range [*Hurley et al*., 1993]. These observations placed a 3σ upper limit of 1.1–5.6 × 10^8 W for hard X-ray emissions from Jupiter. The precipitating electron power required to explain the UV aurora leads to estimates of bremsstrahlung X-ray power which are an order of magnitude below the Ulysses upper limit [*Hurley et al*., 1993], whereas the *Barbosa* [1990a, b] model predicts a bremsstrahlung X-ray power between 9 × 10^7 and 2 × 10^8 W, which should have been detected by the GRB experiment. The Ulysses observations did not completely rule out the electron bremsstrahlung hypothesis but provided more support for the suggestion that the X-ray radiation from Jupiter is mostly K shell line emissions of precipitating S and O ions.

The controversy was further resolved by ROSAT HRI and position-sensitive proportional counter (PSPC) observations of Jupiter made in April 1991 and May 1992, revealing soft (~80–2000 eV) X-ray emissions from auroral latitudes [*Waite et al*., 1994]. Comparison of the observed X-ray photon flux versus energy spectrum with the X-ray spectrum produced by electron bremsstrahlung and recombination line emissions from S and O ions suggested (see Figure 4) that the line spectrum produces a substantially better fit, both spectrally and statistically, than does the best bremsstrahlung fit. The total X-ray power inferred from analysis of the PSPC (0.1- to 2.1-keV energy passband) data was 1.3–2.1 × 10^9 W, which is within a factor of 3 of the 4 × 10^9 W (0.2–3.0

keV) emitted X-ray power reported by *Metzger et al*. [1983] from the Einstein measurements. The difference between the auroral X-ray power inferred from ROSAT and Einstein data may be partly due to differences in the energy passband of the two experiments and/or temporal variations in auroral intensity. *Waite et al*. [1994] used ROSAT HRI observations to study the variation in auroral X-ray intensity as a function of Jupiter's longitude in the northern polar region (see Plate 2); the data set indicated a peak in the northern auroral zone near 180°–200° system III longitude. This longitudinal variability observed by ROSAT at X-ray wavelengths is consistent with the well-known variability in UV emissions in the northern auroral zone [e.g., *Livengood et al*., 1992]. Thus the ROSAT observations support the suggestion of *Metzger et al*. [1983] and model calculations [*Waite et al*., 1988a, 1994; *Waite*, 1991; *Singhal et al*., 1992] that precipitating energetic (>700 keV nucleon^{-1}) S and O ions are most probably responsible for the X-ray emissions from Jupiter. The presence of such energetic ions in the Jovian magnetosphere, and probably the region of their precipitation into the atmosphere (L = 8–12), was demonstrated by the Voyager LECP data [*Gehrels and Stone*, 1983].

The conclusion of *Waite et al*. [1994] was further developed by the detailed modeling of X-ray emission production, assumed to be recombination line emissions from heavy ion precipitation, carried out by *Cravens et al*. [1995]. The model of Cravens et al. was an extension of the previous model of energetic oxygen precipitation at Jupiter developed by *Horanyi et al*. [1988] to include all the charge states of the oxygen (instead of only the lowest four charge states considered by Horanyi et al.), from neutral oxygen up to fully stripped oxygen. Cravens et al. demonstrated that X-ray emissions in the energy region of ROSAT observations occur mainly from highly charged and excited states of the ions; these are q = 5–7 for oxygen ions (i.e., O VI, O VII, and O VIII) and q = 6–13 for sulfur ions. Their modeled X-ray energy spectrum showed a reasonably good resemblance to the ROSAT observations, except at 250- to 400-eV energies. This discrepancy could be due to emissions from other species, such as Na and C, that have not been considered in the model but are observed by Ulysses to be present in the Jovian magnetosphere at a few percent of the oxygen and sulfur fluxes [*Lanzerotti et al*., 1992]. It is also a result of their oversimplified consideration of the PSPC response function. A total auroral X-ray radiated power of $\sim 2 \times 10^8$ W was estimated by these authors, a few times less than the ROSAT observations. The study of *Cravens et al*. [1995] also showed that the X-ray emissions observed by ROSAT and Einstein could be explained by heavy ion precipitation without extrapolating the Voyager energetic ion spectrum [*Gehrels and Stone*, 1983] to lower energies. Recently, *Kharchenko et al*. [1998] performed Monte Carlo calculations that simulate the charge state histories of energetic oxygen ions as they precipitate into Jupiter's atmosphere. They find that the ions are slow to reach the charge state equilibrium assumed by *Cravens et al*. [1995] and previous studies and that this can significantly alter the X-ray spectrum.

In summary, the current status of our understanding of Jovian auroral X rays is that these emissions are dominantly line emissions resulting from recombination and charge exchange transitions in highly charged states of S and O ions which are precipitating into the atmosphere of Jupiter with energies in excess of 300 keV nucleon^{-1} from the L = 8–12 region of the magnetosphere, with at most a minor contribution from electron bremsstrahlung.

It is worth pointing out here that X-ray emissions have also recently been observed by ROSAT from the equatorial latitudes of Jupiter (see Plate 3) which have been interpreted as line emissions from precipitating heavy ions [*Waite et al*., 1997]. The precipitation of these heavy ions at low latitudes can result from pitch angle scattering of ions by plasma waves [*Thorne and Moses*, 1983], whose presence in the inner magnetosphere of Jupiter, with high intensity at lower latitudes, has been detected by Ulysses [*Rezeau et al*., 1997]. These X-ray emissions seem to be organized in solar local time (occurring predominantly between local noon and dusk) and in longitude, and are found to emanate largely from the λ_{III} = 210°–60° region (a broad region of low magnetic field strength along the Jovian magnetic dip equator). Assuming that these equatorial X rays are caused by the precipitation of energetic (>300 keV nucleon^{-1}) S and O ions out of Jupiter's inner radiation belt, *Waite et al*. [1997] studied the implications of these precipitating heavy ions for the heating of the atmosphere. Their model calculations showed that a height-integrated heating rate of 0.08–3 ergs cm^{-2} s^{-1}, with a preferred value of 0.2 ergs cm^{-2} s^{-1}, can result in substantial heating of the atmosphere that may account for a large fraction of the upper atmosphere temperature structure observed by the Galileo probe's atmospheric structure instrument [*Seiff et al*., 1996, 1997].

Most recently, *Gladstone et al*. [1998a] examined the spatial and temporal variations of the Jovian X rays using several years of ROSAT observations. They found that the emitted X-ray power from Jupiter has decreased with time by about 50% from 1994 to 1996, roughly in parallel with solar activity. Also, the distribution of emissions across the disk of Jupiter has an intriguing correlation with the bright limb of the planet (i.e., the X-ray emissions are found to be brightest on the side of the sub-Earth location where the subsolar point resides). This may indicate that reflected or fluoresced solar X rays may contribute to the disk emissions and that they are not entirely the result of ion precipitation.

3.2. Ultraviolet Emissions

3.2.1. Early work. The first positive identification of the aurora on Jupiter was provided by the Voyager

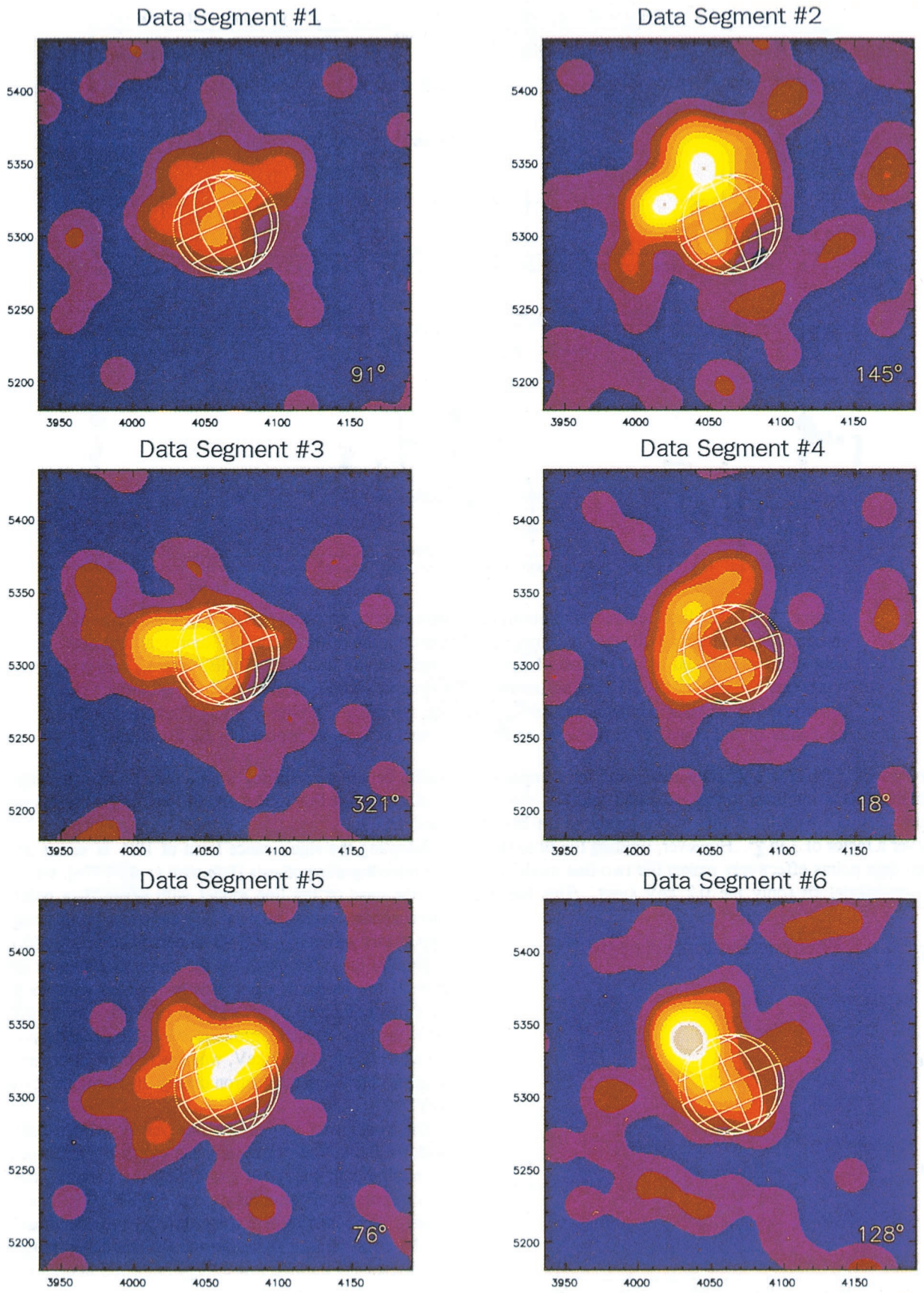

Plate 2. Individual images of six different Röentgensatellit (ROSAT) high-resolution imaging (HRI) observations of Jupiter during May 22, 1992. The orientation and size of the disk of Jupiter and the average central meridian longitude (CML) during the observations are indicated [*Waite et al*., 1994, Plate 2].

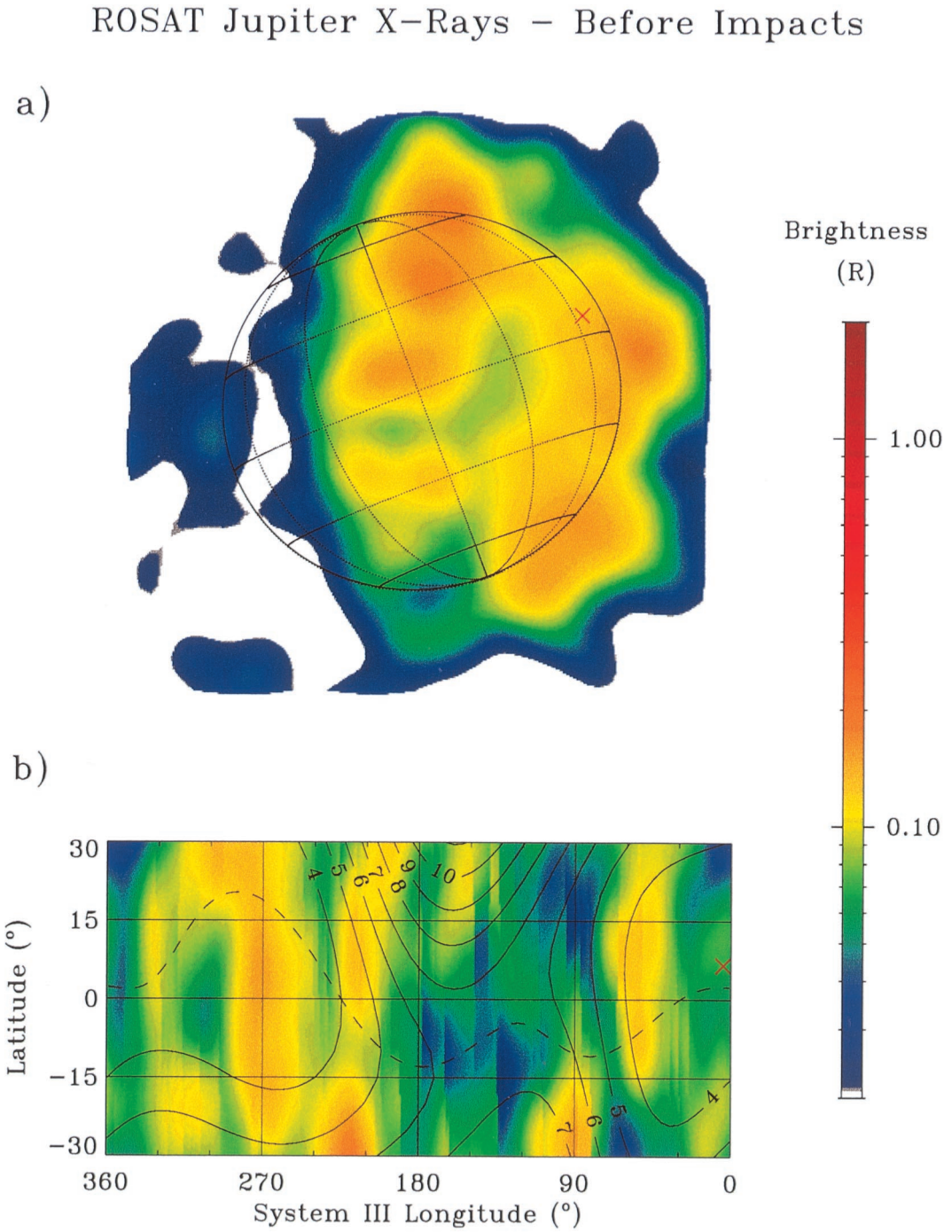

Plate 3. (a) ROSAT HRI X-ray image of Jupiter, produced with data from July 13–15, 1994. The data have been smoothed by the HRI point spread function (PSF) and converted to brightness units. (b) Map of the X-ray emissions, with overlain contours of O6 model surface magnetic field strength (gauss) and a dashed line showing the magnetic dip equator. The red cross marks the entry site of the Galileo probe [*Waite et al*., 1997, Figure 1]. Reprinted with permission from *Science*.

ultraviolet spectrometer (UVS) [*Broadfoot et al*., 1979, 1981a; *Sandel et al*., 1979] (see Figure 5). Assuming the auroral zone width to be 6000 km, the UVS observations inferred about 60 kR of Lyman α and about 80 kR of H_2 Lyman and Werner band emissions [*Broadfoot et al*., 1981a]. These emissions were observed in both hemispheres near 65° magnetic latitudes. The level of emission corresponded to a continuous power input of 10^{13}–10^{14} W into the auroral zone, compared with roughly 10^{11} W for the Earth's aurora. For the precipitating particles to be electrons, an energy flux of about 10 ergs cm^{-2} s^{-1} would be required [*Gérard and Singh*, 1982; *Waite et al*., 1983]. This means that the planet-averaged ratio of auroral to solar radiation input is 20–50 times

more at Jupiter than at the Earth. In addition to electrons, the most commonly accepted primary precipitating species, *Goertz* [1980] suggested proton precipitation may be important, while *Thorne* [1982, 1983] and *Thorne and Moses* [1983] considered heavy ion precipitation, which is supported by observations of 1–20 MeV nucleon^{-1} oxygen, sulfur, and sodium ions in the Jovian inner magnetosphere [*Gehrels and Stone*, 1983] (see *Mauk et al*. [1996] and *Anglin et al*. [1997] for recent results on the analysis of Voyager and Ulysses data). The question of identity of the precipitating particles, however, is still very much a debatable issue [e.g., *Clarke et al*., 1989b; *Waite et al*., 1988a, 1994; *Barbosa*, 1991; *Singhal et al*., 1992; *Mauk et al*., 1996] (see section 3.2.5 for more details).

Jovian auroras were also observed at FUV wavelengths by IUE in the same time period of the Voyager encounter, which gave an indication of a possible temporal variation in the brightness of the emissions [*Clarke et al*., 1980]. *Durrance et al*. [1982] used IUE to observe the north pole of Jupiter during an almost complete rotation of the planet. *Skinner et al*. [1984] modeled the brightness distribution as a function of central meridian longitude corresponding to IUE observations of the north aurora collected between January 1981 and January 1982. (Central meridian longitude, or CML, refers to the longitude on Jupiter (generally in the magnetic field rotational frame known as system III) which is most directly underneath the Earth at a given time.) *Skinner and Moos* [1984] extended this work to south auroral observations from July 1983 to March 1984. The above

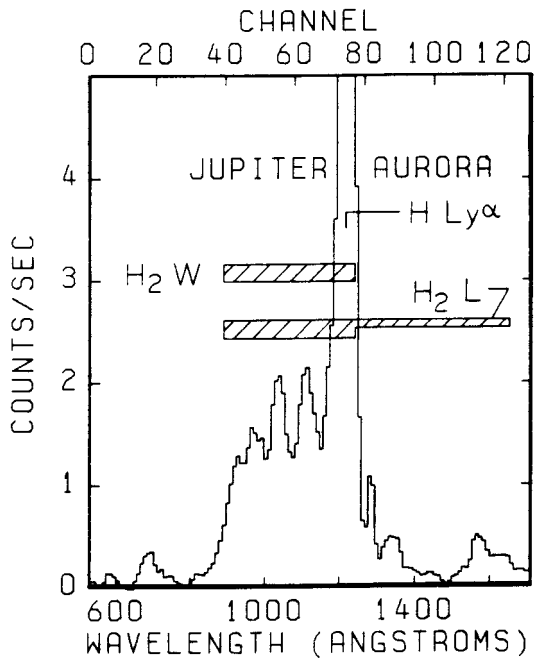

Figure 5. Voyager ultraviolet spectrometer (UVS) discovery spectrum of Jovian auroral FUV emissions from H_2 (Lyman and Werner bands) and H (Lyman α) [*Broadfoot et al*., 1979, Figure 4]. Reprinted with permission from *Science*.

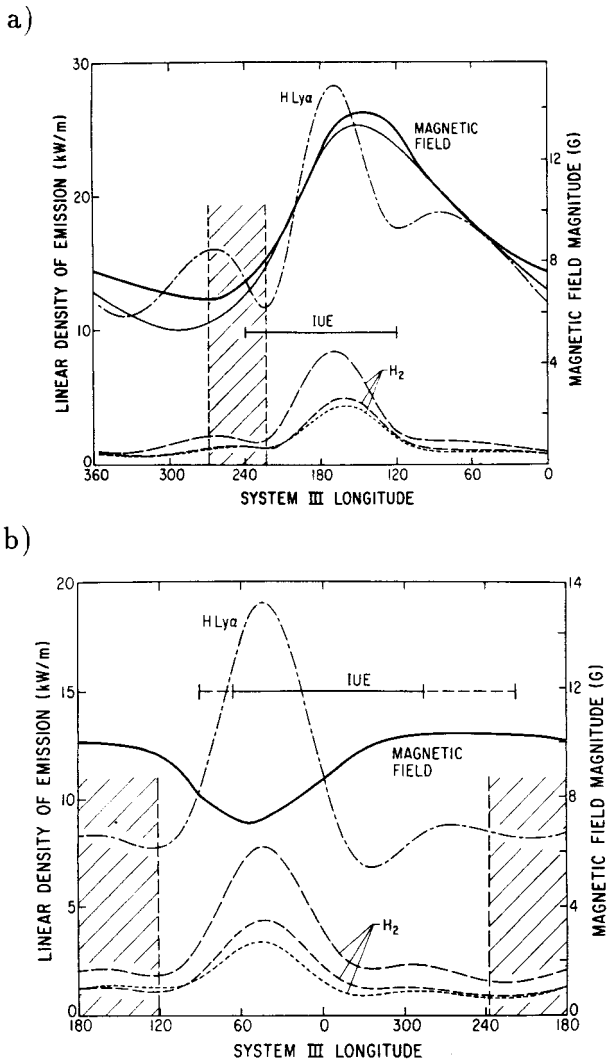

Figure 6. Estimates of relative Jovian (a) northern and (b) southern FUV auroral intensity as a function of system III longitude, as recorded by the Voyager 1 UVS during preencounter observations [*Herbert et al*., 1987, Figures 6 and 8]. The hatched areas indicate regions of poor data constraint. Note the emission maxima near the locations of most negative $dB/d\lambda_{III}$.

studies conducted using IUE data and those using Voyager UVS data [*Herbert et al*., 1987] indicated a longitudinally confined bright region in the northern auroral zone, centered near $\lambda_{III} \sim 180°$, and a more uniform southern aurora with peak emission near $\lambda_{III} \sim 50°$ (see Figure 6). These longitudinal patterns are consistent features over timescales of years, although the brightness of the aurora varies over days and months. *Herbert et al*. [1987] pointed out that these intensity maxima are at longitudes where the mirror point altitude is decreasing with time for particles drifting westward (toward higher longitudes). Such westward drift is expected for electrons due to ordinary gradient curvature drift but could possibly also be exhibited by ions whose drift motion is dominated by corotation lag in the Io plasma

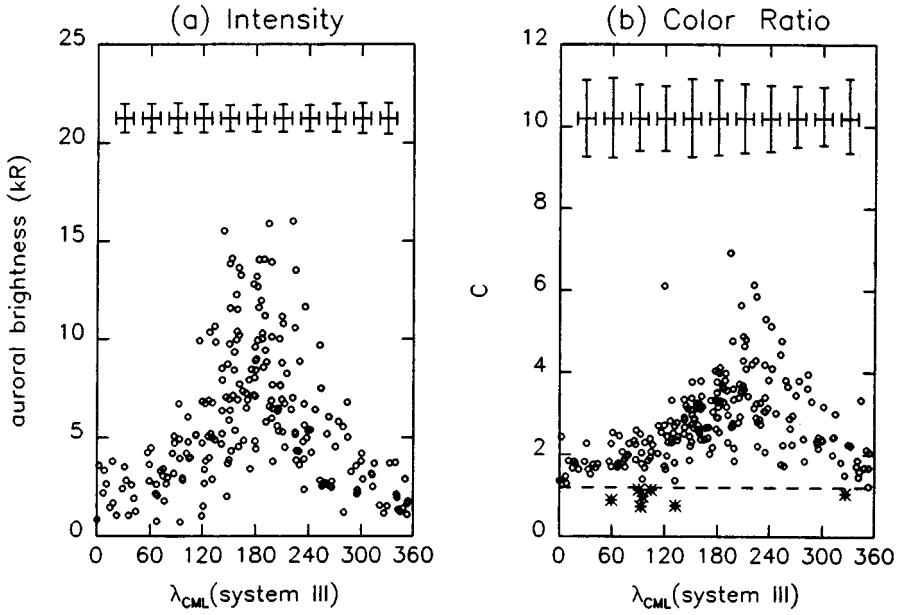

Figure 7. (a) Intensity ($I_{1557-1619}$) and (b) color ratio ($I_{1557-1619}/I_{1230-1300}$) variation of Jovian northern auroral H_2 emissions as observed by International Ultraviolet Explorer (IUE) during 1979–1989 [*Livengood et al*., 1990, Figure 1]. The dashed line in Figure 7b shows the ratio expected for an unattenuated H_2 spectrum, and IUE values lower than this have been plotted as asterisks.

torus. (The Io plasma torus is a doughnut of plasma, mostly electrons plus S and O ions, that encircles Jupiter at Io's orbit. It is nearly self-generated, since torus particles corotating with Jupiter's magnetic field can impact Io's atmosphere and sputter new material into the torus.) The distribution of UV auroral brightness is approximately fixed in magnetic longitude rather than fixed with respect to local time as for the terrestrial aurora.

Long-term studies of Jovian auroras using IUE have been reported by *Livengood et al*. [1988, 1990, 1992] and *Livengood and Moos* [1990]. *Livengood et al*. [1990] analyzed the wavelength-dependent absorption apparent in IUE spectra of Jovian north polar emissions observed over the period of 1978–1989. They found that the hydrocarbon optical depth in front of the auroral emission has a consistent dependence on magnetic longitude (see Figure 7). *Livengood et al*. [1992] used IUE data from 1981 to 1991 to rule out a correlation between the auroral brightness and extreme ultraviolet (EUV) solar cycle variability as predicted by *Eviatar and Barbosa* [1984] and also did not detect any long-term variation in either auroral brightness or morphology. These long-term studies by IUE also confirmed the modulation of emission intensity with central meridian longitude. The UV emission peak at $\lambda_{III} \sim 180°$ CML in the northern auroral zone coincided well with the "IR hot spot" [*Caldwell et al*., 1988], indicating that the processes generating the UV and IR emissions might be the same and that the longitudinal brightness variations might reflect the auroral precipitation pattern [*Prangé*, 1991, 1992]. Later, high-resolution FUV imaging from the Hubble Space Telescope (HST) led to questioning of this conclusion. Even the early (pre-COSTAR) HST images clearly showed that the FUV auroral emissions were of lowest brightness at the location where the IR emission maximized [*Caldwell et al*., 1992]. In retrospect, much of the auroral brightness variation with CML seen by Voyager UVS and IUE was likely due to their large fields of view.

3.2.2. Modeling. Post-Voyager modeling of Jovian auroral and related process has been carried out by several researchers [e.g., *Yung et al*., 1982; *Gérard and Singh*, 1982; *Waite et al*., 1983, 1992; *Gladstone*, 1982; *Horanyi et al*., 1988; *Cravens*, 1987; *Gladstone and Skinner*, 1989; *Barbosa*, 1990a; *Singh*, 1991; *Prangé and Elkhamsi*, 1991; *Kim et al*., 1992; *Singhal et al*., 1992; *Cravens and Eisenhower*, 1992; *Bhardwaj and Singhal*, 1993; *Livengood et al*., 1990; *Rego et al*., 1994; *Prangé et al*., 1995, 1997a, b; *Bisikalo et al*., 1996; *Liu and Dalgarno*, 1996; *Achilleos et al*., 1998; *Gladstone et al*., 1998b; *Rego et al*., 1999]. The study of *Yung et al*. [1982] concluded that the precipitating auroral particles must penetrate the homopause in order to produce the observed absorption of H_2 emissions at wavelengths <140 nm and that electrons in the range of 1–30 keV with an energy flux of about 10 ergs cm^{-2} s^{-1} would suffice. *Gérard and Singh* [1982] computed the expected altitude profiles of ionization, excitation, and heating rates in the upper atmosphere, using the continuous slowing down approximation (CSDA), for 0.1- to 2-keV Maxwellian primary electron spectra. *Waite et al*. [1983] and *Horanyi et al*. [1988] have further studied the detailed aeronomical consequences of 1- to 10-keV monoenergetic electron

precipitation and energetic oxygen and sulfur ion precipitation, respectively, in the upper atmosphere of Jupiter. Their studies showed that atmospheric and ionospheric processes are not very sensitive to the identity of the precipitating particles (effects vary within a factor of ~3) but depend mostly on the total energy input and the atmospheric level at which the energy is deposited.

The first theoretical model of vibrationally excited H_2 in the auroral upper atmosphere of Jupiter was presented by *Cravens* [1987]. He calculated the density for each of the 14 excited vibrational levels of the ground electronic state of H_2 as a function of altitude. He showed that significantly enhanced populations of vibrationally excited H_2 could exist in the atmosphere and that these would affect ionospheric densities by providing an important chemical sink for H^+ ions in the Jovian ionosphere through the reaction

$$H^+ + H_2(v \geq 4) \rightarrow H_2^+ + H,$$

as originally suggested by *McElroy* [1973].

Following the approach of *Yung et al*. [1982], *Gladstone and Skinner* [1989] and *Livengood et al*. [1990] analyzed the effect of the wavelength-dependent atmospheric extinction (due to hydrocarbons near or below the homopause) on the observed H_2 FUV emission spectrum. From a model-dependent analysis of IUE-observed Jupiter polar emission spectra, *Gladstone and Skinner* [1989] inferred equivalent incoming particle energies of ~95 keV, 3.3 MeV, and 6 MeV nucleon^{-1} for electrons, protons, and heavy ions, respectively, while *Livengood et al*. [1990] inferred energy from 10 to 17 keV for electrons and approximately 200–500 keV nucleon^{-1} for ions. Thus these latter studies suggested electrons in the 10- to 100-keV range, while the earlier theoretical studies modeled electrons of $\lesssim$10 keV only.

The effect of Jupiter's strong magnetic field asymmetry on the precipitation distribution of electrons and ions was investigated by *Prangé and Elkhamsi* [1991] for the case of an isotropic and uniform injection mechanism along constant L shells and for various pitch angle distributions. Their model suggested that depending on the real-time precipitation rates of the species (electrons and ions), the longitudinal precipitation profile (and thus the brightness distribution) may have either a single or double peak and that this could possibly explain the longitudinal asymmetry observed in the auroral UV emissions by Voyager and IUE.

Singh [1991] developed a CSDA-based model to calculate the energy degradation of a proton-hydrogen beam precipitating into a H_2-H auroral atmosphere of Jupiter. He found that the overall efficiencies of most excitation processes due to proton and electron impact are fairly similar but that the relative contribution of secondary electrons to the excitation strongly depends on the energy of the primary proton. His calculations suggested that protons carrying an energy flux of 7–10 ergs cm^{-2} s^{-1} with characteristic energy $\lesssim$1 MeV would be required to account for the observed UV intensities.

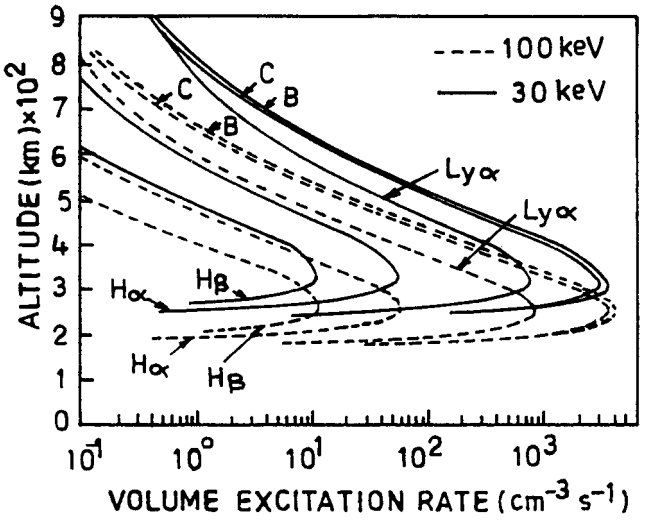

Figure 8. Calculated volume excitation rates of the Lyman (curve B) and Werner (curve C) states of H_2 and the Hα, Hβ, and Lyman α lines of H in a model Jovian atmosphere, for input Maxwellian precipitating electron spectra with characteristic energies of 100 keV (dashed lines) and 30 keV (solid lines) [*Singhal et al*., 1992, Figure 7].

Extending the work of *Horanyi et al*. [1988], *Cravens and Eisenhower* [1992] studied the chemical effects of energetic oxygen ion precipitation on the auroral ionosphere of Jupiter. They found that an auroral oxygen flux of about 10^7 cm^{-2} s^{-1} would be required if all the observed H_2 Lyman and Werner band emissions were due to ion precipitation rather than to energetic electron precipitation. Their calculations further demonstrated that the chemistry associated with the odd auroral oxygen species (i.e., O, OH, and H_2O) could result in about a factor of 4 reduction in the electron density in the auroral ionosphere. Cravens and Eisenhower also studied the implications of O precipitation for CO formation in the atmosphere of Jupiter and noted the possible buildup of S^+ ions above the homopause due to their nonreactivity with hydrogen.

To study the implications of energetic (10–100 keV) electron precipitation in the high-latitude upper atmosphere of Jupiter, *Singhal et al*. [1992] developed a model using the CSDA method. They studied the production of H_2 bands, H I Lyman α, Hα, Hβ emissions (see Figure 8), and X rays via electron bremsstrahlung, as well as ionization rates and subsequent ionospheric chemistry. Singhal et al. found that the Voyager-observed Lyman and Werner band emissions of H_2 may be reconciled with precipitating electrons of characteristic energies 10, 30, and 100 keV having energy fluxes of 10, 18, and 45 ergs cm^{-2} s^{-1}, respectively. The model of Singhal et al. suggested that the most consistent picture, satisfying the Voyager UV observations and the Pioneer and Voyager electron density profiles, is for precipitating electrons with an energy flux of 14–18 ergs cm^{-2} s^{-1} having characteristic energies of 30–50 keV.

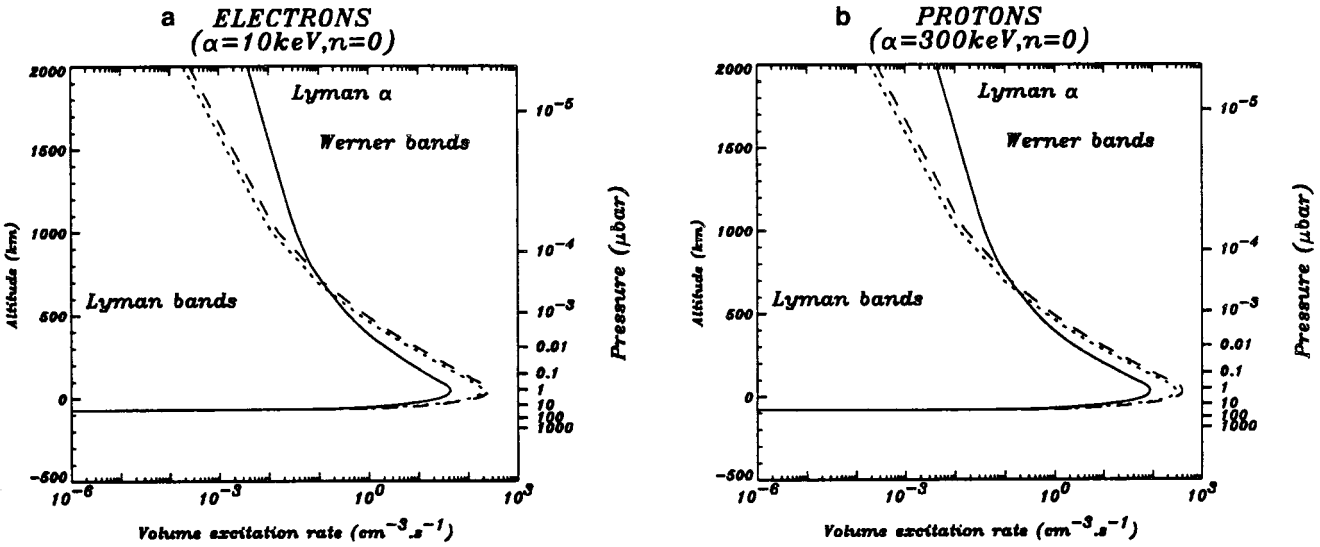

Figure 9. Comparison of the calculated volume excitation rates of H Lyman α and H_2 Lyman and Werner emissions by (a) a 10-keV beam of electrons and (b) a 300-keV beam of protons [*Rego et al*., 1994, Figure 14].

Rego et al. [1994] also developed a code, based on CSDA, for energy degradation of protons and electrons in the Jovian auroral atmosphere. These authors computed altitude profiles of ionization and excitation rates of the H I Lyman α and H_2 bands for electron and proton precipitation in the initial energy ranges of 10–50 keV and 50 keV to 1 MeV, respectively. Rego et al. found that the 10-keV electrons and 300-keV protons produce similar energy degradation profiles (see Figure 9). They pointed out that a beam of protons does not reach equilibrium with H atoms for initial proton energies of $10 \leq E \leq 200$ keV. The ionization process was found to be controlled mainly by the primary precipitating species, with secondary electrons having a negligible contribution. However, in the case of excitation, the contributions of secondary electrons are very important and amount to ~58% for electron primaries and ~69% for a proton aurora. *Prangé et al*. [1995], extending the work of *Rego et al*. [1994], showed that the penetration depth of auroral precipitating particles depends as significantly on their pitch angle distribution as on their initial energy. Therefore primary energies cannot be accurately derived from the "color ratio" (the ratio of auroral brightnesses at 156–162 and 123–130 nm) without taking into account the actual angular distribution of the incoming particles.

A very interesting result reported by *Clarke et al*. [1989a], obtained through high spectral resolution IUE observations, is a pronounced lack of H I Lyman α line emission having large (i.e., 1–2 nm) Doppler (red) shifts in Jupiter's aurora (see Figure 10). The small observed shifts of only about 30–60 km s^{-1} (mainly toward the blue, corresponding to 10- to 20-eV protons and/or H atoms, with higher-velocity wings extending out to a maximum energy of 200 eV) effectively ruled out a substantial magnetospheric proton contribution to the production of Jupiter's aurora. *Clarke et al*. [1989b] suggested that the observed low-Doppler-shift emissions may result from local acceleration of protons by electric fields inside the Jovian ionosphere, analogous to plasma motions observed in Earth's ionosphere. The blue shift indicated plasma motion up out of the atmosphere and raised the possibility that the atmospheric auroral zones supply substantial amounts of protons and H atoms to the magnetosphere. This upward movement and consequent escape of the plasma from the atmospheric auroral zones was supported by the identification of 10- to 100-eV secondary auroral electrons around $L = 7.5$–10 by Voyager [*McNutt et al*., 1990].

Using a modified version of the *Singhal and Bhardwaj* [1991] Monte Carlo model, *Bhardwaj and Singhal* [1993] examined the production of Doppler-shifted H I Lyman α emissions in the auroral atmosphere of Jupiter due to the acceleration of low-energy ionospheric protons in parallel electric fields. Their simulations indicated that an electric field of ~0.5–2.0 mV m^{-1} is required to account for the red-shifted Lyman α emissions and that ~2–5 mV m^{-1} is required to account for the blue-shifted Lyman α emissions of 1–10 kR on Jupiter, when a constant electric field is applied in the neutral number density region of 5×10^{12} to 2×10^{8} cm^{-3}.

More recently, Jovian spectra obtained with the Goddard high-resolution spectrograph (GHRS) on board the HST in the 120.4- to 124.1-nm region with 0.057-nm spectral resolution [*Clarke et al*., 1994] showed highly broadened Lyman α with wings extending symmetrically to ~100 eV (140 km s^{-1}) to either side of line center. The strength of these wings appeared to be correlated with the brightness of H_2 band emission lines also present in the spectra. Consistent with earlier IUE results, no signature of proton precipitation was seen in the GHRS data.

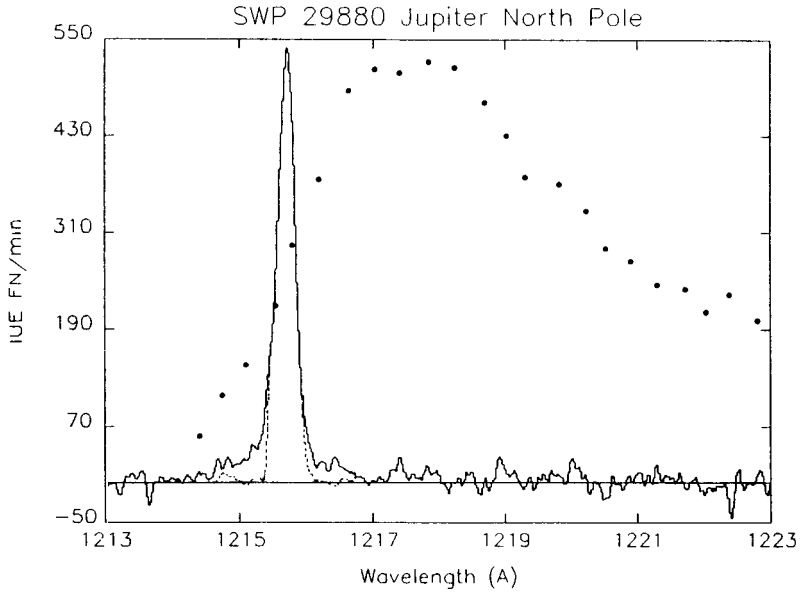

Figure 10. IUE spectrum (solid line) of Jupiter's northern auroral zone, with a representative Earth Hα auroral line profile overplotted as dots with the same velocity scale and normalized to the same peak brightness [*Clarke et al*., 1989a, Figure 1]. The dashed lines indicate the IUE response to a monochromatic emission feature.

Ajello et al. [1995] experimentally measured the kinetic energy distribution of H(2p) atoms using the H I Lyman α emission profile resulting from dissociative excitation of H_2 by electron impact at energies ≤200 eV. They found that the kinetic energies of fast H(2p) atoms span the range 1–10 eV (with a peak near 4 eV) for 100-eV electron impact energy. Ajello et al. concluded that electron impact dissociative excitation of H_2 alone is not sufficient to explain the large broadening of Jupiter's auroral Lyman α emission observed by *Clarke et al*. [1994]. Apparently, a more energetic process is required, one capable of accelerating or producing nascent H atoms of ≳20-eV kinetic energy.

Bisikalo et al. [1996] used a Monte Carlo code to calculate the energy distribution function and the relative number density of nonthermal H atoms for various energies and fluxes of incident electrons and protons in the Jupiter's auroral atmosphere. Only protons were found to yield a nonthermal energy tail extending to energies >10 eV, though the steady state flux of hot atoms for proton as well as electron precipitation was isotropic. They showed that hot H atoms play an important role in determining the shape of the auroral H I Lyman α line profile. Comparison of their modeled Lyman α line profiles with the HST observed spectra [*Clarke et al*., 1994] showed that the model profile obtained with hot H matches better, as it produces much more wing emissions compared with the model without hot H (see Figure 11). However, the modeled line shape is not consistent with observations. Bisikalo et al. suggest that a smaller contribution from much hotter H atoms is required, possibly from accelerated ionospheric protons, as suggested by *Clarke et al*. [1989a]. *Bhardwaj and Singhal* [1993], in their study of low-energy ionospheric proton acceleration in parallel electric fields, found that the energy spectrum of protons runs up to energies of 500 eV or more. Thus it seems plausible that accelerated ionospheric protons could be responsible for producing the observed broadening of the auroral Lyman α line profile; this mechanism should be evaluated in more detail.

A comprehensive analysis of Jovian auroral H I Lyman α emission, which separated the emissions from background sources including Lyman α from the Jovian dayglow, Earth's geocorona, the interplanetary medium, and grating scattered light, has been carried out by *Harris et al*. [1996] using IUE spectra covering the period 1981–1991. They compared the auroral H I Lyman α emission with H_2 emissions in the 123- to 130-nm and 155- to 162-nm band passes. Harris et al. found that both the Lyman α and H_2 emissions show similar long-term variability in intensity and have no correlation with solar cycle variability. A clear linear relationship between the auroral H_2 and H I Lyman α emission and similar distributions with central meridian longitude and CH_4 optical depth was demonstrated (see Figure 12). Using these H_2 and H I Lyman α emission correlations, Harris et al. put a conservative upper limit of 37% for the intensity of Lyman α that can be produced above the altitude where the bulk of the H_2 emissions are produced (say, by electron impact on high-altitude atomic H). The effect of resonant scattering on the emergent Lyman α line intensity and shape was also studied, which indicated that the bulk of the auroral Lyman α emission is produced near the CH_4 homopause.

Prangé et al. [1993] presented observations of an exceptionally bright UV auroral event detected by IUE

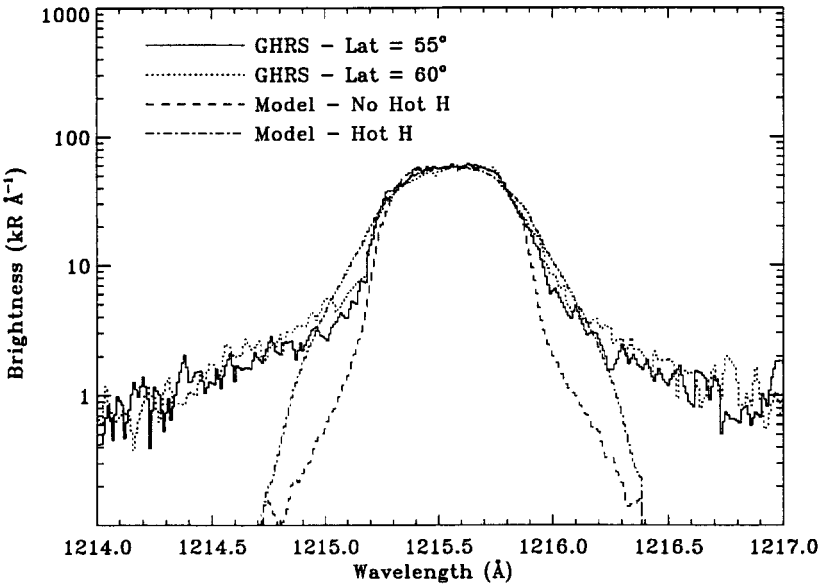

Figure 11. Comparison between Jovian auroral Lyman α profiles observed with the HST Goddard high-resolution spectrograph (GHRS) and model calculations that show the effects of nonthermal H atoms on the width of the expected emission line [*Bisikalo et al*., 1996, Figure 12].

during December 20–21, 1990, whose signatures were also detected simultaneously in auroral decameter radio (DAM) emissions. The DAM and UV emissions exhibited well-correlated variations in intensity and longitude, in particular, with a similar shift of the source region toward larger longitudes from one day to the next (see Figure 13), suggesting that a common cause triggered the variation of the UV and radio emissions during this event. From analysis of Ulysses measurements in the upstream solar wind, *Prangé et al*. [1993] suggested that a large disturbance reached Jupiter at about the time of the auroral event. The correlation between Jovian radio emissions and solar wind activity has already been well established [e.g., *Barrow et al*., 1986; *Barrow and Desch*, 1989; *Zarka and Genova*, 1989].

The effect of the aurora on global thermospheric circulation was first considered by *Sommeria et al*. [1995], who showed that supersonic winds are a likely outcome of such a large energy input. *Achilleos et al*. [1998] have described an ambitious project to create a time-dependent global three-dimensional model of Jupiter's thermosphere and ionosphere, called the Jovian ionospheric model, or JIM. The initial runs suggest that even modest auroral energy input (8 ergs cm^{-2} s^{-1}) can drive large outflows (~0.6 km s^{-1}) by strong chemistry-induced pressure gradients (these gradients are a simple result of the substantial local dissociation of H_2 to 2H in the auroral atmosphere). While the model is still in a preliminary state, with fairly crude discretization and inputs, it is an excellent first step toward a better understanding of how Jupiter's powerful aurora affects the upper atmospheric dynamics and chemistry.

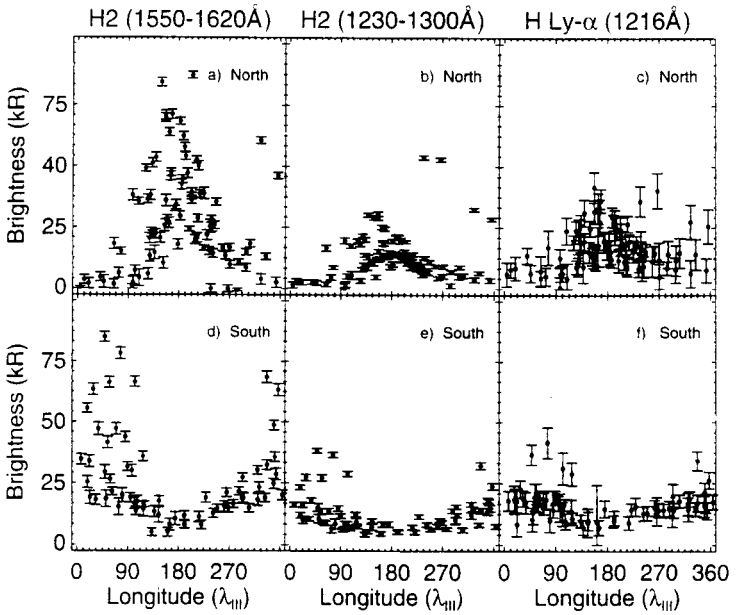

Figure 12. The integrated brightnesses of Jovian auroral H_2 Lyman and Werner band and H Lyman α emissions observed by IUE are shown as a function of central meridian longitude (CML). The H Lyman α pattern is most similar to that of the H_2 Werner band emissions [*Harris et al*., 1996, Figure 8]. Reprinted with permission from Academic Press.

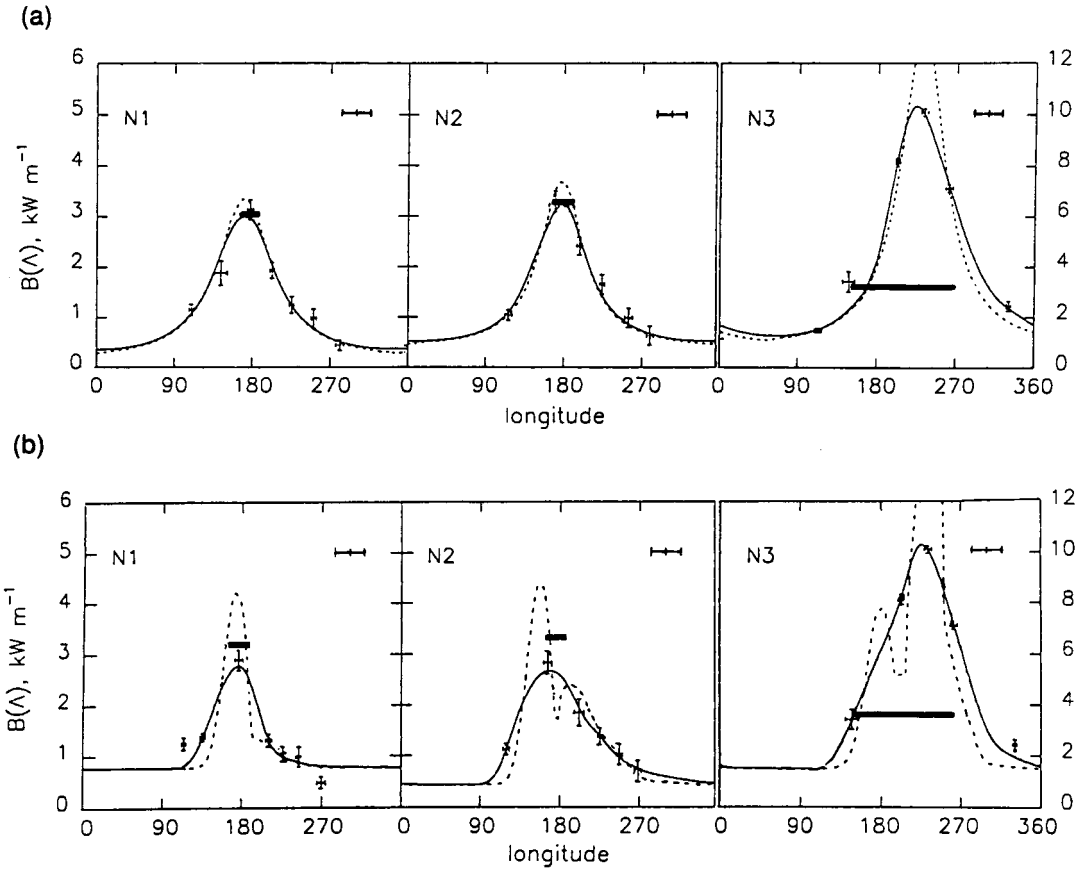

Figure 13. Comparison of IUE observations of FUV emissions from the northern auroral oval (crosses) during three consecutive Jovian days (N1, N2, and N3) and decametric (DAM)-source longitude ranges derived from ground-based decametric observations (bold bars) [*Prangé et al.*, 1993, Figure 5]. The solid lines give the best fit to the observed IUE data, while the dashed lines show model FUV sources based on (a) a Lorentzian distribution and (b) a combination of electron and ion precipitation.

Recently, *Perry et al.* [1999] have begun the difficult process of accurately modeling the auroral region chemistry on Jupiter. While the chemistry in the region above the homopause is fairly straightforward, particles which precipitate below the homopause initiate ion-neutral reactions which quickly lead to the formation of complex hydrocarbon ions. This ion-neutral chemistry is expected to lead to haze formation, as suggested by *Pryor and Hord* [1991]. The initial results of *Perry et al.* [1999] indicate that the auroral ionosphere extends to higher pressures (as large as ~3 μbar) than in nonauroral regions and that the lowest layers are dominated by higher hydrocarbon ions (e.g., $C_3H_n^+$). Larger H-atom column densities in the auroral region were also found, consistent with the results of the JIM model of *Achilleos et al.* [1998].

3.2.3. Imaging. In 1992 a new era opened with the availability of high-resolution UV imaging using the faint object camera (FOC) on board the Hubble Space Telescope (HST). During the Ulysses flyby of Jupiter in February 1992, images of the northern polar regions of Jupiter were obtained by *Dols et al.* [1992] in the FUV near Lyman α and by *Caldwell et al.* [1992] in the bright H_2 Lyman bands near 158 and 161 nm. *Dols et al.* [1992] found that the major part of the observed Lyman α aurora lay poleward of the footprint of L = 15–30 field lines calculated according to the O4 model of *Connerney et al.* [1981]. They also claimed evidence of a more localized source at lower latitudes, possibly connected to the Io plasma torus. The Lyman α images also exhibited considerable longitudinal inhomogeneity, with a minimum intensity near λ_{III} = 180°. Local time–dependent emissions were also seen, in that the H_2 emissions in the few images observed appeared to be enhanced in the late afternoon [*Caldwell et al.*, 1992]. *Caldwell et al.* [1992] determined that the auroral FUV emissions were distributed along a high-latitude oval (contrary to Voyager results), with a minimum at longitude 180° (contrary to IUE results) and with a maximum fixed in local time near the dark limb, which brightened when the CML = 180°. They suggested that the apparent 180° maximum brightness derived from IUE observations was in fact the result of this "dusk limb spot" being seen at the edge of the broad IUE aperture. This hypothesis was recently tested and confirmed by *Prangé et al.* [1997a] and *Ballester et al.* [1996].

Two images taken 3 days apart in June 1992 provided a good view of the $\lambda_{III} \sim 180°$–$200°$ sector of the auroral zone in a passband centered at 153 nm [*Gérard et al*., 1993]. The brighter portions of the aurora were estimated to comprise ~230–350 kR of H_2 Lyman band emissions. These observations basically confirmed the existence of enhanced regions of UV emissions surrounding the north polar regions. The observations showed no indication of bright structured emissions within the polar cap. Their study also suggested that the main magnetospheric source region of the auroral primaries does not lie directly in the vicinity of the Io plasma torus, but appears to originate from a more distant region in the distant magnetosphere, close to the limit of the corotation or even open field lines. The H_2 images exhibited a narrow bright arc in the morning sector, approximately fitting the $L = 30$ magnetic field footprint, and a broader diffuse aurora in the afternoon sector. The total power radiated in the H_2 bands was estimated to be $\sim 2 \times 10^{12}$ W, which is in agreement with earlier IUE and Voyager estimates. However, the high emission rates measured locally in the H_2 arcs imply large local fluxes (~50 ergs cm^{-2} s^{-1} of electron energy precipitation).

In February 1993, *Gérard et al*. [1994a] obtained a series of six UV images of Jupiter's north polar region, covering a complete rotation of the planet, using the HST FOC centered near 153 nm, a region dominated by unabsorbed H_2 Lyman bands and continuum. These images were of better quality than the early HST FOC images obtained in 1992 [*Dols et al*., 1992; *Caldwell et al*., 1992; *Gérard et al*., 1993], owing to the use of a different filter combination and the largest FOC field of view. *Gérard et al*. [1994a] found that the size of the northern auroral oval and its location agree best with the footprint of the $L = 30$ field line in the O6 magnetic field model of *Connerney* [1993], if a small shift were made in the position of the O6 model oval by about 10° parallel to the $\lambda_{III} \sim 270°$ meridian (see Plate 4). Such a conclusion was also supported by another set of their observations acquired with the same instrument in July 1993 [*Gérard et al*., 1994b]. *Gérard et al*. [1994a] observed a systematic variation in emission morphology east and west of the $\lambda_{III} \sim 180°$ meridian; a narrow discrete arc is observed at $\lambda_{III} > 180°$ (parallel but close to the $L = 30$ oval, while a more structured and diffuse emission zone was seen inside the $L = 30$ oval for $\lambda_{III} < 180°$). These morphological features were also observed by *Gérard et al*. [1994b] in their UV images. Emission features similar to those seen in the FUV have been observed in the H_3^+ auroras [*Satoh et al*., 1996], suggesting a common origin.

Gérard et al. [1994b] recorded an exceptionally bright auroral event in July 1993 using the FOC. A local H_2 emission intensity of ~6 MR was observed, which corresponds to a local electron precipitation flux of ~1000 ergs cm^{-2} s^{-1} and a radiated power of $\sim 10^{12}$ W, which is about 3×10^4 times larger than the heating rate due to solar EUV radiation. A decrease in the brightness of the discrete arc by more than an order of magnitude within 20 hours, and its high-latitude location, led Gérard et al. to suggest field-aligned-current-driven auroral precipitation at Jupiter as the cause (in analogy to the Earth's discrete aurora) rather than the usual particle precipitation by pitch angle diffusion [cf. *Herbert et al*., 1987]. Field-aligned currents were detected in the Jovian magnetosphere during the Ulysses flyby of Jupiter [*Dougherty et al*., 1998].

Since the reflected FUV background is large just longward of the 153-nm FOC passband, the equatorward boundary of the aurora may not be correctly determined from the FOC observations at 153 nm, especially in the $\lambda_{III} \sim 140°$–$200°$ region, where the effect of the center and the shape of the auroral oval shift the auroral emission to latitudes ≤50°N. To resolve this, *Grodent et al*. [1996] carried out observations of the Jovian aurora with FOC at 125, 130, and 153 nm. Most of the emissions were found to be confined inside the $L = 6$ oval (as defined by the O6 magnetic field model) and fill a large fraction of polar cap. However, the emissions at 125 and 130 nm extended to significantly lower latitudes, down to ~40°N, between $\lambda_{III} \sim 140°$ and 200°. Such equatorward extensions of the auroral zones were also reported in the IR mapping of the H_3^+ aurora by *Kim et al*. [1994], who found that the H_3^+ emissions are observed down to ~50°N between about $\lambda_{III} = 150°$ and 180°.

Prangé et al. [1996], using post-COSTAR FOC images, showed that the lead angle between the emission features and the foot of the IFT seems to vary with time. Prangé et al. suggested that this variability may result from variations in the mass density of the Io plasma torus. This separation between the magnetic footprint of Io and its auroral footprint obtained by HST observations is different from that obtained by IR observations [*Connerney et al*., 1993]. Analysis of the HST-obtained FUV emissions also indicated that the Alfvén waves carrying the current between Io and Jupiter's ionosphere deposit most of their energy rapidly when they first encounter the ionosphere. This finding was inconsistent with the hypothesis of multiply reflecting Alfvén waves [e.g., *Neubauer*, 1980] that had been invoked successfully to account for the structure observed in Jupiter's decimetric radio emissions, which are also driven by the Io-Jupiter interaction.

One of the more important results from the recent HST images is that the maximum emission along the northern auroral arc was not found at $\lambda_{III} = 180°$ [*Caldwell et al*., 1992; *Dols et al*., 1992; *Gérard et al*., 1993, 1994a, b], as had been inferred from the large aperture spectroscopic studies by IUE [e.g., *Livengood et al*., 1990, 1992; *Skinner et al*., 1984] and from Voyager observations [*Herbert et al*., 1987]. As was mentioned above, recent studies have shown that the modulation of Jupiter's auroral FUV emissions in longitude, with maximum near 180° in the north and near 20° in the south observed by IUE and Voyager, may be explained by viewing

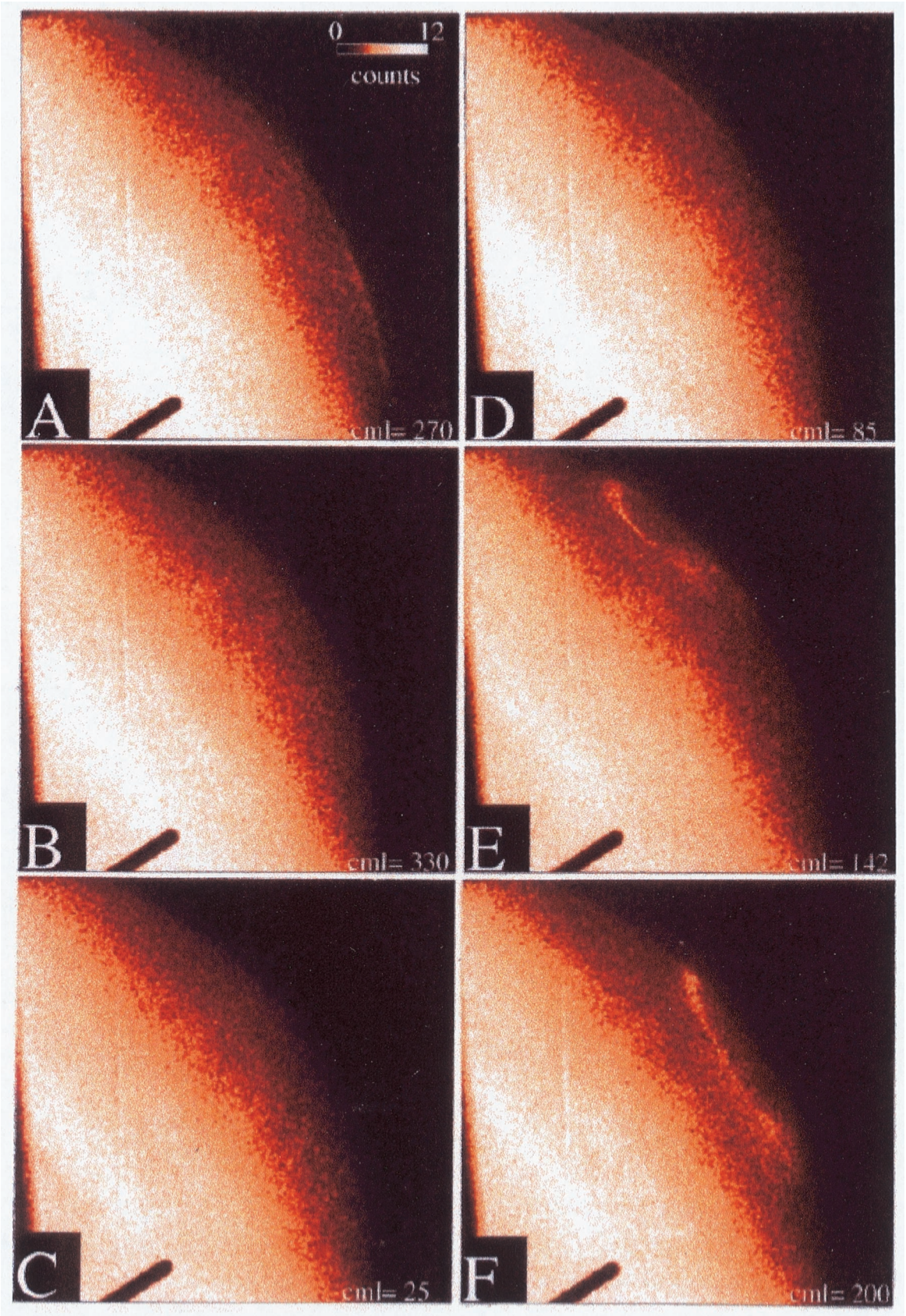

Plate 4. False-color plots of six consecutive HST faint object camera (FOC) FUV images of the northern auroral region of Jupiter, obtained in February 1993. The CML of each exposure is indicated, and the elapsed time between each exposure was about 90 min [*Gérard et al*., 1994a, Plate 4]. Reprinted with permission from Elsevier Science.

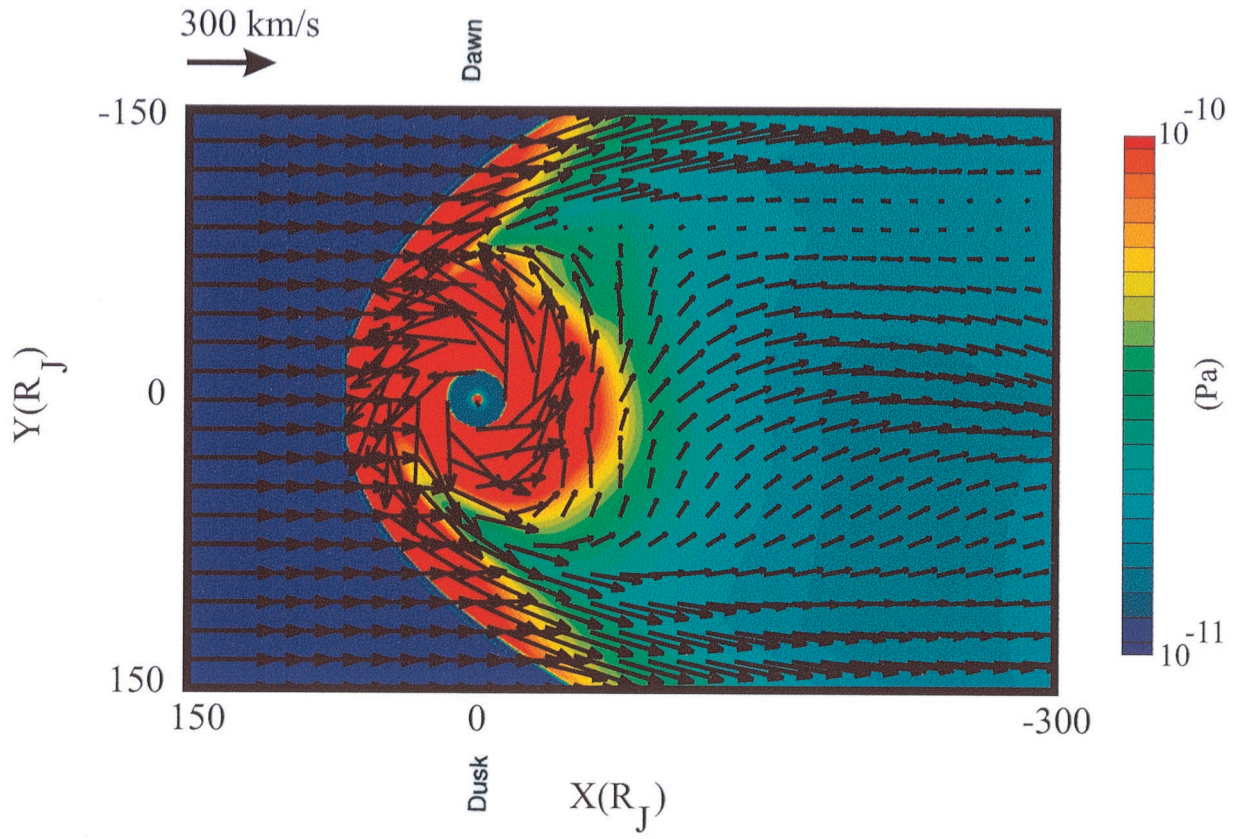

Plate 5. Plasma pressure with superimposed flow vectors in the equatorial plane at a model time of $t = 225$ hours. The dark blue region in the center of the plate is inside the inner magnetosphere boundary of the simulation and is not included in the calculation [*Ogino et al*., 1998, Plate 2].

geometry effects near the east and west ansa (observed extremities) of the auroral oval, combined with IUE point spread function effects [*Ballester et al*., 1996; *Prangé et al*., 1997a]. These effects also affect the color ratio asymmetry, which had been found to exhibit a longitudinal variation very similar to the brightness variation [*Livengood et al*., 1990]. However, the color ratio variation with CML observed with IUE is not solved by geometry considerations alone. *Gérard et al*. [1998] present model results in which a fit to the IUE data required assuming a methane column abundance above the aurora which varied strongly (by factors of 10^7) with longitude: A nonvarying atmosphere produces an opposite dependence to the IUE results. *Prangé et al*. [1997a] also identified an intrinsic brightness modulation due to the transit of a bright possibly transpolar emission aligned along the 160° meridian across the IUE aperture, but with contributions generally smaller than the geometrical effect (15–30% as much). The FOC images taken in a typically strong auroral event also showed similar results.

A comprehensive review of the FOC images was presented very recently by *Prangé et al*. [1998]. They characterize several of the main morphological features of the Jovian aurora, including the IFT footprint and "transpolar emission" arc features that are often seen to stretch from the main oval across the polar cap on its dusk side, occasionally parallel to the noon-midnight meridian (see Plate 1). The brightness of the transpolar feature exhibits considerable variability unrelated to variations in the brightness of the main oval. Surprisingly, these authors suggested that the width of the main oval could be very narrow (80 ± 50 km) with a very high but variable brightness (up to ~2 MR), implying local particle precipitation inputs of 10–200 ergs cm^{-2} s^{-1}.

Clarke et al. [1996] and *Ballester et al*. [1996] present excellent summaries of our current understanding of Jovian FUV auroral morphology, based on numerous HST wide-field planetary camera 2 (WFPC2) observations. From these data it has been determined that (1) the main north and south auroral ovals are robust features that are relatively constant in latitude and system III longitude, although they undergo large brightness variations (occasionally reaching brightnesses of several megarayleighs); (2) inside the polar cap there are patchy regions of emission, primarily on the dusk half of the oval; (3) there is a spot of emission equatorward of each of the main ovals associated with the foot of the IFT; and (4) the north and south auroras exhibit conjugate emission features. The region $90° < \lambda_{III} < 150°$ of the main FUV oval in the north is observed to undergo a curious equatorward shift in latitude, as it rotates from

the morning to the afternoon side of the planet. The HST images conclusively demonstrate that the main Jovian aurora is connected, not to the Io plasma torus region as previously believed, but to the middle magnetosphere $L > 12$. Much of the structure and variability of the aurora is thus likely to be governed by plasma circulation in the middle and outer magnetospheres, and recent modeling [e.g., *Ogino et al*., 1998] suggests that common features of the aurora (e.g., single narrow arcs in the morning, multiple broad arcs in the afternoon) can be explained as the interaction between the regions of corotation and solar wind–driven convection (see Plate 5).

WFPC2 observations in support of Galileo encounters G1, G2, G7, G8, and C9 were presented recently by *Clarke et al*. [1998]. These images confirm the equatorward surge of the 140°–180° region of the main oval as it crosses local noon. Bright "dawn storms" were described in which the main oval brightened significantly at a fixed local time near the dawn terminator and did not rotate with system III. Such features indicate that Jupiter's aurora is not entirely driven by corotation in the magnetosphere but that solar wind–driven convection likely plays a part as well. Finally, several sightings were made of a bright IFT footprint, and a few possible sightings were made of analogous footprints associated with Europa and Ganymede. The imaging database will continue to improve as more HST/STIS observations are made (since STIS has much higher FUV sensitivity than WFPC2), and we can expect that our understanding of Jupiter's auroral morphology will continue to advance for some time to come.

3.2.4. Spectroscopy. The first spectroscopic observation of a Jovian aurora with GHRS aboard HST was made by *Trafton et al*. [1994], at the time of the Ulysses flyby of Jupiter. The targeted region was Jupiter's north polar region at $\lambda_{III} = 180°$ and latitude 67°N, the region near the maximum brightness as derived from the IUE observations. The study concentrated on two 3.5-nm wavelength intervals centered on 127 nm (125.3–128.7 nm) and 159 nm (157.3–160.7 nm), near emission peaks in the H_2 Werner and Lyman bands, respectively. The emission spectra were well explained in terms of excitation of H_2 by electrons except for features at 158.07 and 158.37 nm, which were anomalously bright, and two weak features at 158.02 and 158.74 nm, which were not present in the synthetic spectrum. From the model-dependent analysis of the data, Trafton et al. derived an H_2 rotational-vibrational temperature of 530 ± 100 K, showing that the homopause level is hotter (but not necessarily higher) than observed at nonauroral latitudes. These results, however, were determined for a region of the aurora poleward of the $L = 30$ oval which was only moderately bright, and results may differ in regions of stronger or more energetic auroras.

Clarke et al. [1994] also obtained the UV emission spectrum from Jupiter's north auroral atmosphere with GHRS/HST, but over the wavelength range 120.4–124.1 nm with 0.057-nm spectral resolution. From the fitting of the observed spectra with the synthetic H_2 spectra they derived temperatures from 400–450 to 700–750 K, indicating temporal and/or spatial variability in the temperature of the auroral emission layer. The emissions were found to be emanating from the 50°–60° latitude range at locations consistent with $L = 6$–30 auroral ovals.

Using the GHRS, *Y. Kim et al*. [1995] obtained FUV emission spectra from both polar regions of Jupiter in the 158.6- to 162-nm wavelength range, which is dominated by H_2 Lyman band emissions. Two bright spectra were observed near the western (dusk) limb at latitudes 56°–58°N and CMLs of 190° and 203°. They derived intensities and best fit temperatures of ~240 kR and 300–400 K, respectively, for the bright regions and ~30–120 kR and 200–700 K, respectively, for the fainter regions, with a median temperature of 500 K (i.e., consistent with the results of *Trafton et al*. [1994] and *Clarke et al*. [1994] derived using the same type of experiment but different wavelength ranges). Y. Kim et al. proposed that the generally lower temperatures in the bright regions might indicate that the precipitating particles there may be penetrating to lower altitudes (i.e., might be more energetic), where lower temperatures are expected due to efficient cooling by hydrocarbons.

A theoretical model, developed by *Liu and Dalgarno* [1996] to calculate the detailed FUV emission spectra of H_2 due to electron impact in Jupiter's auroral atmosphere, showed that nearly all the GHRS-observed spectral features of the Jovian aurora can be reproduced with the use of accurate molecular parameters (e.g., the recent laboratory results of *Abgrall et al*. [1993a, b, 1997]) and the inclusion of the effects of secondary electrons (see Figure 14). They found that the auroral UV spectrum is not a sensitive indicator of auroral electron energy because of the similar shape of excitation and ionization cross sections of H_2 at high energies ($\geq$1 keV). Liu and Dalgarno derived a temperature for the Jovian auroral emission region of 400–600 K and challenged the suggestion of *Y. Kim et al*. [1995] that there was a significant correlation between auroral brightness and input energy flux.

Kim et al. [1997] presented GHRS observations of the Jovian aurora in which both short (126–129 nm) and long (159–162 nm) wavelength H_2 emission spectra were obtained in sequence during the same HST orbits. Including short-wavelength spectra in the observations allowed the methane column abundance above the aurora to be determined, along with the ambient H_2 rotational temperatures. Using updated H_2 molecular parameters, Kim et al. confirmed their 1995 result suggesting that the brightest auroras are indeed the coolest (and thus deepest) auroras. This trend was supported by the derived CH_4 columns, which were generally larger for the cooler auroras, in keeping with a deeper source region. The range of inferred temperatures was 400–850 K, and the range of methane column densities was $1–7 \times 10^{16}$ cm^{-2}.

Morrissey et al. [1997] made measurements of FUV flux and morphology of the north polar aurora of Jupiter simultaneously with the shuttle-based Hopkins Ultraviolet Telescope (HUT) and WFPC2 on March 9, 1995. The HUT spectra span the wavelength range 90–165 nm. The H_2 FUV auroral emissions were found from the WFPC2 images to extend over $(4.5 \pm 0.5) \times 10^{-10}$ sr, resulting in an average brightness of 106 kR integrated over the 90- to 165-nm wavelength band (excluding Lyman α) as measured by HUT. The ratio of the total mean brightness for Lyman α to the 123- to 165-nm band and for the 123–130 to 155.7–161.9 nm bands indicated the energy of (assumed) primary electrons to be 3–30 keV, with higher values preferred. The average energy deposition rate was estimated to be 13 ergs cm^{-2} s^{-1}, based on an energy conversion efficiency of 0.123 ergs cm^{-2} s^{-1} kR^{-1} for 10-keV electrons [*Waite et al*., 1983]. Morrissey et al. also provided upper limits for the sulfur emissions caused by the precipitation of sulfur ions. The upper limit for S II 125.6-nm brightness (<210 R) was an order of magnitude lower than that placed by IUE [*Waite et al*., 1988a]. This implied that any heavy ion precipitation must be deposited well below the hydrocarbon homopause. Further analysis of the HUT spectra by *Wolven and Feldman* [1998] demonstrated the presence of strong H_2 self-absorption signatures in the 100- to 110-nm region. These features, which are also seen in the Galileo EUV data [*Ajello et al*., 1998], may be used to determine the fraction of vibrationally excited H_2 in the auroral region.

Recently, observations of the Jovian northern aurora at a resolution of about 0.007 nm in the wavelength range 121.4–122 nm obtained by using the Goddard high-resolution spectrograph (GHRS) aboard the HST [*Prangé et al*., 1997b] have revealed, for the first time, a core reversal of the Lyman α line profile (see Figure 15). This reversal is a common feature of solar and stellar Lyman α emission profiles and has been predicted by models as a consequence of radiative transfer effects on the photons produced deep in the auroral atmosphere [e.g., *Gladstone*, 1982; *Prangé et al*., 1997b], but was never previously observed. Preliminary modeling of the wavelength separation between the line peaks of ~0.01 and 0.015 nm indicated a vertical H column density of about 1.5×10^{16} cm^{-2} above the auroral source, which is much smaller than the low-latitude H column (~10^{17} cm^{-2}). This is a surprising result, since it is expected that auroral particle precipitation yields a much larger H production rate than in the nonauroral atmosphere. Another important result from these observations is that the lines are somewhat asymmetric (i.e., the two peaks are of different intensity). Either the blue or the red wing may be favored, with significant variation in the peak intensity ratio (see Figure 15). The center of the reversal coincides with the Lyman α rest wavelength in the planet's frame, and the auroral Lyman α photons are shifted by about 0.001–0.002 nm (which corresponds to a few thermal Doppler widths) to either the blue or red by multiple scattering. Similar to the IUE observations of *Clarke et al*. [1989a], these Lyman α profiles also exhibited weak wings, which appear nearly symmetric and extend over about ±0.15 nm, suggesting emission from an unknown source of very hot H atoms. It seems likely that the auroral Lyman α line profile asymmetries are due to vertical gradients in the horizontal velocity field in the auroral region atmosphere [*Gladstone et al*., 1998b].

Very recently, initial results from the Galileo EUVS and UVS instruments were presented by *Ajello et al*. [1998] and *Pryor et al*. [1998]. The EUVS data, although of low signal-to-noise ratio due to a low duty cycle, demonstrate that the precipitating particles must be exciting H_2 emissions over a very wide range of altitudes (from 10^{16} to 10^{21} cm^{-2} in H_2 column density), but primarily in the 700- to 250-km region (10^{18}–10^{21} cm^{-2} H_2 column density). These results suggest that high spectral resolution observations of the aurora at wavelengths <110 nm (where the H_2 can be self-absorbed), such as will be possible with the Far Ultraviolet Spectrographic Explorer (FUSE) mission, will be very fruitful. The Galileo UVS data also clearly show C_2H_2 absorption of the auroral emissions near 152 nm. At midultraviolet (MUV) wavelengths the nightside aurora, while very weak (about 8 times dimmer than the simultaneously observed FUV aurora), was clearly detected from the continuum emission of the H_2 *a-b* dissociation transition. This is the first detection of the H_2 *a-b* continuum emission from any astronomical object. This continuum peaks in the 200- to 250-nm range, and its strength relative to the FUV emissions is consistent with excitation by 27-eV secondary electrons (somewhat cooler than the 100-eV secondary electrons found to provide good fits to the FUV auroral emissions).

3.2.5. Identity of precipitating particles. Electrons, protons, and heavy ions (oxygen and sulfur ions) or some combination of these have been suggested as possible candidates for the precipitating particles in Jupiter's auroral regions. Electrons are the most commonly cited primaries responsible to power the aurora. The primary mechanism considered for electron precipitation is the scattering of electrons into the loss cone by wave-particle interactions [*Thorne and Tsurutani*, 1979; *Coroniti et al*., 1980], which is supported by the presence of whistler mode waves in the Jovian magnetosphere [*Gurnett and Scarf*, 1983]. *Yung et al*. [1982] found that

Figure 14. (opposite) Comparisons of HST/GHRS spectra of the Jovian aurora over different FUV wavelength ranges with best fit model H_2 Lyman and Werner band emission spectra resulting from 1-keV electron impact on H_2 at varying temperatures [*Liu and Dalgarno*, 1996, Figures 4, 5, and 3]. (a) *Clarke et al*. [1994] data, H_2 temperature of 500 K. (b) *Trafton et al*. [1994] data, H_2 temperature of 690 K. (c) *Y. Kim et al*. [1995] data, H_2 temperature of 430 K. Reprinted with permission from the American Astronomical Society.

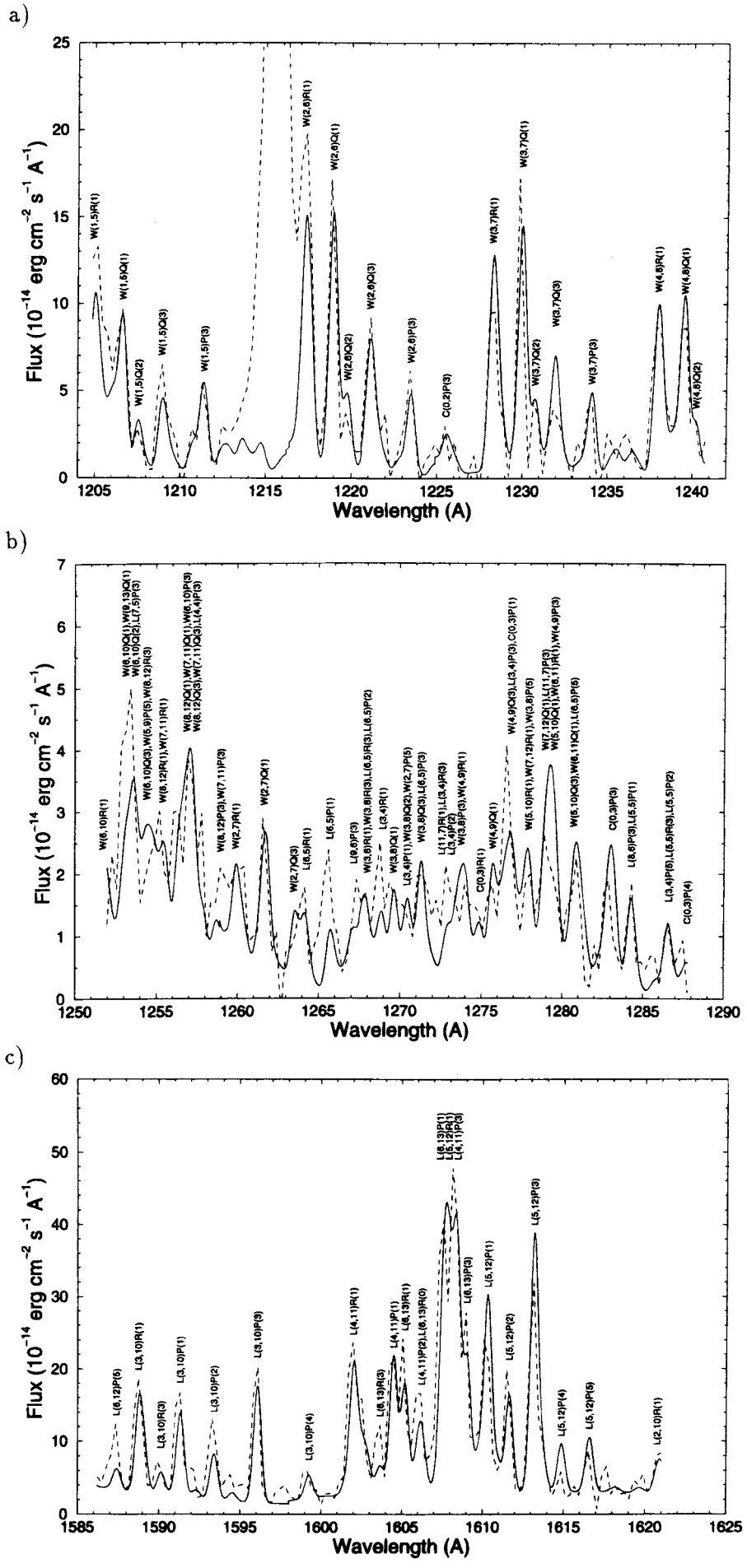
a)
Flux (10^{-14} erg cm^{-2} s^{-1} A^{-1})
Wavelength (A)
W(1.5)R(1)
W(1.5)Q(1)
W(1.5)Q(2)
W(1.5)Q(3)
W(1.5)P(3)
W(2.6)R(1)
W(2.6)Q(1)
W(2.6)Q(2)
W(2.6)Q(3)
W(2.6)P(3)
C(0.2)P(3)
W(3.7)R(1)
W(3.7)Q(1)
W(3.7)Q(2)
W(3.7)Q(3)
W(3.7)P(3)
W(4.6)R(1)
W(4.6)Q(1)
W(4.6)Q(2)
b)
Flux (10^{-14} erg cm^{-2} s^{-1} A^{-1})
Wavelength (A)
W(6.10)R(1)
W(6.10)Q(1),W(9.13)Q(1)
W(6.10)Q(2),L(7.5)P(3)
W(6.10)Q(3),W(6.9)P(5),W(6.12)R(3)
W(6.12)R(1),W(7.11)R(1)
W(6.12)Q(1),W(7.11)Q(1),W(6.10)P(3)
W(6.12)Q(2),W(7.11)Q(3),L(4.4)P(3)
W(6.12)P(3),W(7.11)P(3)
W(2.7)R(1)
W(2.7)Q(1)
W(2.7)Q(3)
L(6.5)R(1)
L(6.5)P(1)
L(9.8)P(3)
W(3.8)R(1),W(3.8)R(3),L(6.5)R(3),L(6.5)P(2)
L(3.4)R(1)
W(3.8)Q(1)
L(3.4)P(1),W(3.8)Q(2),W(2.7)P(5)
W(3.8)Q(3),L(6.5)P(3)
L(11.7)R(1),L(3.4)R(3)
L(3.4)P(2)
W(3.8)P(3),W(4.9)R(1)
C(0.3)R(1)
W(4.9)Q(1)
W(4.9)Q(3),L(3.4)P(3),C(0.3)P(1)
W(5.10)R(1),W(7.12)R(1),W(3.8)P(5)
W(7.12)Q(1),L(11.7)P(3)
W(5.10)Q(1),W(6.11)R(1),W(4.9)P(3)
W(5.10)Q(3),W(6.11)Q(1),L(6.5)P(5)
C(0.3)P(3)
L(6.5)P(3),L(6.5)P(1)
L(3.4)P(5),L(6.5)R(3),L(6.5)P(2)
C(0.3)P(4)
c)
Flux (10^{-14} erg cm^{-2} s^{-1} A^{-1})
Wavelength (A)
L(6.12)P(6)
L(3.10)R(1)
L(3.10)R(3)
L(3.10)P(1)
L(3.10)P(2)
L(3.10)P(3)
L(3.10)P(4)
L(4.11)R(1)
L(6.13)R(3)
L(4.11)P(1)
L(6.13)R(1)
L(4.11)P(2),L(6.13)R(0)
L(6.13)P(1)
L(5.12)P(1)
L(4.11)P(3)
L(6.13)P(3)
L(5.12)P(1)
L(5.12)P(2)
L(5.12)P(3)
L(5.12)P(4)
L(5.12)P(5)
L(2.10)R(1)

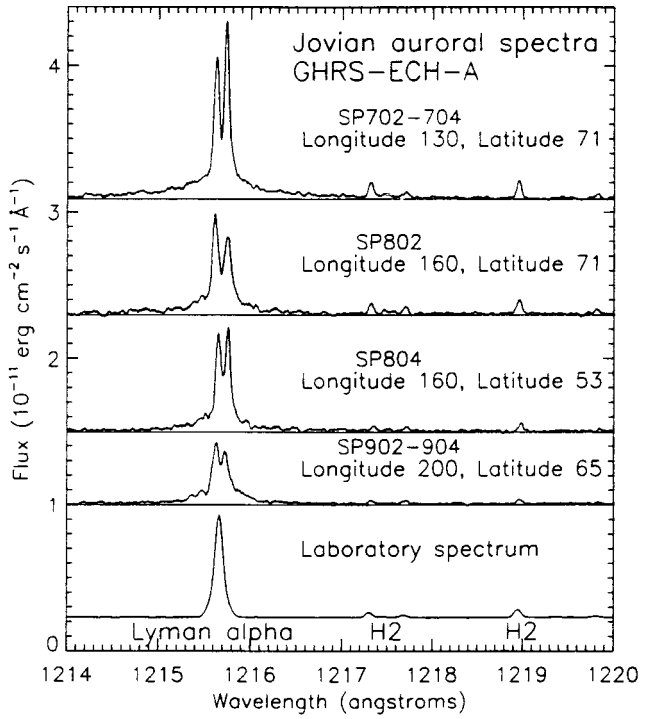

Figure 15. Four HST/GHRS echelle spectra of Jovian auroral Lyman α emissions showing self-reversed and asymmetric line profiles. A laboratory spectrum obtained by 100-eV electron impact on H_2 at a spectral resolution of 7.2 pm is shown for comparison [*Prangé et al*., 1997b, Figure 3]. Reprinted with permission from the American Astronomical Society.

synthetic spectra of H_2 from electron impact closely mimic the spectra observed by IUE [*Durrance et al*., 1982], strengthening the electron's candidacy (although protons and heavy ions would be expected to produce large amounts of secondary electrons while slowing down in H_2).

Owing to a disparity between the estimated power required by the FUV aurora and the power deliverable by electrons, *Goertz* [1980] suggested protons as the possible source of Jovian aurora. However, proton precipitation alone is partially ruled out because it will not generate X rays [*Goertz*, 1980; *Metzger et al*., 1983]. Further, protons should produce Doppler-broadened and red-shifted Lyman α emissions, but no such emissions were observed that would correspond to proton energies >200 eV, effectively ruling out energetic proton precipitation at Jupiter [*Clarke et al*., 1989a; *Prangé et al*., 1997b]. Moreover, hydrogen constitutes only a minor component within the Io plasma torus and inner magnetosphere of Jupiter [*Shemansky*, 1980; *Bagenal and Sullivan*, 1981; *Frank and Paterson*, 1999].

Thorne [1981, 1982, 1983] proposed that heavy ions, which dominate the ion component in the Io torus [*Bagenal and Sullivan*, 1981], are the more likely candidates. Support for the heavy ion precipitation scenario came from the Voyager observations of 1–20 MeV nucleon^{-1} oxygen, sulfur, and sodium ions in the magnetosphere of Jupiter [*Gehrels and Stone*, 1983]. Gehrels and Stone found sharp decreases in the flux of inward diffusing energetic O and S ions at ~6–12 R_J, which they concluded indicated the ions were being scattered into the loss cone and thereby precipitating into Jupiter's atmosphere. These ions are thought to have originally escaped from the Io plasma torus by recombining with electrons to form a "neutral wind" but were photoionized before they could entirely escape the Jovian magnetosphere and gained energy as they diffused in again toward Jupiter [*Eviatar and Barbosa*, 1984]. Additional evidence in favor of a heavy ion aurora was provided by the soft X-ray emissions (0.2–3.0 keV) observed by the Einstein observatory [*Metzger et al*., 1983], which would require unreasonably large (10^{15}–10^{16} W) power input for production via the electron bremsstrahlung process compared with the 10^{13}- to 10^{14}-W input required for emissions expected from excited, highly stripped precipitating oxygen and sulfur ions. Observations of X-ray emissions from ROSAT and subsequent modeling studies support the heavy ion precipitation scenario [*Waite et al*., 1994; *Hurley et al*., 1993; *Cravens et al*., 1995]. Heavy ion precipitation can be driven by pitch angle scattering of ions by plasma waves [*Thorne and Moses*, 1983]. The plasma waves likely to be responsible for such scattering of heavy ions into the loss cone have recently been observed by Ulysses, demonstrating sufficient intensity and having a maximum in the high-latitude part of the torus [*Rezeau et al*., 1997]. However, FUV emissions expected from the recombination of O and S ions during precipitation have not been positively identified in the UV spectra of the aurora [*Waite et al*., 1988a; *Horanyi et al*., 1988; *Morrissey et al*., 1997]. Also, a "pure" ion aurora is unlikely because of very reduced intensities of H_2 band emissions generated [*Horanyi et al*., 1988]. Using HST/GHRS spectra of a bright H_2 aurora near the wavelengths of expected FUV emission features of oxygen and sulfur atoms, *Trafton et al*. [1998] have recently obtained strong upper limits on the contribution of heavy ion precipitation to the main auroral emissions resulting from electron precipitation. They find that for this particular aurora, O ions contributed <13% of the precipitating energy flux and S ions contributed <50%. In addition, no significant evidence was found for the expected accumulation of singly charged S ions in the Jovian auroral ionosphere. While these results are not quite inconsistent with the ROSAT X-ray data, they strongly indicate that the bulk of the FUV aurora is produced by energetic electron impact rather than by heavy ions.

An idea proposed by *Horanyi et al*. [1988] is that electrons as well as heavy ions are precipitating into the upper atmosphere of Jupiter: A consistent picture is obtained when the precipitating heavy ions are mainly responsible for producing X-ray emissions, while most of the UV emissions are produced by electron precipitation. *Mauk et al*. [1996] have extracted some hot plasma parameters for the inner regions of Jupiter's magneto-

sphere from the data sampled by the overdriven LECP experiment on Voyager 1. They concluded that there is a radial ordering to the different auroral sources at Jupiter, with regions of $L < 12$ responsible principally for ion auroras (including X-ray emissions) and regions of $L > 12$ responsible principally for electron auroras. This ordering translates into a latitudinal separation in the auroral emission morphology, with the electron-generated H_2 emissions generally at higher latitudes and the ion-generated X-ray emissions at lower latitudes. Although X-ray observations made until now lack the spatial resolution to distinguish the different regions, the Chandra X-ray facility, with 0.5″ resolution, should provide data to test this idea.

3.2.6. Auroral haze. The Voyager 2 photopolarimeter subsystem (PPS) obtained photometric data on Jupiter at 240 nm and found dark hazes in the polar regions [*Hord et al*., 1979]. An analysis of the PPS data by *Pryor and Hord* [1991] found a good correlation in latitude between regions of strong auroral H_2 band emissions and the UV-dark polar regions in both the north and south. It has been suggested by Pryor and Hord that the dark haze is formed as a result of auroral ionization, which leads to the breakdown of methane followed by polymerizing hydrocarbon chemistry, resulting in the formation of UV-dark haze or soot. The model of *Singhal et al*. [1992] suggested that higher-order hydrocarbons are formed by homopause-penetrating high-energy (~50–100 keV) input electrons, which could promote the formation of more complex hydrocarbons or polymers. The *Singhal et al*. [1992] study thus supported the analysis of *Pryor and Hord* [1991] that auroral ionization plays an important role in creating the UV-dark polar haze on Jupiter. *S. Kim et al*. [1995] found that the reflected 4-μm continuum, like the reflected UV continuum, was also much darker in the polar regions than at equatorial latitudes and suggested condensed benzene (C_6H_6) and diacetylene (C_4H_2) as possible haze components. *Gladstone et al*. [1996] suggested that polyyne (polyynes are H–C≡C– . . . –C≡C–H polymers) formation initiated by ion-neutral reactions in the auroral regions is a likely source for the polar haze observed on Jupiter.

3.3. Visible Emissions

Auroras on Jupiter were also tentatively identified in the visible region by the imaging experiment on Voyager [*Smith et al*., 1979]. *Cook et al*. [1981] concluded that at least one of the limb emissions seen on the nightside by the imaging experiment was most probably auroral emission caused by particle precipitation from the Io torus. The total emission rate in the wavelength range 400–600 nm was estimated to be ~5 kR (an estimated factor of 4 limb enhancement combined with an observed slant intensity of about 20 kR). The double structure observed in the image was attributed by the authors to several causes, such as horizontal structure in the auroral emission or the effects of airglow and twilight processes.

Recently, *Ingersoll et al*. [1998] have presented an analysis of Galileo solid state imaging (SSI) camera observations of Jupiter's nightside aurora. The very high spatial resolution of the SSI (~40 km pixel^{-1}) revealed much new information about the aurora, including (1) a direct measurement of the altitude of the aurora (~240 km above the 1-bar pressure level), (2) apparent widths of <200 km in some cases, and (3) an estimated visible emitted power of 10–100 GW. Most of the visible emissions are thought to be due to the Balmer series of atomic hydrogen. Ingersoll et al. also report the first detection of the IFT footprint at visible wavelengths. They determined a size of about 300 × 500 km for the IFT footprint, with a total radiated power in the visible of ~0.3 GW.

3.4. Infrared Emissions

3.4.1. Thermal emissions. At wavelengths in the range 3–6 μm, Jupiter's spectrum changes from reflected sunlight to thermal emission [*Ridgway et al*., 1976]. A strong absorption band of methane occurring near 7.7 μm (the ν_4 fundamental) was used extensively in the pre-Voyager era to investigate the thermal structure of the Jovian stratosphere as a function of latitude, since the weighting functions for this band peak at pressures of ~10 mbar [e.g., *Orton*, 1975]. Most work concentrated on lower latitudes, where limb-darkening curves allowed the extraction of vertical information. However, observing from the NASA 3-m infrared telescope facility (IRTF) at Mauna Kea, Hawaii, in 1980, *Caldwell et al*. [1980] noticed strong and variable polar limb brightening in meridional scans at 7.7 μm which correlated with CML and suggested that auroral processes were the most likely explanation. In the north polar region the methane emissions were brightest at CML ~170° and were from a distinctly higher latitude than the Io plasma torus footprint, which at the time was the expected location of the UV aurora. Also, no indication of a dependence on Io's orbital position or system III longitude was apparent. In the south the methane emissions were brightest at CML ~50°–60°. The emitted flux in the brightened region was estimated to be ~9 ergs cm^{-2} s^{-1}. The authors noted that even very energetic auroral particle precipitation would be unlikely to reach as deep as the stratospheric regions where the main CH_4 band arises and that the auroral emissions are probably excited higher in the atmosphere. Further IRTF observations in 1981 of the 7.7-μm polar brightenings were reported by *Caldwell et al*. [1983a]. In addition to confirming the earlier results, evidence for rapid time variability was found with two consecutive meridional scans that showed a large change in the north polar emission over a time interval of only 17 min.

Inspired by these results, *Kim et al*. [1985] investigated the 1979 Voyager 1 infrared interferometer spectrometer (IRIS) data for evidence of IR polar brightenings. By binning dozens of individual IRIS 7.1- to 16.7-μm spectra into four latitude/longitude groups, Kim et al. dis-

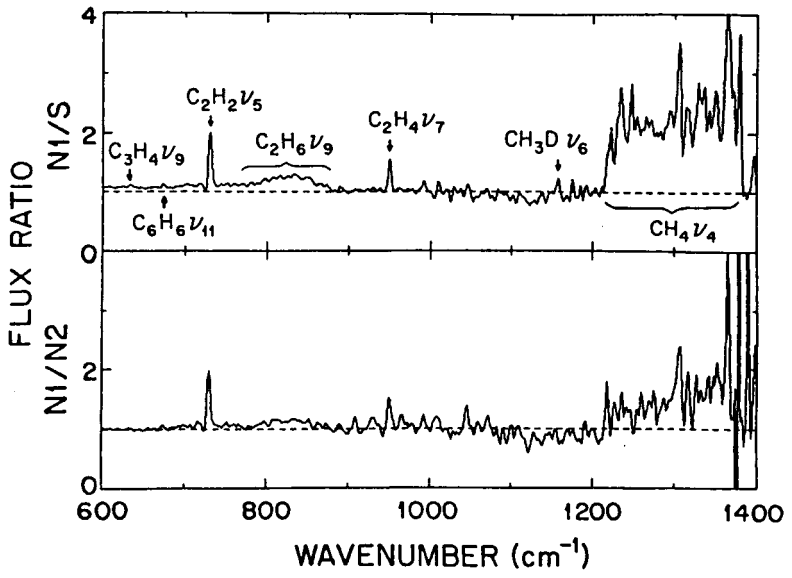

Figure 16. Flux ratios of Voyager infrared interferometer spectrometer (IRIS) (top) "hot spot" to southern (N1/S) auroral spectra and (bottom) hot spot to non-hot-spot (N1/N2) spectra, showing enhanced auroral emissions from several higher hydrocarbons [*Kim et al.*, 1985, Figure 3]. Reprinted with permission from Academic Press.

covered that a composite spectrum of the northern auroral region (latitude $>$ 48°, 120° $<$ system III longitude $<$ 240°) contained enhanced 7.7-μm Q-branch emission from CH_4, in agreement with the expectations based on the discoveries of *Caldwell et al.* [1980, 1983a]. Remarkably, enhancements were also observed in the 13.6-μm Q-branch emissions of C_2H_2 (the acetylene ν_5 fundamental) and the broader 12.2-μm emissions of C_2H_6 (the ethane ν_9 fundamental). Even more remarkably, the auroral IRIS spectra also contained emissions from C_2H_4 (the ethylene ν_7 fundamental at 10.5 μm), CH_3C_2H (the methylacetylene ν_9 fundamental at 15.8 μm), and possibly C_6H_6 (the benzene ν_{11} fundamental at 14.8 μm) (see Figure 16). Upper limits were determined for emissions of C_3H_8 (the propane ν_{26} fundamental at 13.4 μm) and C_4H_2 (the diacetylene ν_8 fundamental at 15.9 μm). Finally, a very tentative identification of CH_3 emission was made (the methyl ν_2 fundamental at 16.5 μm). Kim et al. considered whether the IR emissions might result directly (e.g., impact excitation by precipitating particles) or indirectly (e.g., through aurora-related heating of the local ambient atmosphere) from the aurora. They determined that the observed emissions could be most easily and consistently explained if the auroral region stratosphere ($P \sim 0.1$–3 mbar) were about 15 K warmer than in the corresponding nonauroral regions and the enhanced IR emissions were thermal in nature. The stratospheric temperature profile was adjusted to provide a good spectral fit to the 7.7-μm methane band, and using this somewhat warmer profile, abundance estimates were made for the species detected in the enhanced auroral spectrum. C_2H_2 and C_2H_6 were determined to be about 3 times more abundant than in nonauroral regions, with mixing ratios of 90 ± 20 ppb and 5 ± 1 ppm, respectively. The previously unknown mixing ratios of C_2H_4, CH_3C_2H, and C_6H_6 were estimated at 7 ± 3, 2.5^{+2}_{-1}, and 2^{+2}_{-1} ppb, respectively. Useful upper limits of $<$0.6 ppm and $<$0.3 ppb were set for C_3H_8 and C_4H_2. The observed high ratio of benzene to diacetylene ($>$7) was suggested by Kim et al. as a potential diagnostic of the specific polymerization pathway for polar aerosol (i.e., soot) formation in the Jovian auroral region.

Enhanced acetylene emissions near 13.3 μm from the northern auroral region were also studied by *Drossart et al.* [1986]. In 1984 at the NASA IRTF they performed high spectral (resolving power $\lambda/\Delta\lambda \sim 25{,}000$) and spatial (3″ FWHM) (FWHM is short for "full width at half maximum," which provides a robust measure of the width of a peaked function) resolution observations of the $R(10)$ line in the ν_5 fundamental of C_2H_2 and determined the location of a well-defined bright spot at a latitude of 59° ± 10°N and a system III longitude of 178° ± 10°. This bright spot position was at a somewhat higher latitude than the location of the UV aurora (as known at the time), but considerably closer to the UV emissions than were the *Caldwell et al.* [1980, 1983a] observations. Modeling the observed line emission using temperature profiles derived from Voyager IRIS data, Drossart et al. determined that the bright spot could be explained by an increased abundance of acetylene (to ~100 ppb). Alternatively, they also noted that a stratospheric temperature increase of only 10 K could explain the emission level as well. Both of these conclusions were in excellent agreement with the results of *Kim et al.* [1985].

Continuing toward higher spectral and spatial resolution, *Kostiuk et al.* [1987] presented results of an extensive survey of two individual C_2H_6 emission lines (the ${}^RR_6(14)$ and ${}^RR_8(11)$ lines of the ν_9 fundamental) over the disk of Jupiter. These emissions were observed from Kitt Peak in 1982 and 1983 using an IR heterodyne spectrometer with a spectral resolving power of 10^6 and a spatial resolution of 2″ FWHM. As with the previous investigators, Kostiuk et al. used Voyager IRIS temperature profiles appropriate for the observed location on Jupiter in simulating their observed line profiles, with the derived result being C_2H_6 abundances (assumed to be constant at $P < 100$ mbar and zero at higher pressures) of 3–5 ppm. (Previous heterodyne observation on the south polar region [*Kostiuk et al.*, 1983] had yielded a lower C_2H_6 mole fraction using older molecular parameters.) Also in agreement with the previous work was the fact that the data could be equally well explained by a slightly warmer temperature profile rather than an increase in hydrocarbon abundance. To explore the auroral IR variability in more detail, several experiments were also performed in which the instrument field of view was left on the CML at 60°N while Jupiter rotated for about one half hour (~18° of longitude). Remarkably, in contrast to the results of *Caldwell et al.* [1980, 1983a] for methane and *Drossart et al.* [1986] for acetylene, Kostiuk et al. found that the ethane emissions in 1983 were observed at all system III longitudes except at 180°. The brightest emission was seen at a CML longitude of 234°. With higher spatial resolution and better viewing conditions, *Kostiuk et al.* [1989] also did not observe any apparent longitudinal dependence in the 1986 C_2H_6 12-μm emission data. The lack of C_2H_6 emission in a region where both CH_4 and C_2H_2 excess emission is observed led these authors to conclude that ethane must be strongly depleted in the bright spot region, since any reasonable temperature profile resulted in a model amount of stratospheric emission that would have been measurable. This also suggested that temperature increases alone might not be responsible for the observed enhancements in the CH_4 and C_2H_2 emissions. They suggested that chemical pathways in the auroral stratosphere might lead to the formation of extra C_2H_2 at the expense of C_2H_6, though no specific mechanisms were put forward.

In an effort to learn the morphology of the IR auroral "hot spots" (as they came to be known), *Caldwell et al.* [1988] performed raster scans of Jupiter in the 7.7-μm methane emission during 1984–1986. The instantaneous field of view of the instrument was 2″ FWHM, and 55 × 55 pixel images were obtained over a 42-min period. The location of the northern auroral hot spot was found to be extremely stable, appearing consistently brightest at a latitude of 59°N and a system III longitude of 179°, though at many different local times. A single nondetection out of 19 observations occurred on September 5, 1985, for unknown reasons. The northern hot spot dimensions were about ~40° (25,000 km) in longitude and ~8° (9100 km) in latitude. The extended range in longitude suggested that the hot spot was being smeared out by zonal winds. In marked contrast to the stable northern hot spot, the location of the brightest 7.7-μm emission in the southern aurora constantly changed its location. In one pair of images taken 90 min apart the southern hot spot changed location by 27° in longitude. During three different observation epochs the southern hot spot was found to drift at various rates relative to system III, sometimes moving at the drift rate of the subsolar point and other times drifting more slowly, at about half the apparent solar rate. The southern polar hot spot was found at all possible locations of Io around Jupiter, and its position was not directly correlated with Io's position.

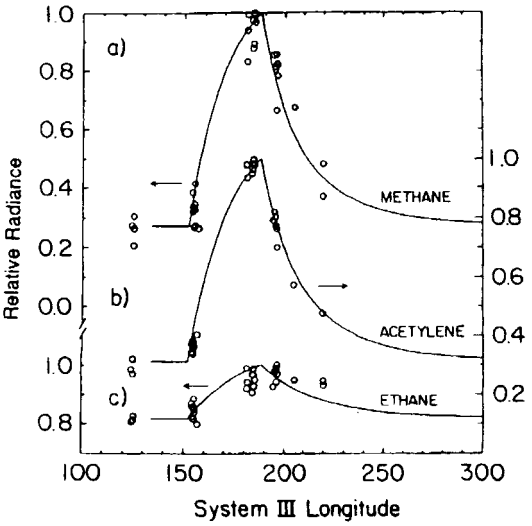

Figure 17. Voyager IRIS measurements (circles) of auroral emissions of CH_4 (top curve), C_2H_2 (middle curve), and C_2H_6 (bottom curve), compared with best fit models based on a two-parameter fit using a combination of zonal wind speed, radiative time constant, and auroral/nonauroral emission strength [*Halthore et al.*, 1988, Figure 3]. Reprinted with permission from Academic Press.

Halthore et al. [1988] used the Voyager 1 IRIS data to study longitudinal asymmetry in the emissions of the three major hydrocarbons, CH_4 (7.8 μm), C_2H_2 (13.6 μm), and C_2H_6 (12.6 μm), near 60° north latitude. Considerably increased emission was observed for CH_4 and C_2H_2 around the hot spot ($\lambda_{III} \sim 180°$), but no significant increase was observed in ethane emission (see Figure 17). They interpreted the longitudinal asymmetry of the emissions as a result of the relative motion between the stratosphere and the location of energy deposition due to precipitating auroral particles. Using a thermal equilibrium model, Halthore et al. estimated an auroral stratospheric zonal wind velocity of 0.6 km h^{-1}. An increase in the temperature of the auroral hot spot region by 50 K was required to explain the intensity of CH_4 emission. However, this temperature enhancement could not satisfy the measured C_2H_2 and C_2H_6 emis-

sions; they required an increase in C_2H_2 abundance by a factor 3.4 and a decrease in C_2H_6 abundance by about 80%.

Kim [1988] developed a theoretical model of vibrational excitation and deexcitation processes of CH_4 and H_2 resulting from the precipitation of monoenergetic electrons of 30 and 100 keV, with input energy fluxes of 10 and 100 ergs cm^{-2} s^{-1}. The calculated intensity of nonthermal CH_4 ν_4 emission was found to be 10^{-3}–10^{-6} times smaller than the Voyager IRIS-observed intensity of ~10 ergs cm^{-2} s^{-1} sr^{-1}, indicating that thermal emission of CH_4 dominates over nonthermal emissions produced by the precipitating particles.

Changes in the average thermal structure of the 10- to 20-mbar pressure level for over a decade were derived by *Orton et al*. [1991] by observing the thermal emission of CH_4 at 7.8 μm with the NASA IRTF during 1980–1990. Since methane is a long-lived species, its abundance is not expected to vary widely with location. Thus the observed changes in the CH_4 emission can be attributed to variations in the temperatures of the emitting regions. The stratospheric temperature was found to have substantial spatial and temporal variability. High-latitude (~60°) temperatures are generally higher, but surprisingly, a peak in the equatorial region is also observed with a periodicity of ~4–5 years (peaks appear in 1980, 1984, and 1989).

The location of the IR methane hot spot in latitude and longitude was found to coincide with the location of the "UVS auroral oval" (as known at that time), suggesting that the processes responsible for the excitation of both of the emissions could be the same, at least in the peak region of the northern aurora [*Prangé*, 1991]. Prangé argued that longitudinal emission profiles in the IR and UV are consistent with those of precipitating electrons in the diffuse aurora. However, more recent findings from the HST are contrary to this conclusion: It is now observed that the UV emission is a minimum at the place where the IR emission is a maximum [*Caldwell et al*., 1992].

Livengood et al. [1993] performed observations of C_2H_6 emissions at 11.9 μm from the northern Jovian auroral region, using the IR heterodyne spectrometer ($\lambda/\Delta\lambda \sim 10^6$) at the IRTF, in order to differentiate the effects of temperature and abundance variations by using line profiles and to identify the pressure level of the source region. In remarkable contrast to the earlier reported observations of C_2H_6 emission [e.g., *Kostiuk et al*., 1987, 1989; *Halthore et al*., 1988], Livengood et al. observed longitudinal asymmetry in the C_2H_6 emission, with maxima in the longitude range 150°–180° near 60° latitude, the traditional IR hot spot location. These observations showed that C_2H_6 emissions in the hot spot can vary by a factor of 5 in 20 hours. They derived a C_2H_6 mole fraction of ~6.5 ppm at the auroral hot spot location, with a temperature of ~183 K, compared with an abundance of 3.8 ± 1.4 ppm outside the hot spot region, where the temperature was ~172 K, at about 1 mbar. The retrieved temperature within the hot spot could be 10–30 K higher than outside the hot spot depending on the C_2H_6 abundance.

The first reliable measurement of C_2H_4 10.5-μm emission from the auroral regions of Jupiter was made by *Kostiuk et al*. [1993] using IR heterodyne spectroscopy. This emission was earlier detected in the equatorial region using the same instrument [*Kostiuk et al*., 1989]. These measurements provided the first direct probe of the ~10-μbar region of Jupiter's auroral atmosphere. Ethylene is a photochemically active species, so its abundance is sensitive to local changes in chemistry. Significantly enhanced C_2H_4 emissions were observed at ~180° longitude and ~60°N latitude (consistent with the location of the CH_4 hot spot) and were confined to <10° in longitude. *Kostiuk et al*. [1993] found that the C_2H_4 abundance had to be increased by a factor of 18 over the Voyager-derived values to explain the observed enhancement at the auroral hot spot. Alternatively, a temperature increase of 67–137 K would be required if the C_2H_4 mole fraction were fixed to the quiescent value. The advantage in studying the C_2H_4 emissions is that the emission region extends from a few millibar to the ~1-μbar pressure level (i.e., the upper stratospheric region, just below the methane homopause), overlapping the formation region of H_2 UV emissions. Thus it can be an effective probe of the energy deposition and coupling of the thermal IR and UV auroral phenomena. Together, the C_2H_6 and C_2H_4 IR emissions, the H_2 UV emissions, and the H_3^+ near-IR emissions can be used to diagnose the Jovian atmosphere from ≤1 mbar to approximately nanobar pressure levels (see Figure 18).

Reanalyzing the Voyager IRIS data, *Drossart et al*. [1993a] found that a good match between modeled and observed auroral hydrocarbon spectra can be obtained by properly adjusting the temperature profile in the upper stratosphere, requiring relatively minor modifications in hydrocarbon abundances compared with previous models. In particular, they showed that large increases in the temperature of the upper stratospheric and lower thermospheric region (~10–50 μbar) can provide the excess hydrocarbon emission bands observed by Voyager and that no modification to the thermal profile deeper in the atmosphere (up to ~1 mbar) is required. The total IR energy flux emitted from the hot spot region, in the 7- to 13-μm band, was found to be 208 ± 15 ergs cm^{-2} s^{-1}, which corresponds to an emitted power of $\sim 4 \times 10^{13}$ W over the IRIS field of view ($\sim 2 \times 10^{18}$ cm^2). This energy is much larger than that thought to be available from auroral particle precipitation alone, implying the need for an additional heat source. Drossart et al. suggested that Joule heating may be one such possible source; however, detailed calculations have to be made to quantify the suggestion.

3.4.2. H_2 emissions. To begin the investigation of Jupiter's near-infrared spectrum, *Kim and Maguire* [1986] modeled the vibrational-rotational excitation of H_2 using an electron precipitation code. They calculated

the line intensities of 2-μm quadrupole emissions from H_2 and suggested that they were strong enough to be observed with ground-based telescopes. Following the success of the thermal IR auroral observations of Jupiter, *Trafton et al*. [1988] followed the suggestion of *Kim and Maguire* [1986] and searched for H_2 quadrupole emission at 2.1 μm. They were only able to establish a marginal detection of the $S_1(1)$ line of H_2 near the north pole around 180° longitude. Further observations at twice the spectral resolution were obtained by *Trafton et al*. [1989b], which confirmed their earlier results, and also showed the presence of H_2 $S_1(1)$ emission at the southern pole, with intensities only ~3–12% of Kim and Maguire's predicted value.

Observing at higher spectral resolution, *Kim et al*. [1990] detected the $S_1(0)$, $S_1(1)$, and $S_1(2)$ emission lines of H_2, the three quadrupole lines of the 1-0 vibrational-rotational band, from Jupiter's southern auroral zone using the Canada-France-Hawaii Telescope (CFHT) Fourier transform spectrometer (FTS). Kim et al. derived a rotational temperature of 730^{+490}_{-200} K in the pressure range 1–0.01 μbar, using the observed 2-μm quadrupole line brightnesses, which were found to be mostly nonthermal in nature. Thus the detection of the 2-μm quadrupole lines provided a new method of deriving the temperature of the high stratosphere (≤1 mbar) of the Jovian auroral zones. *Kim et al*. [1990] also used the 2-μm line emissions of H_2 to study the distribution of polar haze on Jupiter. Using a model spectrum, they found the haze to be widely distributed in both the polar regions, with no particular association with auroral activity, and located mainly in the pressure range of 5–70 mbar for optically thin haze models.

3.4.3. H_3^+ emissions. While observing the 2.1-μm H_2 quadrupole emissions at very high spectral resolution on September 24, 1988, *Drossart et al*. [1989] made the serendipitous discovery of H_3^+ $2\nu_2$ band emission from Jupiter's aurora. The same emissions had also been observed at lower resolution, although they had not been identified, somewhat earlier by *Trafton et al*. [1989a]. By fitting the intensities of the ~25 individual lines detected within the 2.08- to 2.17-μm band pass of the Fourier transform spectrometer (FTS) at the CFHT from the Jovian southern auroral region, *Drossart et al*. [1989] determined a rotational temperature of 1100 ± 100 K for the H_3^+ emissions. It was not possible to determine whether the emission process was thermal or nonthermal (possibly due to either nascent (i.e., prompt) emissions during the formation of H_3^+ or preferential excitation of the $2\nu_2$ level through a resonant exchange with $H_2(v = 1)$).

H_3^+ emissions had been searched for in astronomical sources for nearly 10 years prior to their discovery on Jupiter, and interesting recountings of the Jovian identification and early observations are given by *Oka* [1992] and *Miller et al*. [1994]. The H_3^+ ion as an important component of the Jovian ionosphere has long been predicted by models [e.g., *Atreya and Donahue*, 1976; *Strobel and Atreya*, 1983; *McConnell and Majeed*, 1987], and its presence in the Jovian magnetosphere was inferred by Voyager observations [*Hamilton et al*., 1980]. More recent observations (by the heliosphere instrument for spectra, composition, and anisotropy and low energies (HI-SCALE) and energetic particles composition (EPAC) instruments) from the Ulysses spacecraft have confirmed the presence of H_3^+ ions in the magnetosphere of Jupiter, especially at high magnetic latitudes, where they are being accelerated out of the topside ionosphere [*Lanzerotti et al*., 1993; *Seidel et al*., 1997].

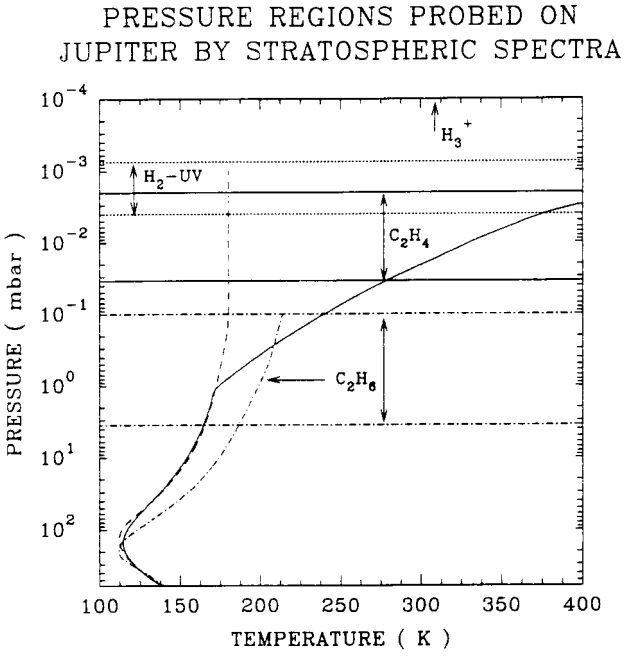

Figure 18. The pressure regions of origin for several important Jovian IR and UV auroral emissions [*Kostiuk et al*., 1993, Figure 11]. The dashed, dash-dotted, and solid lines show the derived temperature profiles for nonauroral emissions, C_2H_6 auroral emissions, and C_2H_4 emissions, respectively.

After the $2\nu_2$ overtone band was discovered, it was natural to look for the fundamental ν_2 band emission at ~4 μm, and it was very quickly discovered by *Oka and Geballe* [1990] and *Miller et al*. [1990]. The 4-μm emissions were observed to be much brighter than the 2.1-μm emissions, and *Miller et al*. [1990] further determined that the vibrational and rotational temperatures were equal, making it seem that the H_3^+ emissions were primarily thermal in origin. It was also clear from these initial studies that the H_3^+ emissions were highly time variable in brightness and derived temperature (*Oka and Geballe* [1990] derived a rotational temperature of 670 K, while the *Miller et al*. [1990] result was identical to the *Drossart et al*. [1989] value of 1100 K). *Maillard et al*. [1990] presented FTS observations of both the north and south auroral regions and found the southern 4-μm aurora to be about twice as bright as in the north, with rotational temperatures of 1000 ± 40 and 830 ± 50 K, respectively. Their high-resolution spectrum showed

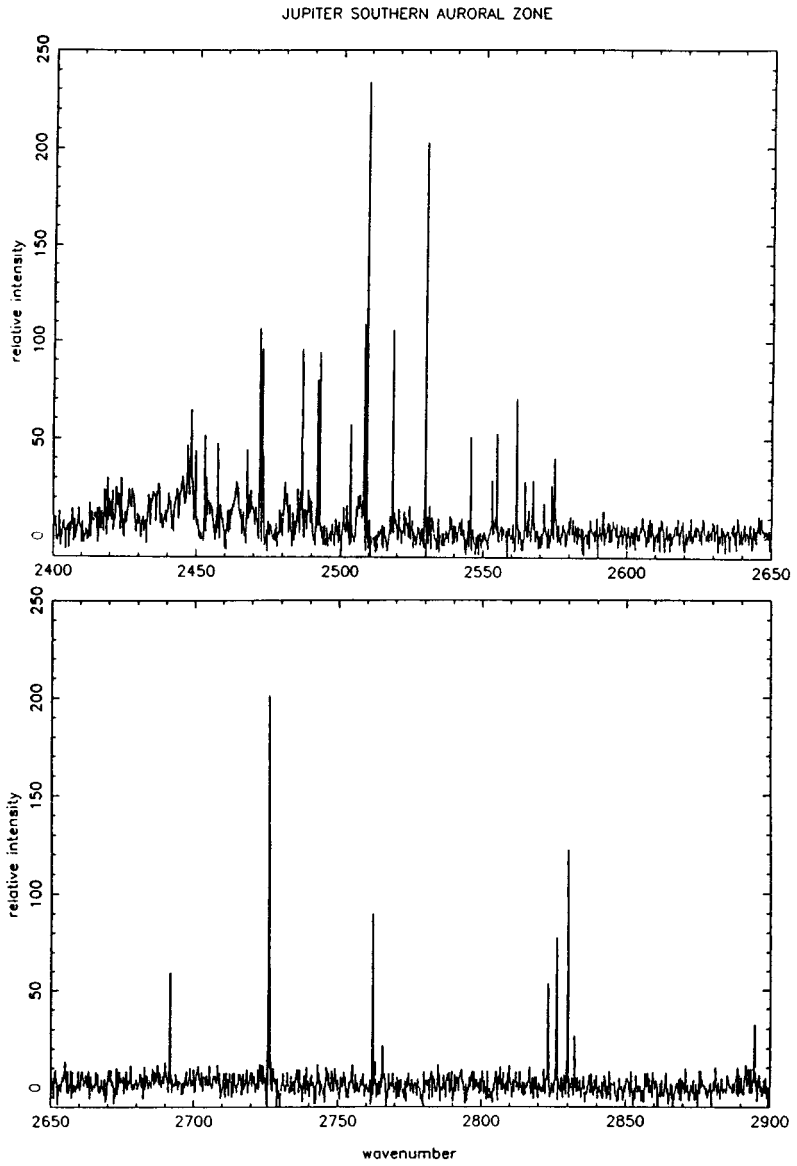

Figure 19. High-resolution Fourier transform spectrometer (FTS) spectrum of Jovian auroral H_3^+ emissions obtained in November 1989 from the Canada-France-Hawaii Telescope (CFHT) [*Maillard et al*., 1990, Figure 1]. A 5-inch-diameter aperture was used, centered on 60°S and 40° CML. Reprinted with permission from the American Astronomical Society.

that the 3.45- to 4.17-μm region was totally dominated by H_3^+ emission, with almost no background, which is due to the fortuitous placement of a CH_4 absorption band in the colder stratosphere underneath the ionosphere (see Figure 19). This study also, like that of *Miller et al*. [1990], suggested that the H_3^+ emissions are thermally produced.

Not long after the spectrometer results were obtained, the infrared camera ProtoCAM was used at IRTF in early 1991 to produce the first images of the H_3^+ 4-μm emissions [*Kim et al*., 1991; *Baron et al*., 1991]. Both studies found strong spatial and temporal variability, as expected for auroral emissions, but found no northern bright spot at the expected location (near 180°) expected from the previous ~10 years of 7.8-μm observations. This suggested that the precipitating particles responsible for the hot spot were depositing most of their energy below the homopause around the 180° longitude. These observations also showed that there are other background emissions at these wavelengths, particularly the CH_4 emissions, whose contributions may be substantial. However, the effect of CH_4 emission was later estimated to be less than 10% [*Kim et al*., 1993]. The reason is that at the temperatures normally prevailing in the Jovian stratosphere, the predicted intensity of the ν_3 band of CH_4 is 1–3 orders of magnitude smaller than could be detected by the IR spectrometers [*Halthore et al*., 1994].

A different followup study of the data reported by *Kim et al*. [1991] was performed by *Drossart et al*. [1992].

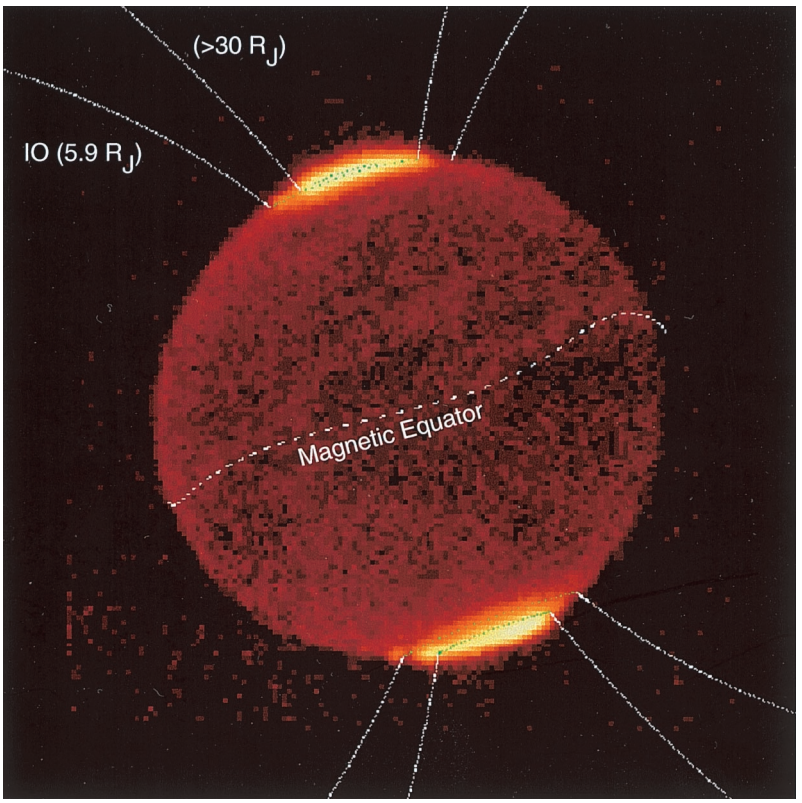

Plate 6. Mosaic of nine ProtoCAM images of H_3^+ emissions from Jupiter at 304° CML, obtained on January 12, 1992. A meridian plane projection of O6 $L = 5.9$ and $L > 30$ magnetic field lines is superimposed on the mosaic, and the leftmost field line is traced from the instantaneous position of Io at a phase of 79°. The main auroral oval emissions are seen to arise near the last open field line, while the faint spots of emission near the dawn limb in each hemisphere at slightly lower latitude are due to the interaction of the IFT with Jupiter's atmosphere [*Connerney et al*., 1993, Figure 1]. Reprinted with permission from *Science*.

After careful subtraction of the background continuum, it was found that the H_3^+ emission in both hemispheres peaked in two spots, separated by about 60° and centered on the CML, with the duskside spots being about twice as bright as the dawnside spots. In the north the spots were found to be relatively fixed in longitude, at about $\lambda_{III} \sim 210°$ (morning) and $\lambda_{III} \sim 150°$ (afternoon). In the south the spots were much more variable in longitude but remained nearly fixed in local time, as if their brightness was modulated by the interaction of both a fixed variation with longitude and a fixed variation with local time.

A theoretical investigation of the H_3^+ emissions by *Kim et al*. [1992], which explicitly considered how the vibrational levels of H_2 and H_3^+ are populated in an aurora, found that radiative decay (leading to the observed emissions) dominates over collisional deexcitation as the major loss rate of vibrationally excited H_3^+, so that the emissions are not in local thermodynamic equilibrium (LTE). However, collisional excitation is a more important source for producing vibrationally excited H_3^+ than is the nascent vibrational excitation following H_3^+ formation, so that the steady state vibrational distribution at the altitude of peak H_3^+ density is close to a Boltzmann (i.e., thermal) distribution. The model calculations of Kim et al. showed that the resulting vibrational distribution and altitude profile of H_3^+ emission produced by precipitating 10-keV electrons having an input flux of 1 ergs cm^{-2} s^{-1} are consistent with the IR observations in the 2- to 4-μm region. This slightly non-LTE result explains why the earlier observations of *Drossart et al*. [1989] and *Miller et al*. [1990] were found to be well fit assuming LTE.

Observations made with the CFHT FTS in March 1992 provided the first very high-resolution H_3^+ spectra of Jupiter's auroral regions [*Drossart et al*., 1993b]. A resolving power of 115,000 allowed the line profiles for 18 individual H_3^+ *R*-branch lines of the ν_2 fundamental to be determined. From the widths of the lines a translational (i.e., Doppler-broadening) temperature of 1150 ± 60 K was derived, as compared with a rotational temperature (i.e., based on the relative line intensities) of 1250 ± 70 K.

Ongoing near-IR imaging of Jupiter's H_3^+ emissions using the IRTF ProtoCAM in January 1992 led to the discovery of emission from the Io flux tube footprint [*Connerney et al*., 1993] (see Plate 6). The IFT contains a large current ($\sim 5 \times 10^6$ A) due to the differential motion of Io in Jupiter's magnetic field. When the particles carrying this current impact the atmosphere of

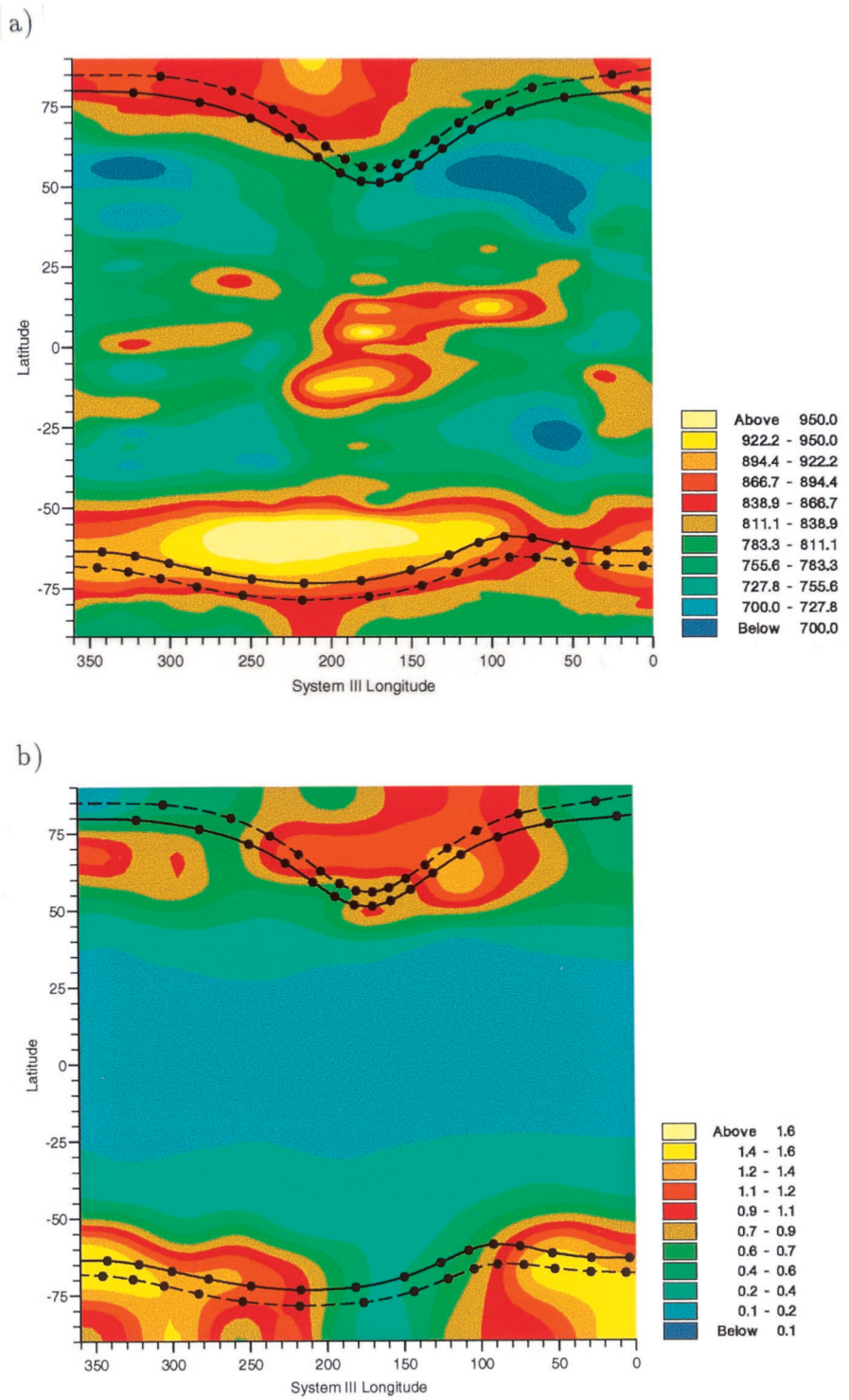

Plate 7. Map of (a) fitted temperature (kelvins) and (b) column density (10^{12} cm^{-2}) as a function of Jovian latitude and longitude, based on CML scans of H_3^+ emissions [*Lam et al.*, 1997a, Figures 4 and 5]. Reprinted with permission from *Icarus*.

Jupiter, an auroral-like spot of emission is produced. Connerney et al. found that the total H_3^+ flux associated with the IFT footprint was about 4.3×10^{-19} W cm^{-2} μm^{-1}, or about 0.3–1% of the total auroral flux. The emissions from the IFT footprint provide a very useful "fiducial mark" for magnetosphere models, since although the longitude of the emission may vary according to the dynamics of the IFT, the latitude of the spot maps out the L shell of Io at 5.9 R_J.

Kim et al. [1994] analyzed ProtoCAM observations of the Jovian aurora from March 1992 and determined that the emissions formed a continuous auroral oval near the

$L = 30$ oval in the O6 magnetosphere model (consistent with HST observations of the FUV aurora [e.g., *Gérard et al*., 1993]). Using a revised limb location, Kim et al. also found that the H_3^+ emissions are dominated by limb brightening (resulting in bright spots at either limb) and extend well off the disk of the planet, with scale heights of 500–1000 km. This result supersedes the earlier characterization of the bright spots as lower-latitude disk features at CML ± 60° [e.g., *Drossart et al*., 1992].

A comprehensive study of the H_3^+ emission morphology was undertaken by *Satoh et al*. [1996] and *Connerney et al*. [1996], using ProtoCAM data obtained at NASA/IRTF during February and March, 1992. Simulating a uniform Jovian auroral oval using a nine-parameter model (width, diameter, height, thickness, center location in latitude and longitude, and three additional parameters describing the strength and extent of diffuse emissions inside and outside the main oval), Satoh et al. were able to obtain reasonable least squares fits to the northern auroral oval observations, while the southern auroral oval observations were not fit as well. They found that by adding two nonuniform components, one varying with local time and the other with system III longitude, the fit to the southern oval data was greatly improved (with the local time variation providing most of the improvement). Their fits to the data at both poles show that the auroral ovals are best fit with an O6 model $L = 30$ size oval centered on latitudes and system III longitudes of 78.8° and 201.3° in the north (shifted by 2.3° along the 280° meridian, relative to the O6 model, consistent with the results from UV observations with HST [*Gérard et al*., 1994a, b; *Clarke et al*., 1996; *Grodent et al*., 1997]) and −84.2° and 57.8° in the south [*Connerney et al*., 1996]. A faint polar collar extends equatorward to $L = 6$ and a brighter diffuse emission fills the polar caps, with an even brighter region on the afternoonside of the cap that is fixed in local time. Broad system III anomalies were found, peaking at ~230° in the north and ~40° in the south, consistent with excitation by westward drifting electrons [e.g., *Herbert et al*., 1987]. It was also found that the brightnesses of the northern and southern auroras are well correlated.

Using the same data set, *Baron et al*. [1996] noticed that the daily variations in H_3^+ auroral brightness were well correlated ($R = 0.65$) with variations in solar wind ram pressure at Jupiter (as determined by instruments on the Ulysses spacecraft, which was near Jupiter at the time). The authors suggested that the correlation was a natural result of "magnetic pumping" [*Goertz*, 1978], in which some of the increase in perpendicular energy of trapped particles (received when the increased solar wind ram pressure compresses the Jovian magnetosphere and thus increases the local magnetic field strength) is converted to parallel energy by pitch angle scattering before the magnetosphere relaxes back to its original state. Some of the particles would have their parallel velocities increased enough to precipitate out into the atmosphere. This result is the first linking the Jovian aurora, previously believed to be entirely dominated by internal processes in the inner magnetosphere (e.g., plasma outflow from the Io plasma torus), to the solar wind (see Figure 20).

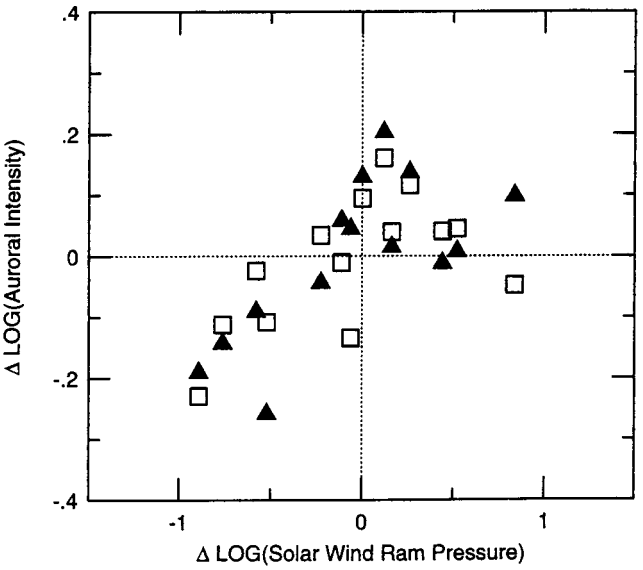

Figure 20. Change (relative to the previous observation) in the integrated H_3^+ auroral brightness of Jupiter as a function of the change in solar wind ram pressure, as measured near Jupiter by instruments on the Ulysses spacecraft. Open symbols are for the northern aurora, and solid symbols are for the southern aurora [*Baron et al*., 1996, Figure 3]. Reprinted with permission from Academic Press.

Recently, *Lam et al*. [1997a] have presented a spectroscopic study of Jupiter's auroral H_3^+ emissions, based on United Kingdom infrared telescope (UKIRT) observations from Mauna Kea, Hawaii, in May 1993. They derived temperatures (typically 700–1000 K) and H_3^+ column densities (~10^{12} cm^{-2}) in the auroral regions and found that these two quantities are generally inversely related (see Plate 7). Lam et al. introduced a parameter $E(H_3^+)$, which allows for the strong coupling between fitted temperature and column densities. This parameter is defined by calculating the total emission per molecule at the appropriate fitted temperature, assuming LTE, and multiplying it by the corresponding fitted column density. Maps of $E(H_3^+)$ show peak values from $\lambda_{III} \sim 300°$–$60°$ in the south and $\lambda_{III} \sim 150°$ in the north. Lam et al. also defined another parameter E(CML), which is the integral of $E(H_3^+)$ along a 1-cm-wide arc following the CML from the lowest-latitude point of the auroral oval to the limb. Together, these parameters can be effectively used to study the temporal and spatial variations and in deriving the total power emitted by H_3^+ emissions. In this way they found the integrated H_3^+ auroral output from each hemisphere to be ~3×10^{12} W. This is roughly equal to the output from the auroral UV emission [e.g., *Livengood et al*., 1992] and is about 10% of the auroral IR output due to hydrocarbon emissions [e.g., *Drossart et al*., 1993a].

Most recently, *Rego et al*. [1999] presented excellent high spectral resolution (14.4 km s^{-1}) observations of H_3^+ lines at 3.95251 and 3.95416 μm along the central meridian of Jupiter (at ~0.8″ spatial resolution), taken with the IRTF CSHELL instrument (an Echelle spectrograph). The signal-to-noise ratio of the data was large enough for the emission lines to be centroided to an accuracy of ±0.3 km s^{-1}, and Doppler shifts of up to ~±3 km s^{-1} were discovered. These Doppler shifts are best explained as due to the line-of-sight projection of large auroral region ion winds in the upper atmosphere, known (as on Earth) as the auroral electrojet. These winds must have true velocities approaching or exceeding the speed of sound (~3 km s^{-1}) and are probably also responsible for driving the neutral winds that are thought to result in the asymmetric Lyman α auroral line profiles described earlier. Thus there are now two independent means for remote study of the dynamics of the violent upper atmosphere of Jupiter; hopefully, these methods will also prove fruitful for the other giant planets.

The Jovian H_3^+ emissions are not confined to the auroral zones alone; they have been detected from the entire disk of the planet [*Ballester et al*., 1994; *Lam et al*., 1997a; *Miller et al*., 1994, 1997a]. These emissions are typically only about 10% as bright as those observed in the polar regions. These nonauroral emissions occur in two midlatitude bands (one in each hemisphere), where the temperatures are relatively lower (~100–300 K less than in the polar regions), and in the equatorial region, where the temperatures are high. The H_3^+ column densities are also lower in the subauroral latitudes (~10^{11} cm^{-3}). The study by *Miller et al*. [1997a] demonstrated that the emission level of H_3^+ in the middle- to low-latitude region is ~0.1 ergs cm^{-2} s^{-1}, indicating the strong cooling effect due to the H_3^+ ions. This high level of H_3^+ emission and its latitudinal profile cannot be explained by solar EUV input alone. The authors suggested the possible causes could be transport of auroral H_3^+ to lower latitudes by atmospheric winds and/or the precipitation of particles at low latitudes (as also indicated by recent X-ray observations [*Waite et al*., 1997] and supported by Galileo probe data from the energetic particles instrument (EPI) experiment [*Fischer et al*., 1996] and Ulysses observations [*Rezeau et al*., 1997]). The observations of H_3^+ at low latitudes are also shown to have links to other low-latitude phenomena, such as the Lyman α bulge [*Ballester et al*., 1994; *Miller et al*., 1997a].

The H_3^+ emissions were also used to monitor the comet Shoemaker-Levy 9 (SL-9) collision with Jupiter [e.g., *Orton et al*., 1995; *Encrenaz et al*., 1995; *Kim et al*., 1996; *Dinelli et al*., 1997; *Miller et al*., 1997b]. During a week in July 1994, twenty-one fragments of comet SL-9 plunged into Jupiter around 44°S latitude. Observations of the auroral regions both during and after the impacts gave a number of interesting and unexpected results. Readers are referred to special issues of *Science* (*267*, 1277–1323, March 1995), *Geophysical Research Letters* (*22*(12), 1555–1636, 1995; *22*(13), 1761–1840, 1995; and *22*(17), 2413–2440, 1995), *Icarus* (*121*, 207–510, 1996), and to *West and Böhnhardt* [1995] and *Noll et al*. [1996], where various aspects of the observations of the SL-9/Jupiter collision and results are presented and discussed. A chronological history of the effects of the SL-9/Jupiter collision on the Jovian auroral emissions, starting from 5 hours before the impact to about 10 days after the impact week, is given by *Miller et al*. [1997b]. One of the most interesting results was that the images taken at 3.5 μm during the week of collision showed the north and south polar intensities at about the same level, while about a week after the last impact, the southern aurora had significantly dimmed and the northern aurora became ~5 times brighter than normal. This effect lasted for about a week before returning to normal.

4. SATURN

4.1. X-Ray Emissions

Since the Saturnian magnetosphere possesses substantial fluxes of energetic electrons and ions, it was expected that Saturn might be a source of X-ray emissions. However, probably due to the nondetection of X rays from Jupiter in early attempts, no attempt was made to observe X-ray photons from Saturn.

During the Voyager 1 flyby of Saturn the LECP experiment detected emission in excess of the background radiation emanating from the vicinity of Saturn, upstream from the bow shock [*Kirsch et al*., 1981b], similar to the detections at Jupiter [*Kirsch et al*., 1981a]. Although the LECP was not equipped for the detection of X rays, the possibility that these excess counts may be due to X-ray radiation produced by the precipitating magnetospheric energetic electrons in the auroral region or through interaction with rings and satellites was considered. The requirement of very large fluxes of precipitating electrons, by a factor of 10^3–10^4 compared with the maximum flux measured by the same LECP instrument in the Saturnian magnetosphere, led *Kirsch et al*. [1981b] to conclude that the observed excess emissions are probably not due to X rays from Saturn but to energetic neutrals (as at Jupiter). Such neutrals are expected to be emitted from Saturn's inner magnetosphere, being produced by charge exchange reactions between radiation belt ions and the neutral corona [*Kirsch et al*., 1981a, b; *Cheng*, 1986].

Prompted by the first detection of X rays from Jupiter [*Metzger et al*., 1983], *Gilman et al*. [1986] made the first systematic attempt to measure X-ray emissions from Saturn using the Einstein observatory. No X-ray emissions from Saturn were detected. The 3σ upper limit of the flux at Earth was found to be ~2–5 × 10^{-13} ergs cm^{-2} s^{-1}, depending on whether ion precipitation (higher value) or electron bremsstrahlung (lower limit) is the source. For bremsstrahlung from keV electrons precipitating into Saturn's atmosphere and satisfying observed

UV aurora constraints, the expected energy flux at Earth in the 0.2- to 3-keV energy range is $\sim 8 \times 10^{-16}$ ergs cm^{-2} s^{-1}, requiring about a 2-order-of-magnitude increase in sensitivity for the detection of Saturn's X-ray emissions [*Gilman et al.*, 1986].

Barbosa [1990b] predicted X-ray intensities at Saturn at 10 and 50 R_S using his electron bremsstrahlung model [*Barbosa*, 1990a], constraining the primary electron beam parameters by UV aurora observations [*Sandel et al.*, 1982; *Atreya et al.*, 1984]. Although the X-ray flux calculated by him for Saturn was $\sim 10^4$ times less than for Jupiter, he considered that it should be still measurable by an orbiting spacecraft (e.g., Cassini). However, in view of the apparent inadequacies in Barbosa's bremsstrahlung model, as discussed in detail in the section on Jovian X-ray emissions, the X-ray photon fluxes predicted by Barbosa should probably be scaled down by a few orders of magnitude in the low-energy region ($\leq$2 keV). The precipitation of nitrogen ions from Titan torus [*Barbosa*, 1987] may also produce significant fluxes of emission line X rays on Saturn; this possibility has not been explored so far.

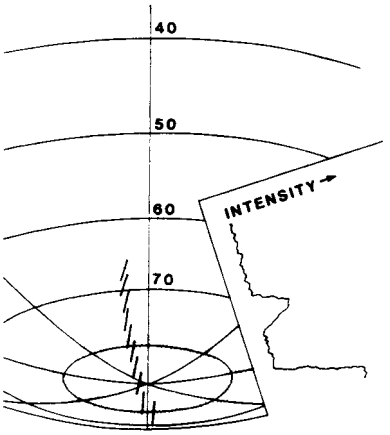

Figure 22. Geometry of Voyager UVS polar auroral scans at Saturn. The range of the spacecraft is 3.6 R_S, and its latitude is 36.6°S. The dashes show the position of the 0.1° × 0.86° UVS slit at 90-s intervals. Auroral emissions were detected at 78°–81.5°S, and relative H_2 band brightnesses are shown as a function of position in the inset [*Sandel and Broadfoot*, 1981, Figure 1]. Reprinted with permission from *Nature*.

4.2. Ultraviolet Emissions

The presence of an aurora on Saturn was suspected from observations made by the UV photometer aboard the Pioneer 11 [*Judge et al.*, 1980] and IUE [*Clarke et al.*, 1981], which found enhancements in the Lyman α brightness near the polar regions. However, it was the UVS instrument on Voyager 1 which provided the first unassailable evidence for the existence of a Saturnian aurora [*Broadfoot et al.*, 1981b]. Aurorally excited emissions were found at H I Lyman α and in the H_2 Lyman and Werner bands (see Figure 21 for the auroral spectrum) around both poles of Saturn, with emission rates varying between 1 and 20 kR. In the south the emissions are confined to an axisymmetric oval between 78° and 81.5°S (see Figure 22), with no emission detected from inside the polar cap region. For the northern aurora the position of the oval is not accurately known, but it is at least poleward of 76°N and may not extend below 78°N [*Sandel and Broadfoot*, 1981]. Brightness variations by factors of $\sim$2–5 times were observed on timescales of a few hours for the auroral emissions. *Sandel and Broadfoot* [1981] noted that the Lyman α component of the Voyager 1 auroral emission was $\sim$5 times fainter than the H_2 band emission, and the lowest burst detected by *Clarke et al.* [1981] compared roughly in intensity with the brightest Lyman α measured by Voyager 1.

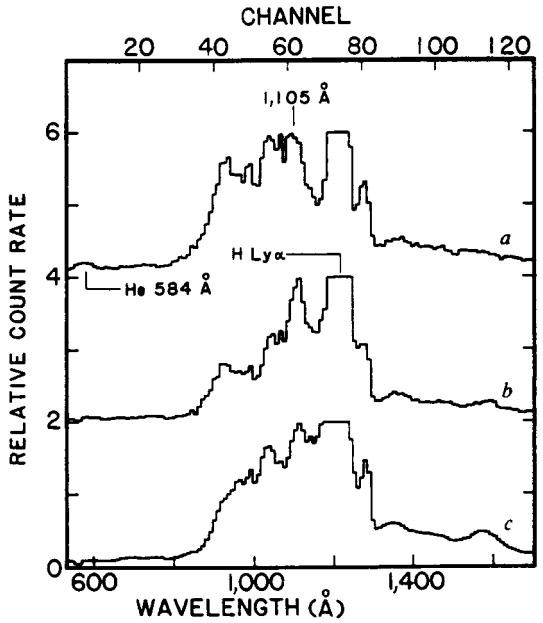

Figure 21. Voyager UVS auroral spectra of Saturn at a local zenith angle of 60° (curve a), Saturn at a local zenith angle of 76° (curve b), and Jupiter (curve c), showing relative differences in H_2 Lyman and Werner band emissions in the 90- to 113-nm range [*Sandel and Broadfoot*, 1981, Figure 4]. The spectra have been normalized at 110.5 nm (note that the strong Lyman α emissions have been clipped in these plots). Reprinted with permission from *Nature*.

The small size of the auroral oval and its location at high magnetic latitudes ($\sim$75°–80°) suggested that the auroral regions map back magnetically to the magnetotail and that the solar wind provides the energy source through an Earth-like interaction with the planet magnetosphere [*Sandel and Broadfoot*, 1981]. The situation at Saturn thus seemed to be quite different than at Jupiter, where the electrodynamical interaction of Io with the Jovian magnetosphere supplies a large part of the auroral power. The power required by precipitating electrons to drive Saturn's aurora is estimated to be about 2×10^{11} W, with an uncertainty of a factor of $\sim$4 [*Sandel and Broadfoot*, 1981], based on an average brightness of 5 kR in the H_2 bands extending over an

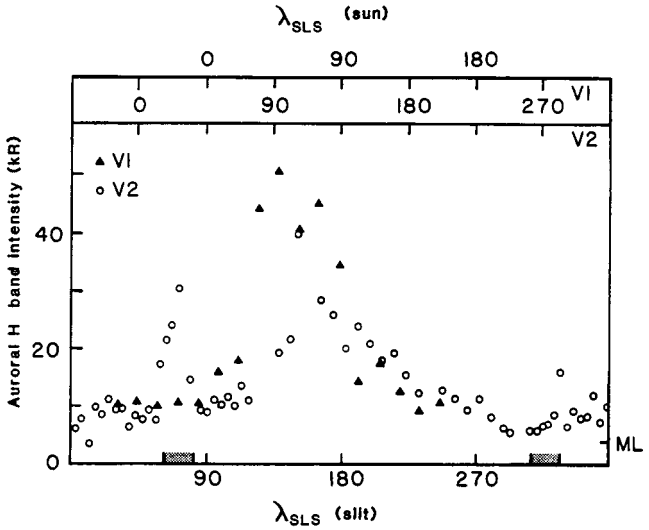

Figure 23. Brightness of Saturn's H_2 110.5-nm auroral emissions measured by the Voyager UVS plotted versus longitude at 80°N [*Sandel et al.*, 1982, Figure 3]. Both Voyager 1 and Voyager 2 observations show brightening near $\lambda_{SLS} \sim 135°$ and when the Sun was near $\lambda_{SLS} \sim 100°$. The tick mark labeled ML indicates the brightness level measured at midlatitudes for this spectral feature. The shaded longitudes were measured by Voyager 2 one planet rotation prior to the main map; the Voyager 1 measurements were contiguous. Reprinted with permission from *Science*.

area of 4.6×10^8 km^2 (the surface area of Saturn between 78° and 81.5° latitude) [*Sandel et al.*, 1982]. The aurora is found to be continuous at both poles with longitudinal asymmetry in the emissions, the brightest intensity appearing at $50° < \lambda_{SLS} < 180°$ (SLS is short for Saturn longitude system) (see Figure 23).

There is an apparent correlation between the location of the peak brightness in UV auroral emissions and the location of the source of Saturn kilometric radiation (SKR) [*Kaiser et al.*, 1981, 1984], suggesting a close link between the two (see Figure 24). This correlation, discovered by *Sandel and Broadfoot* [1981] from Voyager 1 observations, was reaffirmed by *Sandel et al.* [1982] from Voyager 2 observations that the UV aurora is brightest when the subsolar longitude is ~100° (see Figure 23), similar to the effect seen in SKR. Also, there is some indication that the solar wind dynamic pressure is correlated with SKR intensity (see Figure 25) [*Desch*, 1982; *Desch and Rucker*, 1983; *Kaiser et al.*, 1984], which suggests a solar wind power source or at least that the solar wind controls the radiation pattern. However, *Curtis et al.* [1986] have noted that according to the magnetic field model of *Connerney et al.* [1984], the polar source location for SKR could be on closed field lines, which would suggest that an internal, rotationally driven process is responsible for the radio emissions.

The longitudinal asymmetry in the auroral UV and SKR emissions is quite surprising given the perfectly axisymmetric magnetic field of Saturn [*Connerney et al.*, 1984]. The magnetic and rotational axes of Saturn are perfectly aligned with each other, to within 0.1°. This has been a puzzling situation for scientists trying to explain magnetospheric/atmospheric phenomena [e.g., *Hubbard and Stevenson*, 1984]. *Galopeau et al.* [1991] have proposed nonaxisymmetric Saturn magnetic field models based upon observations of SKR emissions, but their conclusions have been contested by *Connerney and Desch* [1992] and *Ness* [1993]. Recent reanalysis of the Voyager-PRA (Planetary Radio Astronomy subsystem) data [*Galopeau et al.*, 1995] shows that the sources of SKR are located at latitudes ≳80° and 1200–1300 LT, with extensions to lower latitudes of ~60° near dawn (0800–0900 LT) and ~75° near dusk (~1900 LT). These locations are consistent with the locations of the bright UV aurora observed by HST [e.g., *Trauger et al.*, 1998; *Zarka*, 1998]. However, owing to their limited data set,

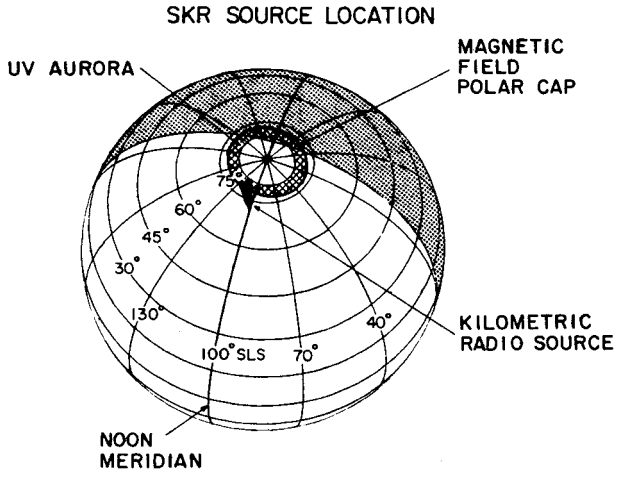

Figure 24. Comparative longitudinal structure of the UV and radio auroras at Saturn. The source regions for right-handed Saturn kilometric radiation (SKR) aurora radio emissions map to a very small region near $\lambda_{SLS} \sim 115°$ [*Kaiser et al.*, 1984, Figure 17].

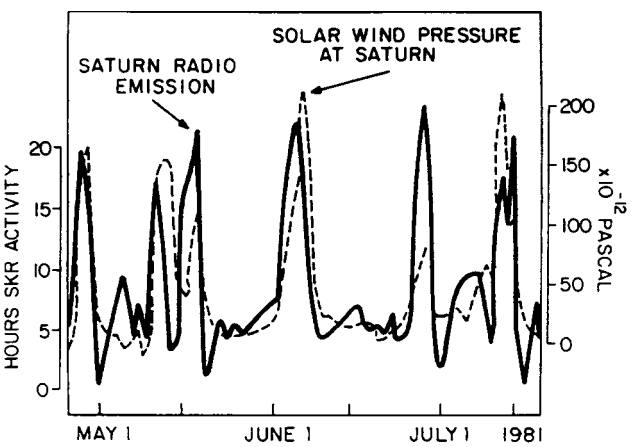

Figure 25. Voyager 2 data showing the close correlation between SKR activity and the solar wind pressure at Saturn [*Kaiser et al.*, 1984, Figure 7].

Trauger et al. were unable to infer anything about the Voyager-observed longitudinal correlation between UV emissions and SKR.

Pre-Voyager calculations of *Waite* [1981] showed that the Lyman α brightness of about 2 kR and the H_2 band brightness of 6–9 kR could be produced by precipitating monoenergetic electrons in the energy range 1–10 keV with an energy flux of 0.75 ergs cm^{-2} s^{-1}. *Gérard and Singh* [1982] modeled the Saturn aurora using the CSDA method for a primary electron flux having a Maxwellian energy distribution with characteristic energies ranging from 0.1 to 2 keV. From comparison with the observed H_2 band intensities, they computed a total energy deposition rate into the auroral zone of 0.2–1.5 ergs cm^{-2} s^{-1} and a globally averaged H atom column production rate of 0.9–7 $\times$ 10^7 cm^{-2} s^{-1}. In contrast, *Shemansky and Ajello* [1983] constructed a synthetic spectral model of the aurora which treats electron-excited H and H_2 emissions at electron energies $\geq$100 eV with an electron differential flux distribution of the form $E^{-1.4}$. They found that H_2 emissions require a foreground H_2 vertical column of only $\sim 10^{16}$ cm^{-2}, which corresponds to a pressure level of $\sim 4 \times 10^{-11}$ bar (well above the homopause), indicating low-energy (<100 eV) exciting electrons. *Atreya et al*. [1984] suggested that electrons in the energy range 1–10 keV are responsible for exciting the aurora. Saturn's UV auroral spectrum shows less atmospheric absorption than Jupiter's (compare curve c with curves a and b in Figure 21), suggesting a relatively higher altitude auroral region corresponding to less energetic primary particles. Modeling the precipitation of protons in Saturn's atmosphere using CSDA [*Singh*, 1991] yielded an excitation efficiency of about 10 kR (erg cm^{-2} $s^{-1})^{-1}$ for the H_2 bands, thus requiring a flux of about 1 erg cm^{-2} s^{-1} to explain the 10 kR of H_2 band emissions observed by Voyager.

Barbosa [1987] proposed that Titanogenic nitrogen ions are a key component of Saturn's magnetospheric particle population and can account for the energetics of the Saturn UV aurora in a corotation-dominated magnetosphere. The nitrogen atoms which are escaping from the sunlit hemisphere of Titan at a rate of $\sim 3 \times 10^{26}$ s^{-1} due to dissociative excitation of N_2 [*Strobel and Shemansky*, 1982] form a torus around Saturn. (A recent estimate of nonthermal photochemical loss of nitrogen from Titan in any chemical form is 1.2 $\times$ 10^7 cm^{-2} s^{-1}, corresponding to a global loss rate of 2.5 $\times$ 10^{25} s^{-1}, of which 70% is atomic nitrogen [*Cravens et al*., 1997]. The same study estimates a sputtering loss of $\sim 1.5 \times 10^{26}$ s^{-1}, while the loss due to polar wind processes is $\sim 2 \times 10^{25}$ s^{-1}). Ionization of the nitrogen torus by both solar EUV and magnetospheric electrons and subsequent pickup of ions produces a population of ~keV N ions which can supply the bulk of mass and energy input to the magnetosphere at a power level of 2 $\times$ 10^{10} W. Thus *Barbosa* [1987] suggests that the aurora on Saturn can be accounted for solely by an internal (Titan) plasma supply in a corotation-dominated magnetosphere, deemphasizing the importance of the solar wind.

In a subsequent paper, *Barbosa* [1990c] estimated the power delivered to the aurora by protons and N^+ ions to be 5 $\times$ 10^9 and 2 $\times$ 10^{10} W, respectively. Taking the flux of superthermal electrons (1–10 keV) from *Sittler et al*. [1983], he estimated $\gtrsim 5 \times 10^{10}$ W of power for the electron aurora and concluded that electrons are most likely the primary precipitation energy source for the aurora as a result of energy transfer from Titanogenic N^+ pickup ions in a corotation-dominated magnetosphere. A suggested mechanism for this energy transfer was ion-generated lower hybrid waves, which could accelerate electrons to keV energies. Recently, combining the electron observations from three Voyager experiments (plasma instrument, LECP, and cosmic ray subsystem), *Maurice et al*. [1996] have generated a composite flux spectrum of electrons in Saturn's magnetosphere which extends over nearly 12 orders of magnitude in intensity (from $\sim 10^{-2}$ to 10^9 particles (cm^2 s sr keV)$^{-1}$) and more than 4 orders of magnitude in energy (from 10 eV to ~2 MeV) (see Figure 26). Such a comprehensive electron spectrum can be employed to better constrain the role of magnetospheric electrons in powering the Saturn aurora.

The IUE observations of auroral H I Lyman α emissions from Saturn over a period of a decade (1980–1990) showed intermittent outbursts of up to 1 kR above the disk brightness (see Figure 27) [*McGrath and Clarke*, 1992]. Voyager observations indicated continuous emissions around the auroral ovals that are apparently not detectable with IUE probably due to the observing geometry and larger slit aperture for IUE (which averages out the intensity). Attempts were made to correlate the auroral activity on Saturn seen with IUE with major solar flares that produced strong geomagnetic activity, but the results were negative [*McGrath and Clarke*, 1992].

Most recently, WFPC2 images of Saturn's FUV aurora were presented by *Trauger et al*. [1998]. They show that the aurora is brightest (~100 kR) near the dawn limb and appears to be fixed in local time (similar to the dawn storms observed at Jupiter). A total radiated FUV power of 40 GW was determined. These results for 1995 were for the northern auroral oval but are consistent with the STIS image highlighting the southern auroral oval shown in Plate 1.

The atmosphere of Saturn contains a variety of particulate material (e.g., aerosols, clouds, haze) which plays an important role in various physical, chemical, and dynamical processes (e.g., radiation and heat budget, chemistry, transport) in the atmosphere [*Tomasko and Doose*, 1984]. The ability of these particles to absorb and scatter sunlight enables us to study their spatial distribution and physical properties through remote sensing at various wavelengths. Voyager photopolarimeter subsystem (PPS) observations at 264 nm have revealed the existence of a layer of small aerosols (radii

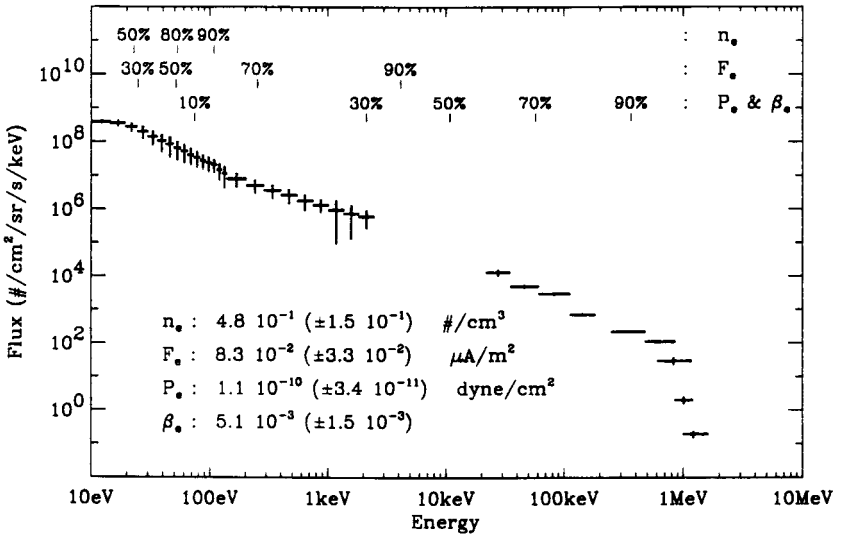

Figure 26. Composite electron flux spectrum for Saturn's magnetosphere at $L = 11.21$, $\lambda_{SLS} = 25.1$, utilizing data from the plasma (PLS) (10 eV to 2.5 keV), Low Energy Charged Particle (LECP) experiment (22 keV to 1 MeV), and cosmic ray subsystem (CRS) (>600 keV) instruments [*Maurice et al*., 1996, Figure 7]. The density (n_e), return current density (F_e), pressure (P_e), and ratio of electron to magnetic pressure (β_e) are listed with $\pm 1\sigma$ uncertainties, and the energies at which these quantities reach various percentages (integrating up from 10 eV) are indicated above with tick marks.

~0.1 μm) in the atmosphere of Saturn which absorbs strongly in the UV region and is located at a pressure level of 30–70 mbar at low to middle latitudes and at pressures ≲20 mbar at higher latitudes (>60°) [*West et al*., 1983; *Tomasko and Doose*, 1984].

The observed UV-darkening of the polar regions of Saturn has been interpreted as the sign of the presence of UV-dark material (auroral haze) in the stratosphere [*West et al*., 1983; *Karkoschka and Tomasko*, 1993]. *Pryor and Hord* [1991] have found that a spatial correlation exists between the regions of strong auroral H_2 band emissions and UV-dark polar haze at Saturn. The observed northern haze region appears to enclose the auroral zone as defined from the Voyager UVS morphological observations. Pryor and Hord have proposed that the source of this haze is auroral ionization and subsequent hydrocarbon chemistry leading to the polymerization of hydrocarbons. The suggestion that auroras may be important in haze formation was made earlier by *Lane et al*. [1982] and is supported by the recent model calculations of *Singhal et al*. [1992] on Jupiter. However, for the auroral mechanism to be an important source of haze production, it is necessary that the precipitating particles be energetic enough to cause substantial ionization at altitudes of appreciable methane abundance (i.e., below the methane homopause) and thus initiate hydrocarbon-ion-polymerization chemistry.

Observations made near 220 nm by the FOC aboard HST (pre-COSTAR) have revealed a dark UV oval enclosing the north pole of Saturn having an equivalent width of ~11° in latitude and centered around 79°N [*Ben*

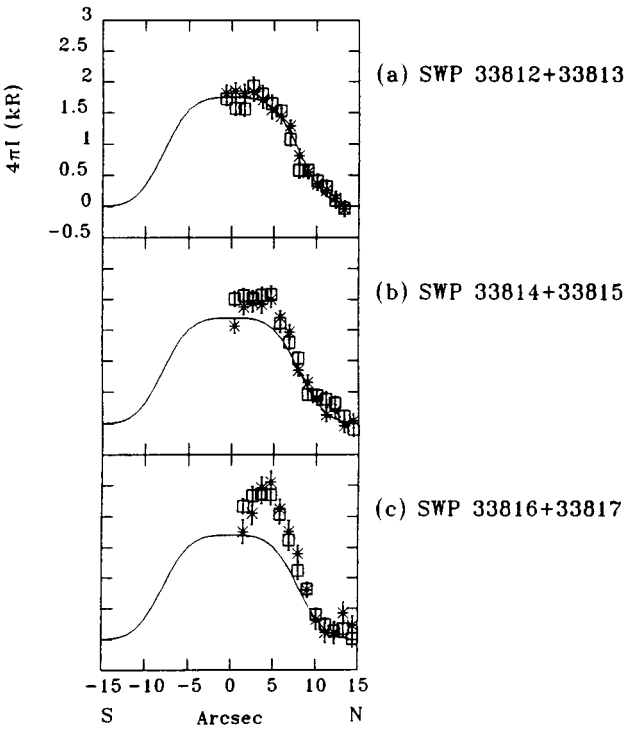

Figure 27. A sequence of IUE observations of Saturn showing the onset of a bright (~1 kR) Lyman α aurora during May 17, 1990 [*McGrath and Clarke*, 1992, Figure 10]. The solid line represents a uniformly emitting disk, smoothed by a 6″ full width at half maximum Gaussian approximation to the IUE point-spread function. Saturn's diameter as seen from Earth at the time of the observations was 17.5″, and the sub-Earth latitude was 22.3°N.

Jaffel et al., 1995]. The oval shape of the dark structure and its correlation with the Voyager UVS location of the aurora suggest that the hydrocarbon aerosol-haze production is indeed linked to the aurora, supporting earlier suggestions [*Pryor and Hord*, 1991; *Singhal et al*., 1992; *Lane et al*., 1982].

Recently, using post-COSTAR FOC observations, *Gérard et al*. [1995] observed Saturn's north polar region at 153 and 210 nm, thus making near-simultaneous measurements of H_2 emissions and the polar haze. The H_2 emissions were found to peak near 80°N, with a total H_2 band brightness of about 180 kR. The maxima of the absorption at 210 nm was found to lie at ~75°N (with optical depth ~0.3), i.e., ~5° equatorward of the UV auroral emission peak. This shift of ~5° was attributed to the equatorward transport of the precursors of the haze particles (during the process of their formation) by meridional winds, which would be generated by the large heat input into the auroral region from the precipitating energetic particles. Preliminary estimates of *Gérard et al*. [1995] suggest that for a 3×10^{10} W H_2 aurora, an aerosol formation efficiency of ~7% is required to explain the observed haze level. Their study also supported the notion of polar haze formation by aurorally produced hydrocarbon aerosols.

4.3. H_3^+ Emissions

The first attempts by T. Geballe and coworkers to detect H_3^+ emissions from Saturn in July 1991 were unsuccessful. A year later, and 3 months after their detection on Uranus [*Trafton et al*., 1993], the Saturnian H_3^+ emissions were eventually detected by *Geballe et al*. [1993] using the cooled grating spectrograph 4 (CGS4) instrument at UKIRT. The intensities of the lines detected were about 1% of those on Jupiter and were even weaker than those detected from Uranus. Geballe et al. derived a temperature of ~800 K and a total H_3^+ column density of $\sim 1.0 \times 10^{11}$ cm^{-2}. The relative weakness of the H_3^+ emissions from Saturn is puzzling: The surface brightness of H_3^+ emissions is similar on Jupiter and Uranus but is about 2 orders of magnitude lower on Saturn. The reason for the apparently intrinsically weak H_3^+ emission on Saturn is still not understood. One suggestion is that H_3^+ is rapidly destroyed by hydrocarbons (particularly methane) in the upper atmosphere of Saturn because of a large eddy diffusion coefficient and thus a high homopause [*Trafton et al*., 1993]. The other suggestion is that transport of water from Saturn's rings into the ionosphere leads to depletion of H_3^+ due to reaction with H_2O (producing H_3O^+). Another possibility is the interference of ring particles in the normal flow of charged particles along magnetic field lines and hence reduced low-latitude auroral activity on Saturn [*Tennyson*, 1995; *Miller et al*., 1994]. *Geballe et al*. [1993] found that their spectra were brightest at the north and south poles but concluded that they had too few data to say if this was due to limb brightening or auroral effects. However, recent observations of the latitudinal profile of H_3^+ emission on Saturn [*Stallard et al*., 1999] show that they are mostly from auroral latitudes, with only a small middle- to low-latitude component, thus making them similar to the morphology of Jovian H_3^+ emissions. More recently, some efforts have been made to observe IR emissions from ions other than H_3^+ (e.g., H_3O^+, CH_5^+) in Saturn's auroral ionosphere, but these have been unsuccessful to date (S. Miller, private communication, 1999).

The questions of (1) whether Saturnian auroras are powered by the solar wind or by particles internal to the magnetosphere, (2) whether an internal source is electron, proton, or heavy ion dominated, and (3) whether auroral particles are energetic enough to initiate hydrocarbon polymerization and haze formation remain open. Understanding the cause of the longitudinal asymmetry in the UV and SKR emissions and the spatial correlation between the UV, SKR, and H_3^+ IR auroral emissions requires further observations at higher spatial and temporal resolution. The data from the Cassini mission will be useful for resolving many of these issues when Cassini reaches Saturn in 2004.

5. URANUS

5.1. Ultraviolet Emissions

Relatively little was known of the planet Uranus prior to the Voyager 2 encounter of January 24, 1986. The planet's 51,200-km diameter at a mean orbital radius of 19.2 AU (AU stands for astronomical unit, the average Earth-Sun distance of 150×10^6 km) subtends less than 4″, making it a very difficult object to observe. The presence of a planetary magnetic field and thus an active magnetosphere and aurora was speculated but was controversial and clearly unknown [e.g., *Desch and Kaiser*, 1984; *Hill and Dessler*, 1985; *Curtis and Ness*, 1985; *Ip and Voigt*, 1985; *Clarke et al*., 1986; *Shemansky and Smith*, 1986]. Experience with auroras on Jupiter and Saturn led to the expectation of similar H Lyman α and H_2 band emissions from Uranus, which would be searched for with IUE and Voyager but would not be well understood until the novel magnetic field geometry of Uranus was discovered.

Preliminary indications of the presence of auroral activity on Uranus were obtained through IUE observations of unexpectedly bright and variable H Lyman α emission from Uranus [*Fricke and Darius*, 1982; *Clarke*, 1982; *Durrance and Moos*, 1982]. *Fricke and Darius* [1982] suggested that the observed high H Lyman α albedo could be due to a large column abundance of H above the absorbing methane layer. However, *Clarke* [1982] and *Durrance and Moos* [1982] argued, based on unreasonably large H column abundance requirements and a rapid factor of ~2 variation in emission brightness, that the resonant scattering of solar Lyman α could not account for the IUE-observed intensity of Lyman α and therefore attributed most of the ~1.5-kR disk-averaged brightness to auroral emissions excited by the precipita-

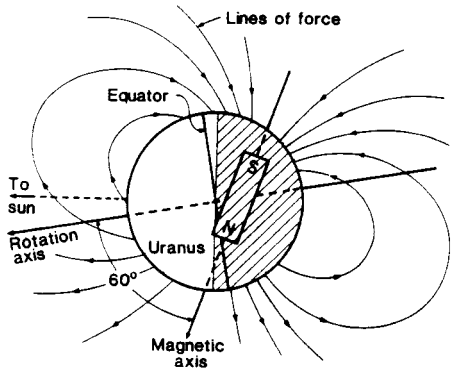

Figure 28. Diagram of the offset tilted dipole (OTD) model of the magnetic field lines of Uranus, in the meridian plane containing the OTD axis and the planetary rotation axis, showing the large spatial and angular offsets from the center and axis of Uranus [*Ness et al*., 1986, Figure 4]. Reprinted with permission from *Science*.

tion of charged particles. This gave the first indirect evidence that Uranus possessed a planetary magnetic field and an active magnetosphere. Subsequently, a marginal detection of the H_2 band emission feature near 160 nm in IUE spectra [*Caldwell et al*., 1983b] further supported the auroral interpretation of the IUE-observed Lyman α emissions. Prompted by these studies, *Hill et al*. [1983] proposed a Faraday disc dynamo model for a Uranian aurora driven by a combination of solar wind and planetary spin, with a magnetic pole pointed toward the Sun.

Four years of observations of the disk-averaged H I Lyman α emissions from Uranus performed with the IUE observatory also supported the view of auroral activity on Uranus [*Clarke et al*., 1986]. The extreme brightness values of 800 R minimum and 2.6 kR maximum indicated a factor of 4 variability in Lyman α emission, if 200 R were assumed to be due to resonant scattering of solar Lyman α. The lack of any correlation of Lyman α variation with solar H I Lyman α flux, or with solar wind density and velocity, together with large variability, was interpreted by *Clarke et al*. [1986] as evidence of the presence of a charged particle excitation process: an aurora on Uranus. They estimated an average power in precipitating particles of 5–10 $\times$ 10^{11} W, suggesting that the Uranus aurora may be comparable, in terms of the total power dissipated, to the Saturnian aurora. In a pre-Voyager paper, *Shemansky and Smith* [1986], citing the nondetection of radio emissions, suggested that the IUE-observed emissions might not be auroral in nature but might be produced by a mechanism (which is now often called "electroglow") similar to that which was thought to be operating in the sunlit atmospheres of Jupiter and Saturn. *Yelle and Sandel* [1986] pointed out that resonant scattering of H I Lyman α emissions from the interstellar wind could be a more potent source for the Uranian Lyman α than the solar scattered component, since the direct sunlight decreases as $1/R^2$ while the flux from the extended interstellar medium decreases more slowly (approximately as $1/R$).

Prior to the Voyager 2 encounter the postulation of IUE-observed strong and apparently variable H I Lyman α emissions being polar auroral emissions was partly based on the fact that the rotation axis of Uranus was known to lie nearly in its orbital plane, and assuming the magnetic axis (granting the existence of a magnetic field) to roughly coincide with the rotation axis, the magnetic pole of Uranus would be expected to more or less face the Earth and Sun. (The inclination of the Uranian orbital plane is $<1°$, while the obliquity of Uranus is 82°. Therefore, twice during its 84-year orbit around the Sun, the rotation axis will be oriented very nearly along the planet-Sun line, so that from Earth one or the other of the planetographic poles of Uranus is viewed. The 1986 encounter of Voyager occurred at such a time.)

Before discussing the Voyager UVS observations, it is worth describing the unusual magnetic field geometry on Uranus. Since a planet's magnetic field strength and orientation control its aurora, information regarding the location of an aurora (in magnetic coordinates) is of great importance, as it indicates from which region of the magnetosphere the aurora-exciting particles originate. The magnetometer on Voyager 2 provided the first measurements of the Uranian magnetic field. The most surprising and highly interesting finding was the large angle (58.6°) between the magnetic and rotation axes and the large offset of the dipole (30% from the planet center). Thus, at the time of the Voyager 2 flyby, Uranus was the first planet known to have the magnetic configuration of an "oblique rotator," a dipole with extended magnetotail rotating about an axis oriented toward the Sun. The preliminary magnetic field representation, the offset and tilted dipole (OTD) model [*Ness et al*., 1986], was characterized by a dipole of moment 0.23 G R_U^3, displaced along the rotation axis by $-0.3\,R_U$ (away from the Sun in 1986), and inclined by 60° from the rotation axis (see Figure 28). However, because of the large dipole offset, there is a strong quadrupole contribution [*Connerney et al*., 1993; *Ness et al*., 1991], causing an order of magnitude variation in the magnetic field strength on the surface, with a minimum of ~0.1 G on the dayside at middle to high northern latitudes and a maximum of ~1 G on the nightside at southern midlatitudes (see Figure 29).

The Voyager 2 UVS observations at the time of closest approach clearly showed emissions associated with the nightside southern magnetic pole [*Broadfoot et al*., 1986]. In the initial UVS data analysis reports the dayside (northern) aurora was ambiguously evident; a more careful analysis later revealed the clear presence of a dayside aurora [*Herbert and Sandel*, 1994]. Higher spatial resolution maps obtained during the Voyager encounter reveal circumpolar UV auroral ovals closer to the planetographic equator than to the pole due to the offset and titled magnetic field [*Herbert and Sandel*, 1994]. The weaker-field (dayside) northern auroral oval

has a considerably larger radius (roughly 35°–40°) than the stronger-field (nightside) southern auroral oval (roughly 7°–10°). The auroral zone covers an area of about 2–4% of the planet's total surface area depending on the width of the dayside ring, which is not well determined. Nightside emission coming from a circular region at the magnetic polar cap with ~20° diameter leads to an auroral brightness of 9.0 kR in H_2 bands and 1.5 kR in H I Lyman α. The ratio of Lyman α to H_2 emissions is consistent with an electron precipitation scenario. Further, the spectra suggest that the UV emissions arise at H_2 column densities of $\sim 10^{20}$ cm^{-2} and that the energy of the precipitating electrons must be about 10 keV to penetrate to this altitude. The disk-averaged auroral brightnesses are ~250 R for the H_2 bands and ~45 R for Lyman α, which may be compared with the corresponding dayglow brightnesses of 1.8 and 1.5 kR, respectively (see *Bhardwaj* [1997a] for a review of outer planet airglow). *Broadfoot et al*. [1986] estimated the total input power to the Uranian aurora to be $\sim 2 \times 10^{11}$ W.

Waite et al. [1988b] have modeled the fate of 1- and 10-keV monoenergetic electron beams precipitating in the atmosphere of Uranus. They found that an input energy flux of about 0.9 ergs cm^{-2} s^{-1} will produce 9 kR of H_2 bands. Their calculations showed that the ratio of Lyman α to H_2 bands for 10-keV precipitating electrons is consistent with the observations of *Broadfoot et al*. [1986].

Whistler-mode emissions from magnetospheric electrons with energies of 10–100 keV were observed by the plasma wave spectrometer (PWS) from the $L < 10$ region during the Voyager flyby [*Gurnett et al*., 1986]. *Coroniti et al*. [1987] have concluded that resonant pitch angle scattering of moderate-energy (5–40 keV) electrons by these waves leads to the precipitation of enough electrons to excite the aurora. Further, examination of the ion and electron phase space densities [*Cheng et al*., 1987; see also *Cheng et al*., 1991] shows (1) injection events which could be associated with substorm activity and (2) evidence for particle precipitation at the strong diffusion rate which may power the observed auroral emissions [*Coroniti et al*., 1987] (see *Kurth et al*. [1991] for review).

Herbert and Sandel [1994] have performed a detailed analysis of the 32 hours of preencounter (sunlit side) and postencounter (dark side) Voyager UVS observations of a Uranus aurora using a singular value decomposition approach to inversion in the two spectral regions: the strong H_2 band region of 87.5–111.5 nm and H Lyman α. Their analysis clearly showed the H_2 aurora to be associated with both magnetic poles (see Figure 30), but the presence of a Lyman α aurora on the dayside (north pole) was not especially convincing because of the strong Lyman α dayglow background emissions. The auroral emissions are found to be somewhat localized in magnetic longitude and thus do not form complete auroral ovals, with peak brightnesses at ~180°, which nearly coincides with the magnetic auroral geographic (MAG)

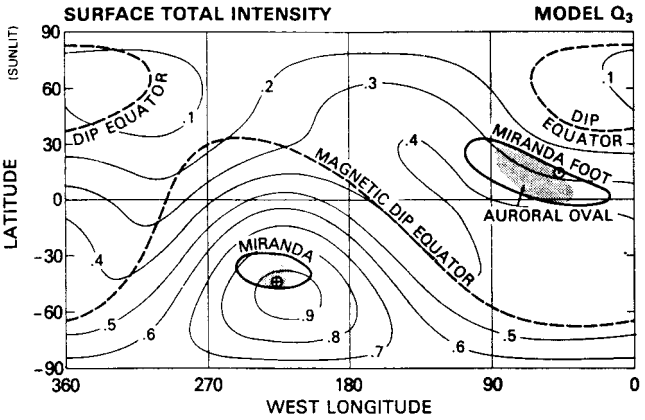

Figure 29. Contours of constant magnetic field magnitude at about 200 mbar on Uranus, calculated using the Q_3 spherical harmonic model [*Connerney et al*., 1987, Figure 5]. The pole tips of the OTD model are shown for comparison, and an estimated auroral oval and Miranda orbit footprint are also indicated.

(see *Herbert and Sandel* [1994] for details) longitude of the highest field strength (see Figure 31). The magnetic field at this longitude is permanently connected with the magnetotail, and therefore it is likely that the aurora is influenced by the magnetospheric convection system, as opposed to the case of an oval-like Earth-type aurora arising at the feet of the last closed field lines. The situation at Uranus is thus dramatically different from that of Jupiter, where the "windshield wiper" effect is important in auroral particle precipitation [*Herbert et al*., 1987; *Prangé and Elkhamsi*, 1991], because the electron mirror points for any given pitch angle are at their highest altitudes at the maximum of magnetic field strength.

The Uranian northern aurora is much brighter (by a factor of 2–4) in H_2 emissions and is centered around a magnetic latitude of 60° compared with the southern aurora, which peaks at about 65° magnetic latitude (see Figure 31). The larger H_2 emission from the northern (dayside) aurora compared with the southern (nightside) aurora is due presumably to the lower magnetic field strength in the north (see Figure 29). According to *Herbert and Sandel* [1994], the precipitating particles lie at relatively low L shell values ($L = 5$–10), indicating that their energies may be ≤10 keV. The lower energies of precipitating electrons estimated from the UVS data are consistent with the Voyager photopolarimeter subsystem (PPS) observations, which found that Uranus is bright in the auroral regions and reveals no sign of the presence of UV-dark auroral haze common to the other giant planets [*Pryor and Hord*, 1991]. This supports the idea that the precipitating electrons are not energetic enough to penetrate the methane homopause and initiate haze formation.

It is interesting to note a close correlation between the location of UV auroral intensity maxima with the

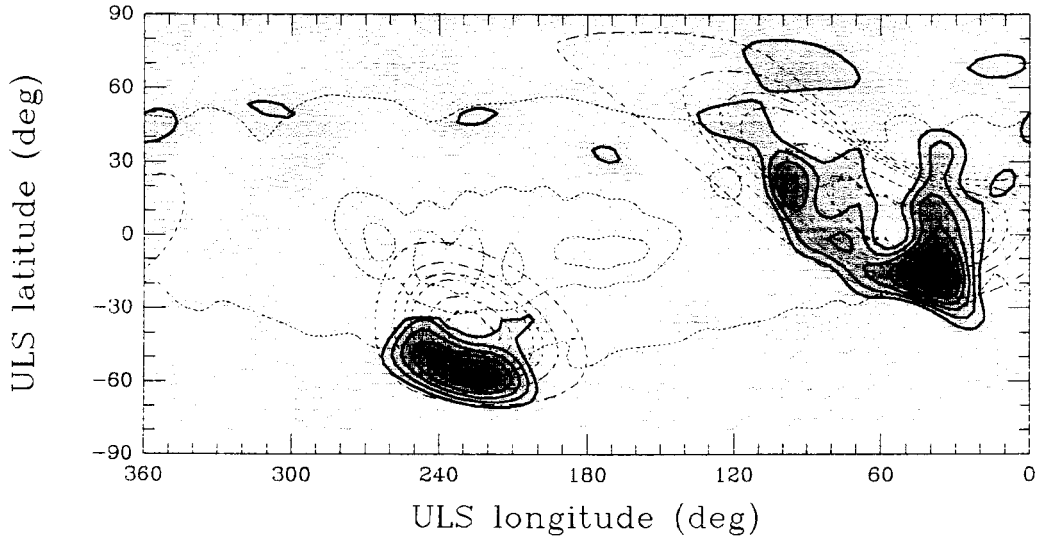

Figure 30. Voyager UVS H_2 emission map for Uranus, with the bold lines and shaded contours indicating relative H_2 brightness (only brightness values exceeding the measured variance, shown by dotted contours, are shown) and with the dashed lines indicating L values of 2, 3, 4, 5, 10, 20, and 30 (outermost to innermost) [*Herbert and Sandel*, 1994, Figure 2].

locations of the source of Uranian kilometric radiation (UKR) [*Desch et al*., 1991], the strongest whistler-mode emissions [*Gurnett et al*., 1986; *Coroniti et al*., 1987], and the most intense 22- to 35-keV electron fluxes [*Krimigis et al*., 1986]. The location of the brightest southern UV aurora coincides with the location of the source of the broadband bursty and broadband smooth UKR, while the northern polar UV auroral intensity maxima seem to lie near the source region of dayside O-mode UKR emissions (see Figure 32). The intensity maxima of both north and south UV auroras lie at the feet of the flux tubes in which maximum whistler-mode plasma wave emission and 22- to 35-keV electrons were observed by Voyager (see *Kurth et al*. [1991] and *Cheng et al*. [1991] for detailed discussions). Recent observations in IR of H_3^+ ion from Uranus [*Lam et al*., 1997b] have revealed spatial variations in the emissions that indicate an association with the aurora; the evidence, however, is not as conclusive as for the case of Jupiter [*Ballester et al*., 1994].

The Voyager UVS data show [*Broadfoot et al*., 1986; *Herbert and Sandel*, 1994] that the aurora at H I Lyman α is considerably weaker than in the H_2 bands, a situation opposite to that found at Jupiter [*Herbert et al*.,

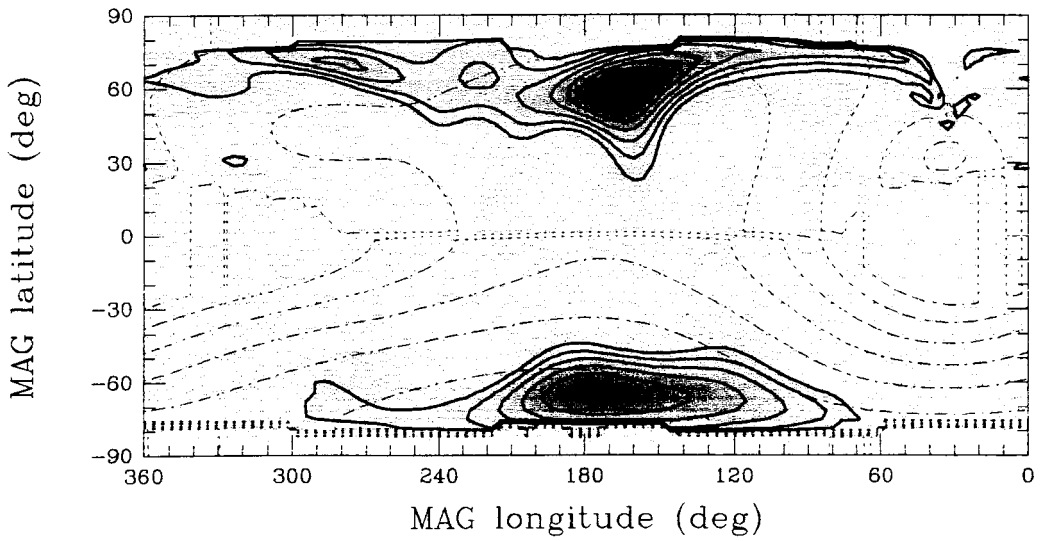

Figure 31. Voyager UVS H_2 emission map for Uranus in magnetic field coordinates, with brightnesses plotted as in the previous figure and with contours of surface magnetic field magnitude at 0.1-G intervals (with the northern maximum near 0.4 G and the southern maximum near 0.9 G) [*Herbert and Sandel*, 1994, Figure 10].

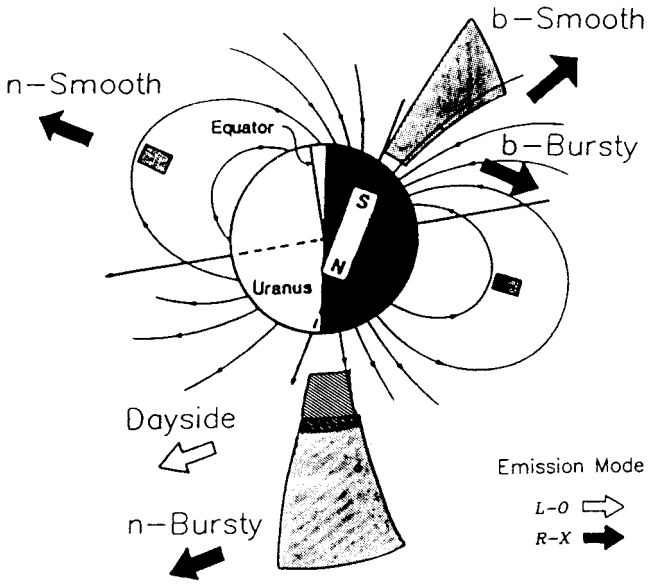

Figure 32. Meridian plane diagram indicating the source locations for Uranian kilometric radiation (UKR), which agree well with the locations of H_2 FUV emission [*Desch et al*., 1991, Figure 10]. Reprinted with permission from University of Arizona Press.

1987; *Broadfoot et al*., 1981a]. Because the north pole was in the sunlit hemisphere at the Voyager encounter, and the Lyman α dayglow is several times brighter than the H_2 band emissions in 87.5–111.5 nm [cf. *Bhardwaj*, 1997a], the Lyman α emissions from the northern aurora are obscured by resonantly scattered solar Lyman α. The reason that the auroral Lyman α/H_2 band intensity ratio is diminished at Uranus relative to Jupiter may be that the atomic H column abundance in the Uranian aurora is smaller than at Jupiter. *Herbert and Sandel* [1994] have estimated the total auroral power output of the H_2 bands and H I Lyman α at 3–7 × 10^9 W. For a presumed 10% UV excitation efficiency, the particle input power is likely around 3–7 × 10^{10} W, corresponding to a disk-averaged deposition rate of about 0.003–0.008 ergs cm^{-2} s^{-1}.

Recently, *Herbert and Hall* [1996] have examined the spatial distribution of hot (≲2 eV) H atoms (at the exosphere temperature of 800 K the thermal energy is 0.07 eV) [*Herbert*, 1988; *Stevens et al*., 1993] detected by the Voyager UVS in the extended Uranian H corona [*Broadfoot et al*., 1986]. The extended H corona has significant consequences for the magnetospheric plasma, which can charge exchange with coronal H, resulting in the production of fast neutrals that can escape from the magnetosphere [*Cheng*, 1986; *Krimigis et al*., 1988] or precipitate into the upper atmosphere [*Ip*, 1987; *Bhardwaj and Singhal*, 1993; *Bhardwaj*, 1997b]. The H corona density distribution has a radial profile ∝ $1/r^2$, which is characteristic of an escaping population with high temperature $T_{\text{nonthermal}} \gg T_{\text{thermal}}$. The nonthermal H coronal density is higher on the sunlit side (typically 400–500 cm^{-3} at 2 R_U) than on the nightside (200–300 cm^{-3} at 2 R_U) [*Herbert*, 1988; *Herbert and Hall*, 1996]. The hot H density distribution is found to maximize near the dayside (north) magnetic pole, with the minima near the darkside (south) magnetic pole (see Figure 33). The ratio of about 5:2 of the H densities between the two poles is approximately the same (~2:1) as obtained for the ratio of the total brightness of the two UV auroras [*Herbert and Sandel*, 1994] and is also consistent with the 1:2 ratio of the magnetic field strengths of the north and south magnetic poles. The coincidence between the UV auroral intensity ratio and hot H coronal density ratio at the two poles probably indicates a common source of the

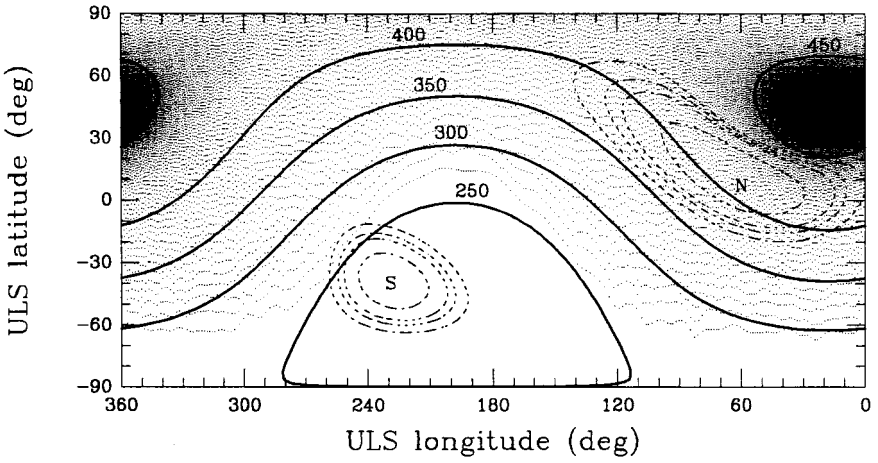

Figure 33. Density map of the H corona of Uranus at 2 R_U derived from Voyager UVS observations of Lyman α emissions, with solid contours labeled in per cubic centimeters, and with L values of 10, 5, 4, and 3 indicated (proceeding outward from each magnetic pole) [*Herbert and Hall*, 1996, Figure 3]. The uncertainty in density is estimated to vary from ±50 cm^{-3} near the equator to ±90 cm^{-3} near the poles. At the time of the Voyager 2 flyby the northern hemisphere was sunlit.

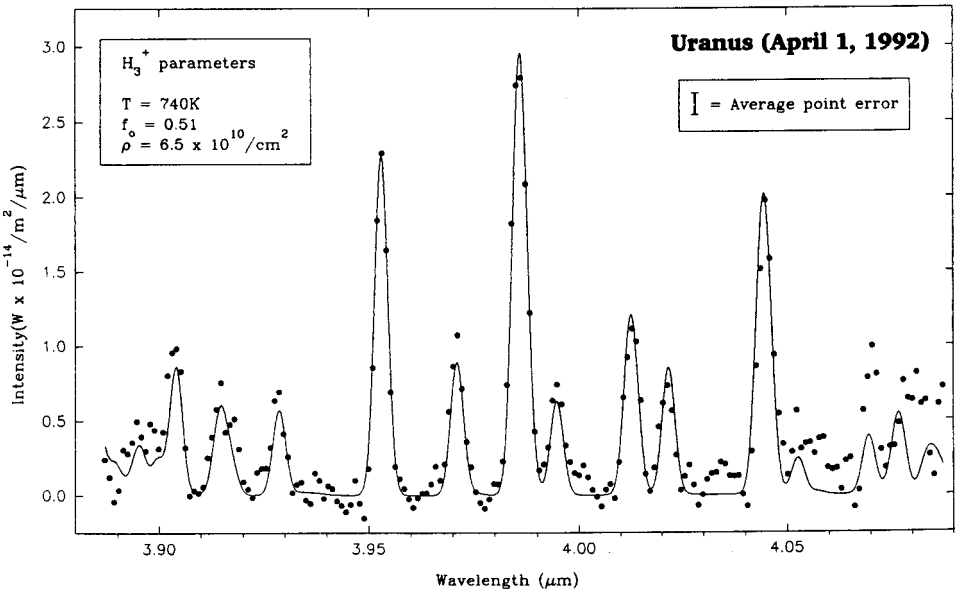

Figure 34. Spectrum of Uranus from 3.89 to 4.09 μm observed on April 1, 1992 (dots), compared with best fit H_3^+ spectrum (solid line), with parameters listed [*Trafton et al.*, 1993, Figure 1]. Reprinted with permission from the American Astronomical Society.

production of these two. However, such a conclusion is hampered by the statistical constraints of the data. Other possible sources of the nonthermal H corona investigated by *Herbert and Hall* [1996] are Jeans escape, solar EUV dissociation of H_2, electroglow, auroral plasma sheet H^+ cascade [*Herbert*, 1993], satellite tori, charge exchange of polar wind H^+ with thermospheric H, and exothermic ionospheric reactions. On the basis of geometric, energy, and power constraints they suggested that the most plausible sources are aurora and electroglow, in order of preference. Another possible source of the nonthermal H atoms could be ionospheric protons accelerated in the auroral region by wave-particle interactions and electric fields [*Bhardwaj and Singhal*, 1993], which should also be explored. Recently, *Gao et al.* [1998] presented results showing how the octupole component terms (OCT) magnetic field model (which combines the Q3 magnetic field model with an octopole component) provides a much better correspondence with the FUV auroral emissions observed by the Voyager UVS.

5.2. H_3^+ Emissions

Uranus was the second of the giant planets (after Jupiter) from which H_3^+ emissions were detected. On April 1, 1992, *Trafton et al.* [1993] detected 11 emission features of the H_3^+ fundamental vibrational-rotational band at 3.89–4.09 μm, using the CGS4 spectrometer on the UKIRT telescope, in perhaps one of the purest H_3^+ spectra ever recorded (see Figure 34). Peak intensities were a few percent of those normally measured in the Jovian auroral spectrum. Fitting of the spectrum using the parameters of *Kao et al.* [1991] implied a rotational temperature of 740 ± 25 K, a vertical column density of 6.5×10^{10} cm^{-2} (±10%), and an ortho-H_3^+ fraction of 0.51 ± 0.03. Trafton et al. estimated a planet-wide total H_3^+ emitted power of 5×10^{10} W, which is considerably larger than the UV emitted auroral power of ~3–7 × 10^{10} W.

Attempts to look at the distribution of H_3^+ emissions on Uranus are very difficult because of the small angular size of the planet. *Lam et al.* [1997b] recorded a series of images in the 3- to 4-μm region in April 1993. These images show H_3^+ emissions over the entire disk but also pronounced structure suggestive of enhanced auroral activity in the region about the magnetic pole. However, the spatial variation on Uranus is more limited than in the case of Jupiter. Because of the uncertainty in the period of rotation of Uranus, the positions of the magnetic poles are not known with sufficient accuracy to allow unambiguous correlation of the region of strongest emission with the north magnetic pole. It seems that auroral activity on Uranus plays a far less significant role in the production of H_3^+ compared with the situation at Jupiter. The overall brightness of H_3^+ emissions of Uranus is found to vary by a factor of 2 on a timescale of years [*Lam et al.*, 1997b]. *Lam et al.* [1997b] have suggested that the H_3^+ emissions are dominated on Uranus by a planet-wide dayglow rather than are associated with the polar regions. This suggestion has been supported in recent observations by *Trafton et al.* [1999], which indicate that the typical auroral contribution is no more than 20% of the total H_3^+ emission from Uranus. Trafton et al. also measured H_2 quadrupole emissions from Uranus and showed that both H_3^+ and H_2 emissions display a significant dependence on solar flux variations.

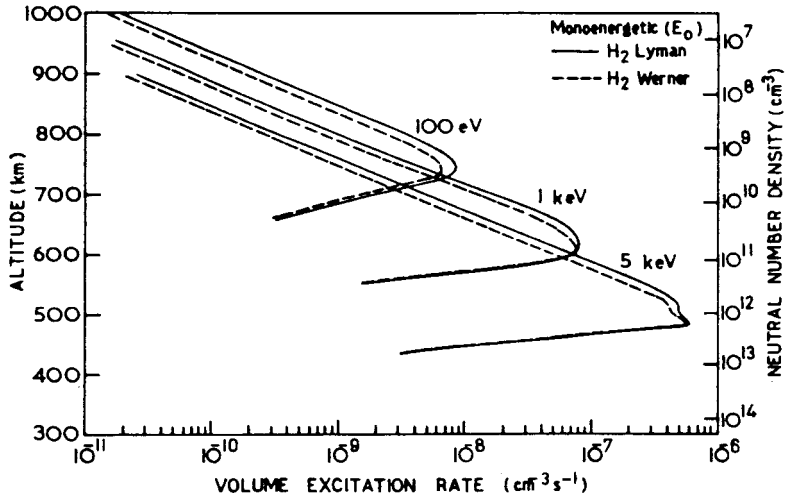

Figure 35. Calculated volume excitation rates for the Lyman and Werner bands of H_2 at three monoenergetic unit fluxes (E_0) [*Bhardwaj and Singhal*, 1990, Figure 7]. Reprinted with permission from the *Indian Journal of Radio and Space Physics*.

6. NEPTUNE

6.1. Early Work

Since polar auroras had been observed on the other three outer planets, it was logical in the pre-Voyager period to expect that an aurora should be present on Neptune too. This expectation seemed quite reasonable because Neptune was anticipated to have a substantial magnetic field [*Curtis and Ness*, 1986; *de Pater and Goertz*, 1989], along with the well-known fact that Neptune possesses a dense atmosphere [*Clarke*, 1988; *Cheng*, 1989; *Shingawa and Waite*, 1989; *Bhardwaj and Singhal*, 1990]. *Curtis and Ness* [1986] predicted an equatorial cloud-top field for Neptune of 0.4–0.5 G using a planetary dynamo model. From simulation studies of Neptune's synchrotron radiation, which were observed from Earth at 20 cm, together with energy budget considerations, *de Pater and Goertz* [1989] estimated a magnetic field strength of 1–2 G.

However, prior to the closest approach of Voyager, the lack of detectable radio and UV emissions at 0.4 AU from Neptune by Voyager, and the absence of significant UV emissions in the IUE data [*Clarke*, 1988], caused some doubts [*Dessler and Sandel*, 1989]. This prompted *Dessler and Sandel* [1989] to propose a "quiescent" magnetosphere for Neptune. Other alternatives suggested at that time for the absence of auroral-magnetospheric activity included (1) the presence of a large methane abundance in Neptune's upper atmosphere to cloak the auroral UV emissions, (2) a weak or negligible magnetic moment, or (3) the orbit of Neptune lying beyond the heliospheric shock front [*Suess and Dessler*, 1985], thereby excluding the presence of an Earth-like aurora driven by solar wind–driven convection. *Cheng* [1989] speculated that inverted-V events might be observed by Voyager over Neptune's auroral zones at energies of several tens of keV.

Since Uranus and Neptune orbit around the Sun at large distances and are more similar in size and composition, *Bhardwaj and Singhal* [1990] assumed that the energy flux of precipitating electrons on Neptune might be of the same order as that on Uranus. Taking the energy flux as 0.9 ergs cm^{-2} s^{-1} on Neptune (the same as on Uranus), they predicted the auroral H_2 band intensity on Neptune to be about 900 R (see Figure 35 for excitation rates of H_2 bands). On the basis of relatively much lower strength of H I Lyman α emission observed by IUE from Neptune, *Clarke* [1988] suggested that polar auroras might be weak on Neptune, although he did not rule out an active Neptunian magnetosphere. *Curtis* [1988] argued that if the magnetic field of Neptune was not tilted and offset similar to the Uranian magnetic field, then Neptune would lack a major source of auroral precipitation, which in turn would imply a much colder exospheric temperature of ~200 K at Neptune.

6.2. Ultraviolet Emissions

During the Voyager 2 flyby of Neptune the UVS detected extremely weak emissions from the nightside of the planet at longitudes of ~30° and 200°W (see Figure 36) classified as "auroral emissions" by *Broadfoot et al.* [1989]. The integrated intensity in the 96.7- to 111.5-nm wavelength band was ~10 R. No H I Lyman α emissions were detected from the nightside because the expected brightness was below the detection limit of the instrument. The presence of an aurora on Neptune was also supported by Voyager measurements of plasma wave [*Gurnett et al.*, 1989] and radio [*Warwick et al.*, 1989] emissions as well as by the charged particle population experiments [*Krimigis et al.*, 1989]. The UV aurora radiates ~5×10^7 W, implying an input power of precipitating particles ~10^9 W (i.e., 2–3 orders of magnitude less than at Uranus). *Broadfoot et al.* [1989] proposed a

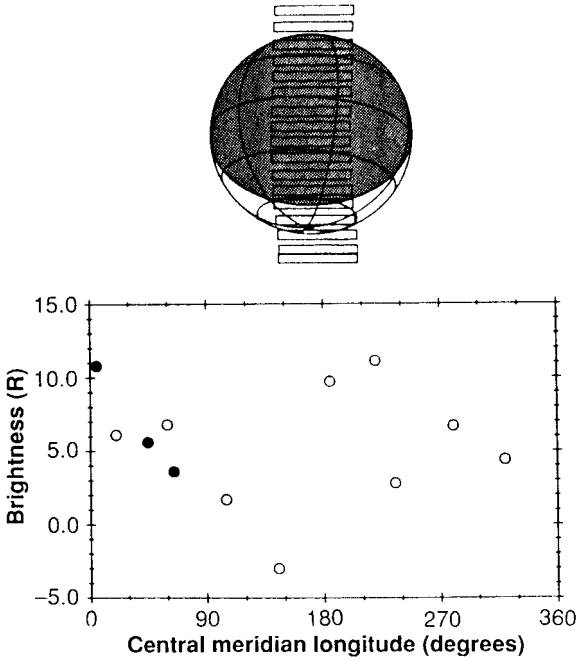

Figure 36. Voyager UVS observations of H_2 (96.7–111.5 nm) emissions from the nightside of Neptune, shown as a function of central meridian longitude [*Broadfoot et al*., 1989, Figure 5]. The observations consisted of north-south scans, as indicated in the top diagram, with the data selected to avoid the sunlit crescent. The solid circles are from the beginning of a second 16.06-hour rotation of Neptune. Reprinted with permission from *Science*.

centrifugally driven torus model in which the energy source for Neptune's aurora is plasma mass loading and/or outward transport in the Triton torus (see Figure 37), requiring a plasma source of around 1 kg s^{-1} if corotation is maintained out to 20 R_N. However, the model of *Cheng* [1990a] showed that the Triton torus plasma source is much smaller and hence the centrifugally driven torus model is unable to power Neptune's aurora. Cheng proposed that Neptune's aurora may be driven by a solar wind–Neptune interaction generating field-aligned currents and producing field-aligned potential drops above the polar caps. He showed that solar wind interactions could, in principle, provide a power of 3.2×10^{11} W incident on a circle of 26 R_N radius, for $n_{sw} = 0.0045$ cm^{-3} and $v_{sw} = 403$ km s^{-1}, given an efficiency for converting solar wind power to emissions of about 0.3% (about one third the value at Earth).

Sandel et al. [1990] investigated the latitudinal and longitudinal distribution of the nightside H_2 emissions (96.7–111.5 nm) of Neptune. Two distinct types of Neptunian auroral emissions were found (see Figure 38). The first, a spatially distributed emission with almost uniform brightness, extends from 55°S to 50°N latitude and longitudes of 0°–60°W. These emissions are weak, with integrated intensity over the wavelength range and field of view of ~2.5 R, corresponding to an emitted power of 6×10^7 W for the areal coverage of 13% of the planet's surface. The second, a more localized emission in both longitude and latitude, was confined mainly in the southernmost latitudes at ~240°W, with an integrated intensity of about 5 R over the same band pass. Although the brightness of this region was larger, the UVS spectrum is of poorer quality because of a smaller integration time. The spectrum is consistent with H_2 band emissions, but the level of confidence is lower than for the diffuse type emissions. Assuming an emitting area of 2.5% of the surface, the emitted power is 2×10^7 W.

The more localized and brighter auroral emissions from the southern magnetic latitudes may be a classical aurora. This interpretation is supported by the observations of the characteristics of the magnetospheric plasma population [*Krimigis et al*., 1989] and nonthermal radio

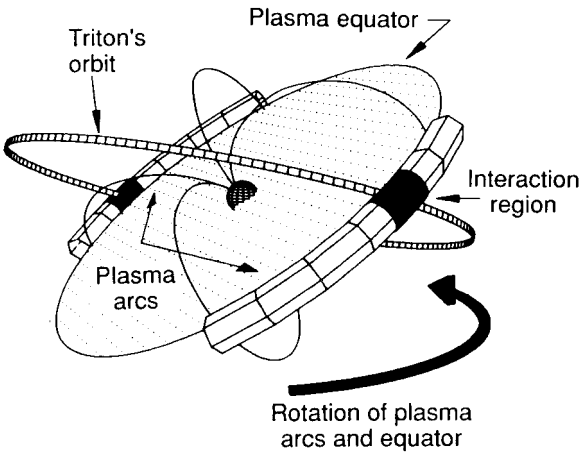

Figure 37. Diagram showing the possible formation of plasma arcs at 140°–210°W and 310°–25°W, due to the ionization of gases escaped from Triton (tilted 21° with respect to Neptune's equator) as they encounter the plasma equatorial plane (which rotates with the planet but is canted at a large angle (here shown as 40°) to the equator) [*Broadfoot et al*., 1989, Figure 6]. Reprinted with permission from *Science*.

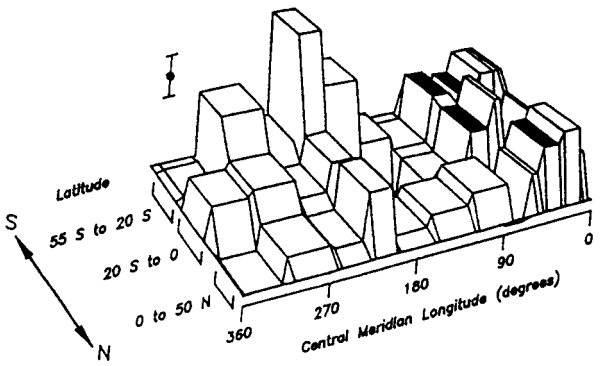

Figure 38. Voyager UVS map of H_2 96.7- to 111.5-nm emissions from the dark side of Neptune [*Sandel et al*., 1990, Figure 1]. The large peak near 240° CML is thought to be a southern hemisphere aurora; the latitudinally broad region of emission near 0°–60° CML may be due to precipitation of conjugate photoelectrons from the daylit side of the planet.

emissions [*Gurnett et al*., 1989; *Warwick et al*., 1989] of the type normally associated with auroral particle acceleration. This interpretation implies a brighter aurora at the northern pole, owing to weaker field strength there, which escaped detection because the 51°N latitude of that pole places it mostly outside the viewing area of UVS. Thus we lack a reliable measurement of auroral emission from the northern pole.

Sandel et al. [1990] proposed, following the suggestion of *Broadfoot et al*. [1989], that the brighter and spatially confined component of the aurora could be powered by Neptune's rotational energy extracted from Neptune's ionosphere through its electrodynamical coupling with Triton's plasma arcs [cf. *Hill and Dessler*, 1990]. The implied upper limit for mass loading of the magnetosphere by Triton is estimated to be $\sim$1 kg s^{-1}. The consequences of such a mass loading rate for convection in Neptune's magnetosphere are discussed by *Hill and Dessler* [1990], who concluded that a mass loading rate of this magnitude is consistent with results from the Voyager PLS and LECP [*Belcher et al*., 1989; *Krimigis et al*., 1989].

However, *Cheng* [1990a] estimated a net injection rate of only $\sim$45 g s^{-1} for H^+ (taking charge exchange and gravity into account) and $\sim$6 g s^{-1} for N^+ (scaling from the inferred injection rate in the Saturn system from Titan) and therefore argued that the injection rates are too low (compared with $\sim$1 kg s^{-1}) to drive the aurora. He suggested that Neptune's aurora is driven mainly by the solar wind via a low-latitude boundary layer (LLBL) interaction [*Cheng*, 1989].

Mauk et al. [1991] have conjectured that the more localized and brighter auroral emissions from the southern magnetic latitudes are caused by the diffuse precipitation of energetic electrons trapped at L values $\gtrsim 8\,R_N$. The observed electrons in the $L > 8\ R_N$ region have broad pitch angle distribution, and the analysis of *Mauk et al*. [1994] suggested that pitch angle scattering can fill up the pitch angle distribution in about 2 hours. The emission energy flux observed by the Voyager UVS is $\sim 10^{-4}$ ergs cm^{-2} s^{-1}, which requires (according to the conversion efficiencies of *Sandel et al*. [1990]) an electron input power of greater than 10^{-3} ergs cm^{-2} s^{-1}. The required auroral power could be obtained from a trapped electron population with $\sim$0.03% of the trapped radiation belt intensities, since the hot electrons observed by the LECP experiment [*Krimigis et al*., 1989; *Cheng et al*., 1991], if isotropic, could deliver up to $\sim$3 ergs cm^{-2} s^{-1} of power to the atmosphere [*Mauk et al*., 1991]. Also, the $L > 8\ R_N$ regions map onto Neptune's surface with a size of $\sim$3.2% of the planets surface for each hemisphere with central dipole. This value agrees well with the size of the auroral emission region of $\sim$2.5% seen by the UVS [*Sandel et al*., 1990]. The study of *Mauk et al*. [1994] indicated that the pitch angle scattering rate of energetic electrons near $L = 8\ R_N$ is large enough to cause electrons to precipitate in sufficient quantities to power the aurora. These authors proposed that this brighter component of Neptune's aurora is analogous to the diffuse aurora at Earth.

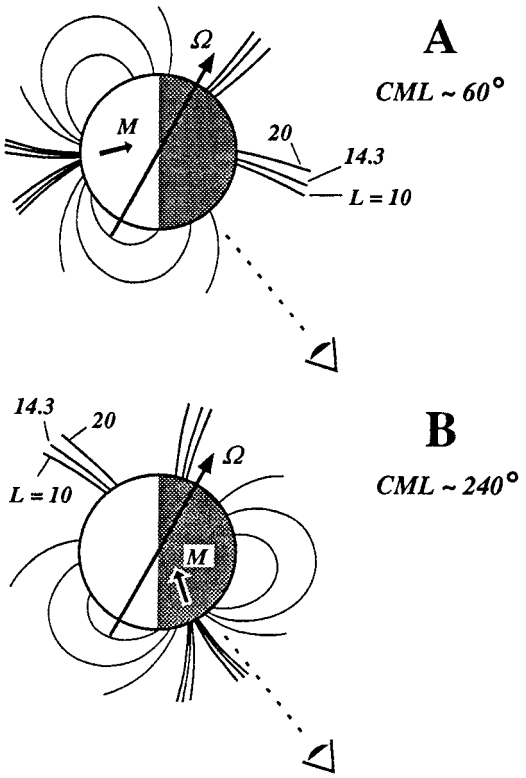

Figure 39. (a) Diagram showing how the Voyager UVS observations near 60° CML would tend to see emissions from conjugate photoelectrons produced on the daylit side of Neptune, while (b) those taken near 240° CML see more of an open-field-line configuration with few emissions [*Sandel et al*., 1990, Figure 2].

For the latitudinally diffuse nightside emissions, which are not consistent with usual auroral morphology, two alternative models have been proposed. *Sandel et al*. [1990] suggested that the diffuse emissions are excited by photoelectrons precipitating from the magnetically conjugate sunlit hemisphere. The order of magnitude estimates made by Sandel et al. showed that this mechanism requires an overall solar flux to emission conversion efficiency of $\sim$0.5% (scaling the solar photon flux with energies >30 eV at 1 AU to the heliocentric distance of Neptune), which seemed not unreasonable, but no detailed model calculations have been performed to assess quantitatively the effectiveness of the proposed photoelectron excitation mechanism. This mechanism will occur only in the nearly pole-on configuration (see Figure 39) that occurs once each Neptune rotation. (The orientation of Neptune's spin axis (28.8° obliquity) coupled with the large magnetic tilt angle (46.8°) allows Neptune's magnetosphere to change every 8 hours (a half rotation) from an "Earth-like" magnetosphere with two polar cusps to a "pole-on" magnetosphere with only one polar cusp. One consequence of such a magnetospheric geometry is that every half rotation Neptune's magneto-

TABLE 2. Comparative Emitted Power at Different Wavelengths in Giant Planet Auroras

Emission	*Jupiter*	*Saturn*	*Uranus*	*Neptune*
X rays (0.1–3 keV)	~1–4 GW[a]	<5–15 GW	NIA	NIA
FUV[b] (80–180 nm)	2–10 TW	≤50 GW	≤40 GW	≤100 MW
Visible (385–1000 nm)	~10–100 GW	NIA	NIA	NIA
IR (H_3^+) (3–4 μm)	4–8 TW	~150–300 GW	~250 GW	<12 GW
IR (hydrocarbons) (7–14 μm)	~40 TW	NIA	NIA	NIA
Radio (10 kHz to a few megahertz)	~10 GW[c]	~1 GW	~30 MW	~20 MW

NIA, no information available.
[a]A 3σ upper limit for X-ray emissions at 27–48 keV is 0.11–0.56 GW [*Hurley et al*., 1993].
[b]Galileo UVS data indicate that MUV (162–320 nm) auroral emissions from Jupiter contain about 8 times less flux than FUV auroral emissions [*Pryor et al*., 1998].
[c]Jupiter's decametric emission power is ~100 GW [*Zarka*, 1998].

tail changes between a planar plasma sheet (where the plasma currents close over the tail magnetopause) as at Earth, and a cylindrical one (where the plasma currents close entirely within the magnetospheric cavity) [*Ness et al*., 1989; *Voigt and Ness*, 1990]). Recently, the use of a more accurate magnetic field model has confirmed the suggestion of *Sandel et al*. [1990] and also showed that a region near the southern bright aurora is also magnetically conjugate to the dayside hemisphere [*Bishop et al*., 1995].

Cheng [1990b] proposed an alternative model to account for the diffuse emissions. According to this model, the emissions are generated due to the excitation caused by the precipitation of energetic charged particles (electrons and protons) in the magnetic anomaly region (a region of anomalously low surface magnetic field), which arises from the large offset and tilt of Neptune's dipole magnetic field [*Ness et al*., 1989]. On Neptune's surface this anomaly region extends from 51°N, 48°W (the north magnetic pole) to 38°S, 167°W (on the magnetic equator). The energetic trapped particles drifting along the magnetic field lines precipitate into Neptune's atmosphere after being transported radially into the atmospheric drift-shadow region, where they encounter the weak-field region (i.e., the "windshield wiper" effect). In the model of *Cheng* [1990b] the latitudinally diffuse emissions peaking around 0°–60°W longitude are excited by westward drifting electrons precipitating at the eastern edge of the magnetic anomaly region. The protons drift to the east, and they precipitate on the other side of the western longitude, possibly accounting for the enhanced UV emission near 240°W. This scenario of an atmospheric drift-shadow precipitation pattern is supported by the observations of energetic particle dropouts seen in the Voyager LECP experiment data [*Krimigis et al*., 1989; *Mauk et al*., 1990] and the agreement between the required precipitating power and what can be explained by anomaly precipitation [*Cheng*, 1990b].

Paranicas and Cheng [1994] followed up on the work of *Cheng* [1990b] using the O8 model of Neptune's magnetic field. With the new model, drift L shell footprints are found to have unusual morphologies, with cusps, thin necks, and double loops forming over the planet at 1 R_N. Using test particles launched uniformly from near Neptune, the precipitation pattern at the planet matched the UVS observations of *Sandel et al*. [1990] quite well, with normal auroral precipitation occurring near the 30°S pole and magnetic-anomaly precipitation (low surface magnetic field, as in Earth's South Atlantic anomaly region) in the 0°–90° longitude region. This model predicts precipitation in regions not measured by the Voyager UVS: near 90°W and south of 55°S, near 45°W and northward of 55°N, and weak precipitation above 60°N over a range of longitudes near 200°W.

Recently, *Huang et al*. [1998] modeled the drift of particles in Neptune's plasmasphere and showed that even with pitch angles of near 90°, low-energy (tens of eV) particles will precipitate into the atmosphere as they drift around the magnetic equator. These particles could also contribute to the observed UV emissions.

In summary, there are several models proposed for each of the two types of auroral emissions, but it remains to be established which of these mechanisms actually dominates the aurora on Neptune. The resolution would appear to require more refined knowledge of the magnetic field geometry close to Neptune, in terms of both locating the magnetic poles and improving the surface-to-surface mappings (see *Connerney et al*. [1993] for a review). At present, the low signal-to-noise ratio of the available UVS data makes it difficult to choose among the various suggested mechanisms. Since no space mission is planned for Neptune in the near future, we will have to concentrate our efforts on making remote sensing observations from ground- and satellite-based instruments to further our understanding of auroral processes on Neptune.

6.3. H_3^+ Emissions

Trafton et al. [1993] attempted to detect H_3^+ emissions from Neptune a night after their successful detection of Uranus. No lines were detected in the 3.9- to 4.1-μm spectrum despite integrating for nearly an hour. *Trafton et al*. [1993] placed upper limits of 5×10^{-18} W m^{-2} for H_3^+ line fluxes from Neptune, which are several times greater than the typical H_3^+ line strengths detected from

TABLE 3. Summary of Characteristics of UV Auroras on the Giant Planets

Property	*Jupiter*	*Saturn*	*Uranus*	*Neptune*
Emissions observed	H_2 (80–170 nm), H Ly α; V1, V2 H_2 (115–170 nm), H Ly α; IUE, HST H_2 (83–170 nm), H Ly α; HUT H_2 (85–250 nm), H Ly α; GLL	H_2 (80–170 nm), H Ly α; V1, V2 H Ly α; IUE H_2 (115–170 nm), H Ly α; HST	H_2 (88–112 nm), H Ly α; V2 H Ly α; IUE	H_2 (98–112 nm); V2
Surface brightness[a]	H_2, ~100–500 kR (up to ~2 MR) H Ly α, ~50–150 kR	H_2, ~10–100 kR (up to ~150 kR) H Ly α, ~2–20 kR	H_2, ~10 kR H Ly α, ~1.5 kR	diffuse, ~2.5 R discrete, ~5 R
Emitted power	~2–10 TW	≲50 GW	≲40 GW	≲0.1 GW
Basic morphology	continuous ovals at each pole; approximately corotating; main ovals near $L \sim 15$–30; morning shows single narrow arc (~200–2000 km wide); afternoon shows multiple arcs (with emission inside polar cap); emission altitude ~240 km	high-latitude (~80°) ovals; brightest in morning sector; emission altitude ~1000 km	emissions from both poles at 60°–65° magnetic latitude; brightest at ~180° longitude; northern aurora ~2–4 times brighter than southern aurora	diffuse emissions at 55°S–55°N, 0°–60° longitude (13% of surface); discrete emissions at high southern latitudes, 180°–270° longitude (2.5% of surface)
Generation scenario	e^- precipitation at $L \sim 15$–30; primary e^- energy ~10–50 keV (penetrates CH_4 homopause), with e^- flux ~30–300 ergs cm^{-2} s^{-1}; S and O ion precipitation at $L \sim 8$–12 produces X-ray emissions	e^- precipitation; primary e^- energy ≲10 keV, with e^- flux ~1 erg cm^{-2} s^{-1}; possible N ion precipitation (originating from Titan)	e^- precipitation at $L \sim 5$–10; primary e^- energy ≲10 keV, with e^- flux ~1 erg cm^{-2} s^{-1}	e^-, ion precipitation (N^+ from Triton); possible sources are conjugate photoelectrons (diffuse) and whistler-induced pitch angle scattering (discrete)
Related observations	UV-dark, high-altitude haze (likely aurorally produced)	UV-dark, high-altitude haze (likely aurorally produced); maximum haze UV-absorption 5°–8° equatorward of main oval	peak N and S UV brightness coincident with maxima in whistler-mode plasma waves and 22- to 35-keV e^- flux	

The various auroral-UV observing platforms are V1, Voyager 1; V2, Voyager 2; IUE, International Ultraviolet Explorer; HST, Hubble Space Telescope; HUT, Hopkins Ultraviolet Telescope (part of the Astro-1 and Astro-2 space shuttle missions); and GLL, Galileo.

[a]The rayleigh (R) is a unit of surface brightness equivalent to 10^6 photons cm^{-2} s^{-1} $4\pi sr^{-1}$.

TABLE 4. Summary of Characteristics of H_3^+ Auroras on the Giant Planets

Property	*Jupiter*	*Saturn*	*Uranus*
Wavelength	2 μm, 3–4 μm	3–4 μm	3–4 μm
Emitted power	4–8 TW	~150–300 GW	~250 GW
Morphology and related information	highly localized near auroral ovals (typically 80% of emissions from aurora, 20% from disk); continuous oval near $L = 30$ at each pole; derived $T \sim 650$–1100 K, $N(H_3^+) \sim 10^{12}$ cm^{-2}; emitting region about 500–1000 km above the $P = 1$-bar level, with an emission scale height of about 200–1000 km; similar brightnesses are observed at each pole; brightness variations seem to correlate with solar wind ram pressure	highly localized near auroral ovals (few percent disk emissions); derived $T \sim 800$ K, $N(H_3^+) \sim 10^{11}$ cm^{-2}; emissions are ~100 times less intense than at Jupiter (even weaker than from Uranus); emissions comparable in strength to the brightest observed UV emissions	widely distributed over disk (only ~20% auroral emissions); derived $T \sim 670$–740 K, $N(H_3^+) \sim 10^{11}$ cm^{-2}; variable by factor of 2 over timescale of years, similar to solar cycle; brightness ~5–10% of Jupiter
Generation mechanism	particle precipitation from $L = 6$–30 region, resulting in H_2^+ production, followed by chemical reaction to form excited H_3^+	particle precipitation at high latitudes, producing H_2^+, followed by chemical reaction to form excited H_3^+	solar EUV photoionization of H_2, followed by chemical reaction to form excited H_3^+; minor contribution from particle precipitation

Saturn. A subsequent, longer observation of Neptune by T. Geballe and coworkers also failed to detect any H_3^+ emissions [*Tennyson*, 1995]. Given the unusually weak auroral activity on Neptune as observed by the Voyager UVS (i.e., 2–3 orders of magnitude less than at Uranus), it is perhaps unsurprising that no H_3^+ emissions on Neptune have been detected so far. Note that the magnetic field strength at Neptune is about half that at Uranus, and being 10 AU farther from the Sun than Uranus, Neptune receives only about 35% of the solar wind flux at Uranus. Compounding the detection difficulty is the fact that Neptune is only one third the solid angle of Uranus when viewed from Earth.

7. SUMMARY

We have reviewed some of the history of auroral observations of the giant planets, with the intent of summarizing the last 2 decades or so of work in this area of planetary science. As was mentioned in the introduction, owing to the impressive advances being made in observing technology (primarily the instrumentation of HST but also many other spacecraft and ground-based facilities), the discipline of planetary auroral research has a wealth of excellent data, which are resulting in a rapid evolution of our understanding. With the recent launch of the Chandra X-ray and FUSE EUV satellites, this trend is very likely to continue for years to come. The future version of HST, the next generation space telescope, when realized sometime in the first or second decades of the new millennium, will also enhance our aurora-studying capability by providing even higher spatial resolution data from the giant planets.

After providing the history of auroral observations at each of the giant planets, we close this review by briefly outlining our current understanding of the subject, through the use of some comparative tables. Table 2 compares estimates of the total emitted power from each planet as a function of spectral region. It is clear that Jupiter is the auroral powerhouse among the giant planets, especially at IR and FUV wavelengths (for comparison, the current world energy consumption is about 13 TW [*Doman et al.*, 1999]). It is likely that much of the huge 7- to 14-μm IR output of Jupiter not only results from energetic particle impact, but is also supplemented by Joule heating. Saturn and Uranus are of comparable strength, each emitting a few percent of what Jupiter puts out. Neptune appears to have an intrinsically weak aurora, although its radio output is comparable to that of Uranus.

The major characteristics of the giant-planet UV auroras are compared in Table 3. The descriptions of morphology for Jupiter and Saturn may be compared with Plate 1. It is currently believed that most of the UV emissions on each of the giant planets are the result of energetic electron precipitation, with perhaps a small contribution from energetic heavy ion precipitation (S and O from Io at Jupiter; perhaps N at Saturn and Neptune from Titan and Triton, respectively). Brightness estimates for FUV auroral emissions from Jupiter have been generally increasing over the years, from tens to hundreds or even thousands of kilorayleighs, as ob-

TABLE 5. Characteristics of the Io Flux Tube Footprint at UV, Visible, Near IR, and Radio Wavelengths

Property	*Ultraviolet*[a,b,c,d] *(H_2)*	*Visible*[e] *(385–935 nm)*	*Infrared*[f] *(H_3^+)*	*Radio*[g] *(Decametric S-Bursts)*
Size	400^{+100}_{-200} km[b] 1000–2000 km[c]	300 × 500 km	N/A	1000–2000 km
Brightness	50–300 kR[c,d]	250–460 kR	N/A	10^{-18}–10^{-16} W m^{-2} Hz^{-1} at 1 AU
Lag angle with respect to instantaneous Io flux tube footprint	0°–10°[c,d] <15°[a,b] (variable)	N/A	15°–20° (variable)	10°–20° (variable)
Energy of precipitating particles	e^-, 1–200 keV[a] H^+, 25–500 keV	N/A	N/A	e^-, ~5 keV
Emitted power	5×10^{10} W[a,b]	3×10^8 W	3–10 × 10^{10} W	10^8–10^9 W
Incident power	0.8–5 × 10^{11} W[b]	N/A	2–4 × 10^{11} W	≥10^{11} W
Remarks	factor of ~6 variation in brightness with time, north footprint slightly brighter than south			duration, 50–100 ms bandwidth, ~10 kHz T_B, ≥10^{17} K emitted flux, 10% of Io decametric frequencies, ~0.5 to −40 MHz

N/A, not available.
[a]*Prangé et al*. [1996].
[b]*Prangé et al*. [1998].
[c]*Clarke et al*. [1996].
[d]*Clarke et al*. [1998].
[e]*Ingersoll et al*. [1998].
[f]*Connerney et al*. [1993].
[g]*Zarka* [1998].

servations at higher spatial resolution reveal narrower arcs than previously assumed.

A summary of the H_3^+ auroral characteristics observed for Jupiter, Saturn, and Uranus (Neptune is currently undetected, in keeping with its intrinsic auroral weakness) is provided in Table 4. On Jupiter and Saturn the emissions are highly localized in the auroral regions, so that they are believed to result when H_3^+ ions are created by auroral ion chemistry. On Uranus, however, the emissions are widespread and may be due to solar EUV production of H_3^+.

Finally, we present in Table 5 a list of multispectral characteristics of the Io flux tube footprint emissions, which may be considered an aurora of sorts. The IFT footprint is apparent as a spot of emission equatorward of the main auroral oval (in both the north and south) in H_2 FUV emissions in Plate 1 (the nature of the UV emission composing the extended tail stretching "downstream" from the IFT footprint is currently a mystery), in H_3^+ IR emissions in Plate 6, and in visible emissions [*Ingersoll et al*., 1998]. Since the position of Io is well known, the IFT footprint location provides a useful fiducial mark for evaluating models of Jupiter's inner magnetic field [e.g., *Connerney et al*., 1998].

Tables 2–5 show that while not much is known yet about the auroras of Uranus and Neptune, and not much more is known about Saturn (although the Cassini mission will soon change this), for Jupiter there is an impressive number of data, much of which are waiting to be analyzed in detail. A comprehensive understanding of auroral physics on the giant planets is still a long way off. However, we hope that by presenting the key results from X-ray, UV, and IR observations in summary form, we will facilitate the eventual development of such an understanding.

ACKNOWLEDGMENTS. We thank J. H. Waite Jr. and W. S. Lewis for many useful discussions and the referees for many helpful suggestions.

James Horwitz was the Editor responsible for this paper. He thanks Jane Fox and one anonymous reviewer for the technical review and Bridget Scanlon for the cross-disciplinary review.

REFERENCES

Abgrall, H., E. Roueff, F. Launay, J.-Y. Roncin, and J. L. Subtil, Table of the Lyman band system of molecular hydrogen, *Astron. Astrophys. Suppl. Ser*., *101*, 273–321, 1993a.

Abgrall, H., E. Roueff, F. Launay, J.-Y. Roncin, and J. L. Subtil, Table of the Werner band system of molecular hydrogen, *Astron. Astrophys. Suppl. Ser*., *101*, 323–362, 1993b.

Abgrall, H., E. Roueff, X. Liu, and D. E. Shemansky, The emission continuum of electron-excited molecular hydrogen, *Astrophys. J*., *481*, 557–566, 1997.

Achilleos, N., S. Miller, J. Tennyson, A. D. Aylward, I. Mueller-Wodarg, and D. Rees, JIM: A time-dependent, three-dimensional model of Jupiter's thermosphere and ionosphere, *J. Geophys. Res*., *103*, 20,089–20,112, 1998.

Ajello, J. M., I. Kanik, S. M. Ahmed, and J. T. Clarke, Line profile of H Lyman α from dissociative excitation of H_2 with application to Jupiter, *J. Geophys. Res*., *100*, 26,411–26,420, 1995.

Ajello, J. M., et al., Galileo orbiter ultraviolet observations of Jupiter aurora, *J. Geophys. Res*., *103*, 20,125–20,148, 1998.

Akasofu, S.-I., The aurora, in *Light From the Sky: Readings From Scientific American*, pp. 13–20, W. H. Freeman, New York, 1980.

Anglin, J. D., J. R. Burrows, J. L. Mu, and M. D. Wilson, Trapped energetic ions in Jupiter's inner magnetosphere, *J. Geophys. Res*., *102*, 1–36, 1997.

Atreya, S. K., *Atmospheres and Ionospheres of the Outer Planets and Their Satellites*, 224 pp., Springer-Verlag, New York, 1986.

Atreya, S. K., and T. M. Donahue, Model ionospheres of Jupiter, in *Jupiter*, edited by T. Gehrels, pp. 304–318, Univ. of Ariz. Press, Tucson, 1976.

Atreya, S. K., Y. L. Yung, T. M. Donahue, and E. S. Barker, Search for Jovian auroral hot spots, *Astrophys. J*., *218*, L83–L87, 1977.

Atreya, S. K., J. H. Waite Jr., T. M. Donahue, A. F. Nagy, and J. C. McConnell, Theory, measurements and models of the upper atmosphere and ionosphere of Saturn, in *Saturn*, edited by T. Gehrels and M. S. Matthews, pp. 239–277, Univ. of Ariz. Press, Tucson, 1984.

Bagenal, F., and J. D. Sullivan, Direct plasma measurements in the Io torus and inner magnetosphere of Jupiter, *J. Geophys. Res*., *86*, 8447–8466, 1981.

Ballester, G. E., Magnetospheric interactions in the major planets, in *Ultraviolet Astrophysics Beyond the IUE Final Archive*, *Eur. Space Agency Spec. Publ*., *ESA-SP-413*, 21–28, 1998.

Ballester, G. E., S. Miller, J. Tennyson, L. M. Trafton, and T. R. Geballe, Latitudinal temperature variations of Jovian H_3^+, *Icarus*, *107*, 189–194, 1994.

Ballester, G. E., et al., Time-resolved observations of Jupiter's far-ultraviolet aurora, *Science*, *274*, 409–413, 1996.

Banks, P. M., C. R. Chappell, and A. F. Nagy, A new model for the interaction of auroral electrons with the atmosphere: Spectral degradation, backscatter, optical emission, and ionization, *J. Geophys. Res*., *79*, 1459–1470, 1974.

Barbosa, D. D., Titan's atomic nitrogen torus—Inferred properties and consequences for the Saturnian aurora, *Icarus*, *72*, 53–61, 1987.

Barbosa, D. D., Bremsstrahlung X-rays from Jovian auroral electrons, *J. Geophys. Res*., *95*, 14,969–14,976, 1990a.

Barbosa, D. D., Bremsstrahlung X ray spectra of Jupiter and Saturn: Predictions for future planetary spacecraft, *Geophys. Res. Lett*., *17*, 1029–1032, 1990b.

Barbosa, D. D., Auroral precipitation flux of ions and electrons in Saturn's outer magnetosphere, *Planet. Space Sci*., *38*, 1295–1304, 1990c.

Barbosa, D. D., Reply to "Comment on 'Bremsstrahlung X-rays from Jovian auroral electrons by D. D. Barbosa' by J. H. Waite Jr.," *J. Geophys. Res.*, *96*, 19,533–19,534, 1991.

Baron, R. L., R. D. Joseph, T. Owen, J. Tennyson, S. Miller, and G. E. Ballester, Imaging Jupiter's aurorae from H_3^+ emissions in the 3–4 μm band, *Nature*, *353*, 539–542, 1991.

Baron, R. L., T. Owen, J. E. P. Connerney, T. Satoh, and J. Harrington, Solar wind control of Jupiter's H_3^+ auroras, *Icarus*, *120*, 437–442, 1996.

Barrow, C. H., and M. D. Desch, Solar wind control of Jupiter's hectometric radio emission, *Astron. Astrophys*., *213*, 495–501, 1989.

Barrow, C. H., F. Genova, and M. D. Desch, Solar wind control of Jupiter's decametric radio emission, *Astron. Astrophys*., *165*, 244–250, 1986.

Belcher, J. W., et al., Plasma observations near Neptune: Initial results from Voyager 2, *Science*, *246*, 1478–1483, 1989.

Ben Jaffel, L., V. Leers, and B. R. Sandel, Dark auroral oval on Saturn discovered in Hubble Space Telescope ultraviolet images, *Science*, *269*, 951–953, 1995.

Berge, G. L., and S. Gulkis, Earth-based radio observations of Jupiter: Millimeter to meter wavelengths, in *Jupiter*, edited by T. Gehrels, pp. 621–692, Univ. of Ariz. Press, Tucson, 1976.

Bhardwaj, A., Airglow on the outer planets, *Sci. Rep. SPL-SR-01-97*, 65 pp., Space Phys. Lab., Vikram Sarabhai Space Cent., Trivandrum, India, 1997a.

Bhardwaj, A., Ring current H atom precipitation on the outer planets, *Adv. Space Res*., *20*(2), 233–237, 1997b.

Bhardwaj, A., and G. R. Gladstone, Auroras on Saturn, Uranus, and Neptune, *Adv. Space Res*., *26*(10), 1551–1558, 2000.

Bhardwaj, A., and R. P. Singhal, Auroral and dayglow processes on Neptune, *Indian J. Radio Space Phys*., *19*, 171–176, 1990.

Bhardwaj, A., and R. P. Singhal, Optically thin H Lyman alpha production on outer planets: Low-energy proton acceleration in parallel electric fields and neutral H atom precipitation from ring current, *J. Geophys. Res*., *98*, 9473–9481, 1993.

Bigg, E. K., Influence of the satellite Io on Jupiter's decametric emission, *Nature*, *203*, 1008–1010, 1964.

Bishop, J., S. K. Atreya, P. N. Romani, G. S. Orton, B. R. Sandel, and R. V. Yelle, The middle and upper atmosphere of Neptune, in *Neptune and Triton*, edited by D. P. Cruikshank, pp. 427–487, Univ. of Ariz. Press, Tucson, 1995.

Bisikalo, D. V., V. I. Shematovich, J.-C. Gérard, G. R. Gladstone, and J. H. Waite Jr., The distribution of hot hydrogen atoms produced by electron and proton precipitation in the Jovian aurora, *J. Geophys. Res*., *101*, 21,157–21,168, 1996.

Broadfoot, A. L., et al., Extreme ultraviolet observations from Voyager 1 encounter with Jupiter, *Science*, *204*, 979–982, 1979.

Broadfoot, A. L., B. R. Sandel, D. E. Shemansky, J. C. McConnell, G. R. Smith, J. B. Holberg, S. K. Atreya, T. M. Donahue, D. F. Strobel, and J. L. Bertaux, Overview of the Voyager ultraviolet spectrometry results through Jupiter encounter, *J. Geophys. Res*., *86*, 8259–8284, 1981a.

Broadfoot, A. L., et al., Extreme ultraviolet observations from Voyager 1 encounter with Saturn, *Science*, *212*, 206–211, 1981b.

Broadfoot, A. L., et al., Ultraviolet spectrometer observations of Uranus, *Science*, *233*, 74–79, 1986.

Broadfoot, A. L., et al., Ultraviolet spectrometer observations of Neptune and Triton, *Science*, *246*, 1459–1466, 1989.

Burke, B. F., and K. L. Franklin, Observations of a variable radio source associated with the planet Jupiter, *J. Geophys. Res*., *60*, 213–217, 1955.

Caldwell, J., A. T. Tokunaga, and F. C. Gillett, Possible infrared aurora on Jupiter, *Icarus*, *44*, 667–675, 1980.

Caldwell, J., A. T. Tokunaga, and G. S. Orton, Further observations of 8-μm polar brightenings of Jupiter, *Icarus*, *53*, 133–140, 1983a.

Caldwell, J., R. Wagener, T. Owen, M. Combes, and T. Encrenaz, Tentative confirmation of an aurora on Uranus, *Nature*, *303*, 310–312, 1983b.

Caldwell, J., R. Halthore, G. Orton, and J. Bergstralh, Infrared polar brightenings on Jupiter, 4, Spatial properties of methane emission, *Icarus*, *74*, 331–339, 1988.

Caldwell, J., B. Turgeon, and X.-M. Hua, Hubble Space Telescope imaging of the north polar aurora on Jupiter, *Science*, *257*, 1512–1515, 1992.

Carr, T. D., M. D. Desch, and J. K. Alexander, Phenomenology of magnetospheric radio emissions, in *Physics of the Jovian Magnetosphere*, edited by A. J. Dessler, pp. 226–284, Cambridge Univ. Press, New York, 1983.

Cheng, A. F., Energetic neutral particles from Jupiter and Saturn, *J. Geophys. Res*., *91*, 4524–4530, 1986.

Cheng, A. F., Magnetosphere of Neptune: Auroral zone field-

aligned potential drops?, *Geophys. Res. Lett*., *16*, 953–956, 1989.
Cheng, A. F., Triton torus and Neptune aurora, *Geophys. Res. Lett*., *17*, 1669–1672, 1990a.
Cheng, A. F., Global magnetic anomaly and aurora of Neptune, *Geophys. Res. Lett*., *17*, 1697–1700, 1990b.
Cheng, A. F., S. M. Krimigis, B. H. Mauk, E. P. Keath, C. G. Maclennan, L. J. Lanzerotti, M. T. Paonessa, and T. P. Armstrong, Energetic ion and electron phase space densities in the magnetosphere of Uranus, *J. Geophys. Res*., *92*, 15,315–15,328, 1987.
Cheng, A. F., S. M. Krimigis, and L. J. Lanzerotti, Energetic particles at Uranus, in *Uranus*, edited by J. T. Bergstralh, E. D. Miner, and M. S. Matthews, pp. 831–893, Univ. of Ariz. Press, Tucson, 1991.
Clarke, J. T., Detection of auroral hydrogen Lyman-alpha emission from Uranus, *Astrophys. J*., *263*, L105–L109, 1982.
Clarke, J. T., IUE observations of Neptune for H Lyman-α emission, *Geophys. Res. Lett*., *15*, 701–704, 1988.
Clarke, J. T., H. W. Moos, S. K. Atreya, and A. L. Lane, Observations from Earth orbit and variability of the polar aurora on Jupiter, *Astrophys. J*., *241*, L179–L182, 1980.
Clarke, J. T., H. W. Moos, S. K. Atreya, and A. L. Lane, IUE detection of bursts of H Lyman-alpha emission from Saturn, *Nature*, *290*, 226–227, 1981.
Clarke, J. T., et al., Continued observations of the H Ly α emission from Uranus, *J. Geophys. Res*., *91*, 8771–8781, 1986.
Clarke, J. T., J. T. Trauger, and J. H. Waite Jr., Doppler-shifted H Ly α emissions from Jupiter's aurora, *Geophys. Res. Lett*., *16*, 587–590, 1989a.
Clarke, J. T., J. J. Caldwell, T. E. Skinner, and R. V. Yelle, The aurora and airglow of Jupiter, in *Time-Variable Phenomena in the Jovian System*, edited by M. J. S. Belton, R. A. West, and J. Rahe, *NASA Spec. Publ*., *SP-494*, 211–220, 1989b.
Clarke, J. T., L. Ben Jaffel, A. Vidal-Madjar, G. R. Gladstone, J. H. Waite Jr., R. Prangé, J.-C. Gérard, J. Ajello, and G. James, Hubble Space Telescope Goddard High-Resolution Spectrograph H_2 rotational spectra of Jupiter's aurora, *Astrophys. J*., *430*, L73–L76, 1994.
Clarke, J. T., et al., Far-ultraviolet imaging of Jupiter's aurora and the Io "footprint," *Science*, *274*, 404–409, 1996.
Clarke, J. T., et al., Hubble Space Telescope imaging of Jupiter's UV aurora during the Galileo orbiter mission, *J. Geophys. Res*., *103*, 20,217–20,236, 1998.
Clary, R. S., and J. H. Hunter Jr., Hydrogen-alpha auroral activity on Jupiter, *Astrophys. J*., *199*, 517–521, 1975.
Connerney, J. E. P., Magnetic fields of the outer planets, *J. Geophys. Res*., *98*, 18,659–18,679, 1993.
Connerney, J. E. P., and M. D. Desch, Comment on "Evidence of Saturn's magnetic field anomaly from Saturnian kilometric radiation high-frequency limit" by P. Galopeau et al., *J. Geophys. Res*., *97*, 8713–8717, 1992.
Connerney, J. E. P., M. H. Acuña, and N. F. Ness, Modeling the Jovian current sheet and inner magnetosphere, *J. Geophys. Res*., *86*, 8370–8384, 1981.
Connerney, J. E. P., L. Davis Jr., and D. L. Chenette, Magnetic field models, in *Saturn*, edited by T. Gehrels and M. S. Matthews, pp. 354–377, Univ. of Ariz. Press, Tucson, 1984.
Connerney, J. E. P., M. H. Acuña, and N. F. Ness, The magnetic field of Uranus, *J. Geophys. Res*., *92*, 15,329–15,336, 1987.
Connerney, J. E. P., R. L. Baron, T. Satoh, and T. Owen, Images of excited H_3^+ at the foot of the Io flux tube in Jupiter's atmosphere, *Science*, *262*, 1035–1038, 1993.
Connerney, J. E. P., T. Satoh, and R. L. Baron, Interpretation of auroral "light curves" with application to Jovian H_3^+ emissions, *Icarus*, *122*, 24–35, 1996.
Connerney, J. E. P., M. H. Acuña, N. F. Ness, and T. Satoh, New models of Jupiter's magnetic field constrained by the Io flux tube footprint, *J. Geophys. Res*., *103*, 11,929–11,939, 1998.
Cook, A. F., II, A. Vallance Jones, and D. E. Shemansky, Visible aurora in Jupiter's atmosphere?, *J. Geophys. Res*., *86*, 8793–8796, 1981.
Coroniti, F. V., F. L. Scarf, C. F. Kennel, W. S. Kurth, and D. A. Gurnett, Detection of Jovian whistler mode chorus: Implications for the Io torus aurora, *Geophys. Res. Lett*., *7*, 45–48, 1980.
Coroniti, F. V., W. S. Kurth, F. L. Scarf, S. M. Krimigis, C. F. Kennel, and D. A. Gurnett, Whistler mode emissions in the Uranian radiation belts, *J. Geophys. Res*., *92*, 15,234–15,248, 1987.
Cravens, T. E., Astrophysical applications of electron energy deposition in molecular hydrogen, Ph.D. thesis, Harvard Univ., Cambridge, Mass., 1975.
Cravens, T. E., Vibrationally excited molecular hydrogen in the upper atmosphere of Jupiter, *J. Geophys. Res*., *92*, 11,083–11,100, 1987.
Cravens, T. E., and G. M. Eisenhower, The chemical effects of auroral oxygen precipitation at Jupiter, *Icarus*, *100*, 260–270, 1992.
Cravens, T. E., E. Howell, J. H. Waite Jr., and G. R. Gladstone, Auroral oxygen precipitation at Jupiter, *J. Geophys. Res*., *100*, 17,153–17,161, 1995.
Cravens, T. E., C. N. Keller, and B. Ray, Photochemical sources of nonthermal neutrals for the exosphere of Titan, *Planet. Space Sci*., *45*, 889–896, 1997.
Curtis, S. A., A prediction for Neptune exospheric temperature, *Geophys. Res. Lett*., *15*, 1319–1321, 1988.
Curtis, S. A., and N. F. Ness, Are Uranus's rings black because they are in the solar wind?, *Geophys. Res. Lett*., *12*, 855–858, 1985.
Curtis, S. A., and N. F. Ness, Magnetostrophic balance in planetary dynamos: Predictions for Neptune's magnetosphere, *J. Geophys. Res*., *91*, 11,003–11,008, 1986.
Curtis, S. A., R. P. Lepping, and E. C. Sittler Jr., The centrifugal flute instability and the generation of Saturnian kilometric radiation, *J. Geophys. Res*., *91*, 10,989–10,994, 1986.
de Pater, I., and C. K. Goertz, Synchrotron radiation from Neptune: Neptune's magnetic field and electron population, *Geophys. Res. Lett*., *16*, 97–100, 1989.
Desch, M. D., Evidence for solar wind control of Saturn radio emission, *J. Geophys. Res*., *87*, 4549–4554, 1982.
Desch, M. D., and M. L. Kaiser, Predictions for Uranus from a radiometric Bode's law, *Nature*, *310*, 755–757, 1984.
Desch, M. D., and H. O. Rucker, The relationship between Saturn kilometric radiation and the solar wind, *J. Geophys. Res*., *88*, 8999–9006, 1983.
Desch, M. D., M. L. Kaiser, P. Zarka, A. Lecacheux, Y. Leblanc, M. Aubier, and A. Ortega-Molina, Uranus as a radio source, in *Uranus*, edited by J. T. Bergstralh, E. D. Miner, and M. S. Matthews, pp. 894–925, Univ. of Ariz. Press, Tucson, 1991.
Dessler, A. J., and B. R. Sandel, A quiescent magnetosphere for Neptune, *Geophys. Res. Lett*., *16*, 957–960, 1989.
Dinelli, B. M., S. Miller, N. Achilleos, H. A. Lam, M. Cahill, J. Tennyson, M.-F. Yagod, T. Oka, J.-C. Hilico, and T. R. Geballe, UKIRT observations of the impact and consequences of comet Shoemaker-Levy 9 on Jupiter, *Icarus*, *126*, 107–125, 1997.
Dols, V., J. C. Gérard, F. Paresce, R. Prangé, and A. Vidal-Madjar, Ultraviolet imaging of the Jovian aurora with the Hubble Space Telescope, *Geophys. Res. Lett*., *19*, 1803–1806, 1992.
Doman, L. E., et al., International energy outlook 1999, *DOE/EIA-0484(99)*, 224 pp., Dep. of Energy, Washington, D. C., 1999.

Dougherty, M. K., M. W. Dunlop, R. Prangé, and D. Rego, Correspondence between field-aligned currents observed by Ulysses and HST auroral emission, *Planet. Space Sci*., *46*, 531–540, 1998.

Drossart, P., B. Bézard, S. K. Atreya, J. Lacy, E. Serabyn, A. Tokunaga, and T. Encrenaz, Enhanced acetylene emission near the north pole of Jupiter, *Icarus*, *66*, 610–618, 1986.

Drossart, P., et al., Detection of H_3^+ on Jupiter, *Nature*, *340*, 539–541, 1989.

Drossart, P., R. Prangé, and J.-P. Maillard, Morphology of infrared H_3^+ emissions in the auroral regions of Jupiter, *Icarus*, *97*, 10–25, 1992.

Drossart, P., B. Bézard, S. K. Atreya, J. Bishop, J. H. Waite Jr., and D. Boice, Thermal profiles in the auroral regions of Jupiter, *J. Geophys. Res*., *98*, 18,803–18,811, 1993a.

Drossart, P., J.-P. Maillard, J. Caldwell, and J. Rosenqvist, Line-resolved spectroscopy of the Jovian H_3^+ auroral emission at 3.5 micrometers, *Astrophys. J*., *402*, L25–L28, 1993b.

Dulk, G. A., J. A. Eddy, and J. P. Emerson, Search for visual aurora on Jupiter, *Astrophys. J*., *159*, 1123–1124, 1970.

Durrance, S. T., and H. W. Moos, Intense Ly-α emission from Uranus, *Nature*, *299*, 428–429, 1982.

Durrance, S. T., P. D. Feldman, and H. W. Moos, The spectrum of the Jovian aurora 1150–1700 Å, *Geophys. Res. Lett*., *9*, 652–655, 1982.

Edwards, P. J., and K. G. McCracken, Upper limits to the hard X-ray flux from the quiet Sun and Jupiter, *J. Geophys. Res*., *72*, 1809–1812, 1967.

Encrenaz, T., R. Schulz, J. A. Stüwe, G. Wiedemann, P. Drossart, and J. Crovisier, Near-IR spectroscopy of Jupiter at the time of comet Shoemaker-Levy 9 impacts: Emissions of CH_4, H_3^+, and H_2, *Geophys. Res. Lett*., *22*, 1577–1580, 1995.

Evans, D. S., Precipitating electron fluxes formed by a magnetic field aligned potential difference, *J. Geophys. Res*., *79*, 2853–2858, 1974.

Eviatar, A., and D. D. Barbosa, Jovian magnetospheric neutral wind and auroral precipitation flux, *J. Geophys. Res*., *89*, 7393–7398, 1984.

Fischer, H. M., E. Pehlke, G. Wibberbez, L. J. Lanzerotti, and J. D. Mihalov, High-energy charged particles in the innermost Jovian magnetosphere, *Science*, *272*, 856–858, 1996.

Fisher, P. C., D. B. Clark, A. J. Meyerott, and K. L. Smith, Upper limit to Jupiter's X-ray flux on September 30, 1972, *Nature*, *204*, 982–983, 1964.

Fox, J. L., Models for aurora and airglow emissions from other planetary atmospheres, *Can. J. Phys*., *64*, 1631–1656, 1986.

Frank, L. A., and W. R. Paterson, Production of hydrogen ions at Io, *J. Geophys. Res*., *104*, 10,345–10,354, 1999.

Fricke, K. H., and J. Darius, Observation of the Lyman-alpha albedo of Uranus, in *Proceedings of the Third European IUE Conference*, *ESA SP-176*, pp. 463–469, Eur. Space Agency, Paris, 1982.

Galopeau, P., A. Ortega-Molina, and P. Zarka, Evidence of Saturn's magnetic field anomaly from Saturnian kilometric radiation high-frequency limit, *J. Geophys. Res*., *96*, 14,129–14,140, 1991.

Galopeau, P., P. Zarka, and D. Le Queau, Source location of Saturn's kilometric radiation: The Kelvin-Helmholtz instability hypothesis, *J. Geophys. Res*., *100*, 26,397–26,410, 1995.

Gao, S., C. W. Ho, T.-S. Huang, and C. J. Alexander, Uranus's magnetic field and particle drifts in its inner magnetosphere, *J. Geophys. Res*., *103*, 20,257–20,265, 1998.

Geballe, T. R., M.-F. Jagod, and T. Oka, Detection of H_3^+ infrared emission lines in Saturn, *Astrophys. J*., *408*, L109–L112, 1993.

Gehrels, N., and E. C. Stone, Energetic oxygen and sulfur ions in the Jovian magnetosphere and their contribution to the auroral excitation, *J. Geophys. Res*., *88*, 5537–5550, 1983.

Gehrels, N., E. C. Stone, and J. H. Trainor, Energetic oxygen and sulfur in the Jovian magnetosphere, *J. Geophys. Res*., *86*, 8906–8918, 1981.

Gérard, J.-C., and V. Singh, A model of energy deposition of energetic electrons and EUV emission in the Jovian and Saturnian atmospheres and implications, *J. Geophys. Res*., *87*, 4525–4532, 1982.

Gérard, J.-C., V. Dols, F. Paresce, and R. Prangé, Morphology and time variation of the Jovian far UV aurora: Hubble Space Telescope observations, *J. Geophys. Res*., *98*, 18,793–18,801, 1993.

Gérard, J.-C., V. Dols, R. Prangé, and F. Paresce, The morphology of the north Jovian ultraviolet aurora observed with the Hubble Space Telescope, *Planet. Space Sci*., *42*, 905–917, 1994a.

Gérard, J.-C., D. Grodent, R. Prangé, J. H. Waite, G. R. Gladstone, V. Dols, F. Paresce, A. Storrs, L. Ben Jaffel, and K. A. Franke, A remarkable auroral event on Jupiter observed in the ultraviolet with the Hubble Space Telescope, *Science*, *266*, 1675–1678, 1994b.

Gérard, J.-C., V. Dols, D. Grodent, J. H. Waite, G. R. Gladstone, and R. Prangé, Simultaneous observations of the Saturnian aurora and polar haze with the HST/FOC, *Geophys. Res. Lett*., *22*, 2685–2688, 1995.

Gérard, J.-C., D. Grodent, V. Dols, and J. H. Waite Jr., The longitudinal variation of the color ratio of the Jovian ultraviolet aurora: A geometric effect?, *Geophys. Res. Lett*., *25*, 1601–1604, 1998.

Giles, J. W., H. W. Moos, and W. R. McKinney, The far ultraviolet (1200–1900 Å) spectrum of Jupiter obtained with a rocket-borne multichannel spectrometer, *J. Geophys. Res*., *81*, 5797–5806, 1976.

Gilman, D. A., K. C. Hurley, F. D. Seward, H. W. Schnopper, J. D. Sullivan, and A. E. Metzger, An upper limit to X-ray emission from Saturn, *Astrophys. J*., *300*, 453–455, 1986.

Gladstone, G. R., Radiative transfer with partial frequency redistribution in inhomogeneous atmospheres: Application to the Jovian aurora, *J. Quant. Spectrosc. Radiat. Transfer*, *27*, 545–556, 1982.

Gladstone, G. R., and T. E. Skinner, Spectral analysis of Jovian auroral emissions, in *Time-Variable Phenomena in the Jovian System*, edited by M. J. S. Belton, R. A. West, and J. Rahe, *NASA Spec. Publ*., *SP-494*, 221–228, 1989.

Gladstone, G. R., M. Allen, and Y. L. Yung, Hydrocarbon photochemistry in the upper atmosphere of Jupiter, *Icarus*, *119*, 1–52, 1996.

Gladstone, G. R., J. H. Waite Jr., and W. S. Lewis, Secular and local time dependence of Jovian X ray emissions, *J. Geophys. Res*., *103*, 20,083–20,088, 1998a.

Gladstone, G. R., J. H. Waite Jr., and J.-C. Gérard, Jovian auroral Lyman-α self-reversals: A window on Jupiter's auroral electrojet?, *Bull. Am. Astron. Soc*., *30*, 1078, 1998b.

Goertz, C. K., Energization of charged particles in Jupiter's outer magnetosphere, *J. Geophys. Res*., *83*, 3145–3150, 1978.

Goertz, C. K., Proton aurora on Jupiter's nightside, *Geophys. Res. Lett*., *7*, 365–368, 1980.

Grodent, D., V. Dols, J.-C. Gérard, and D. Rego, The equatorial boundary of the ultraviolet Jovian north aurora observed with multispectral Hubble Space Telescope images, *J. Geophys. Res*., *101*, 2163–2168, 1996.

Grodent, D., G. R. Gladstone, J.-C. Gérard, V. Dols, and J. H. Waite Jr., Simulation of the morphology of the Jovian UV north aurora observed with the Hubble Space Telescope, *Icarus*, *128*, 306–321, 1997.

Gurnett, D. A., and F. L. Scarf, Plasma waves in the Jovian magnetosphere, in *Physics of the Jovian Magnetosphere*, edited by A. J. Dessler, pp. 285–316, Cambridge Univ. Press, New York, 1983.

Gurnett, D. A., W. S. Kurth, F. L. Scarf, and R. L. Poynter,

First plasma wave observations at Uranus, *Science*, *233*, 106–109, 1986.

Gurnett, D. A., W. S. Kurth, R. L. Poynter, L. J. Granroth, I. H. Cairns, W. M. Macek, S. L. Moses, F. V. Coroniti, C. F. Kennel, and D. D. Barbosa, First plasma wave observations at Neptune, *Science*, *246*, 1494–1498, 1989.

Haider, S. A., and R. P. Singhal, Analytical yield spectrum approach to electron energy degradation in Earth's atmosphere, *J. Geophys. Res*., *88*, 7185–7189, 1983.

Halthore, R., A. Burrows, and J. Caldwell, Infrared polar brightenings on Jupiter, 5, A thermal equilibrium model for the north polar hot spot, *Icarus*, *74*, 340–350, 1988.

Halthore, R., J. E. Allen, and P. L. Decola, A non-LTE model for the Jovian methane infrared emissions at high spectral resolution, *Astrophys. J*., *424*, L61–L64, 1994.

Hamilton, D. C., G. Gloeckler, S. M. Krimigis, C. O. Bostrom, T. P. Armstrong, W. I. Axford, C. Y. Fan, L. J. Lanzerotti, and D. M. Hunten, Detection of energetic hydrogen molecules in Jupiter's magnetosphere by Voyager 2: Evidence for an ionospheric plasma source, *Geophys. Res. Lett*., *7*, 813–816, 1980.

Harris, W., J. T. Clarke, M. A. McGrath, and G. E. Ballester, Analysis of Jovian auroral H Ly-α emission (1981–1991), *Icarus*, *124*, 350–365, 1996.

Haymes, R. C., D. V. Ellis, and G. J. Fishman, Upper limits to the hard X-ray fluxes from Mars, Venus, and Jupiter, *J. Geophys. Res*., *73*, 867–870, 1968.

Heaps, M. G., The roles of particle precipitation and Joule heating in the energy balance of the Jovian thermosphere, *Icarus*, *29*, 273–281, 1976.

Heaps, M. G., J. N. Bass, and A. E. S. Green, Electron excitation of a Jovian aurora, *Icarus*, *20*, 297–303, 1973.

Heaps, M. G., B. C. Edgar, and A. E. S. Green, Jovian proton aurora, *Icarus*, *24*, 78–85, 1975.

Herbert, F., Constraints on the neutral hydrogen corona at Uranus from its interaction with magnetospheric plasma, *Geophys. Res. Lett*., *15*, 705–708, 1988.

Herbert, F., The Uranian corona as a charge exchange cascade of plasma sheet protons, *J. Geophys. Res*., *98*, 3999–4011, 1993.

Herbert, F., and D. T. Hall, Atomic hydrogen corona of Uranus, *J. Geophys. Res*., *101*, 10,877–10,885, 1996.

Herbert, F., and B. R. Sandel, The Uranian aurora and its relationship to the magnetosphere, *J. Geophys. Res*., *99*, 4143–4160, 1994.

Herbert, F., and B. R. Sandel, Ultraviolet observations of Uranus and Neptune, *Planet. Space Sci*., *47*, 1119–1139, 1999.

Herbert, F., B. R. Sandel, and A. L. Broadfoot, Observations of the Jovian aurora by Voyager, *J. Geophys. Res*., *92*, 3141–3154, 1987.

Hill, T. W., and A. J. Dessler, Remote sensing of the magnetic moment of Uranus: Predictions for Voyager, *Science*, *227*, 1466–1469, 1985.

Hill, T. W., and A. J. Dessler, Convection in Neptune's magnetosphere, *Geophys. Res. Lett*., *17*, 1677–1680, 1990.

Hill, T. W., A. J. Dessler, and M. E. Rassbach, Aurora on Uranus: A Faraday disc dynamo mechanism, *Planet. Space Sci*., *31*, 1187–1198, 1983.

Holman, B. L., and J. H. Hunter Jr., Hydrogen-alpha auroral activity on Jupiter, 2, *Astrophys. J*., *213*, 906–907, 1977.

Horanyi, M., T. E. Cravens, and J. H. Waite Jr., The precipitation of energetic heavy ions into the upper atmosphere of Jupiter, *J. Geophys. Res*., *93*, 7251–7271, 1988.

Hord, C. W., R. A. West, K. E. Simmons, D. L. Coffeen, M. Sato, A. L. Lane, and J. T. Bergstralh, Photometric observations of Jupiter at 2400 angstroms, *Science*, *206*, 956–959, 1979.

Huang, T.-S., C. W. Ho, and C. J. Alexander, The plasmasphere of Neptune, *J. Geophys. Res*., *103*, 20,267–20,278, 1998.

Hubbard, W. B., and D. J. Stevenson, Interior structure of Saturn, in *Saturn*, edited by T. Gehrels and M. S. Matthews, pp. 47–87, Univ. of Ariz. Press, Tucson, 1984.

Hunten, D. M., and A. J. Dessler, Soft electrons as a possible heat source for Jupiter's thermosphere, *Planet. Space Sci*., *25*, 817–821, 1977.

Hunter, J. H., Hα auroral activity on Jupiter, *Nature*, *223*, 388–389, 1969.

Hurley, K. C., A search for X rays from the planet Jupiter, *J. Geophys. Res*., *77*, 46–53, 1972.

Hurley, K. C., Upper limits to Jovian X-ray emission from the UHURU satellite, in *The Magnetospheres of the Earth and Jupiter*, edited by V. Formisano, pp. 241–244, D. Reidel, Norwell, Mass., 1975.

Hurley, K. C., M. Sommer, and J. H. Waite Jr., Upper limits to Jovian hard X radiation from the Ulysses gamma ray burst experiment, *J. Geophys. Res*., *98*, 21,217–21,219, 1993.

Ingersoll, A. P., A. R. Vasavada, B. Little, C. D. Anger, S. J. Bolton, C. Alexander, K. P. Klaasen, and the Galileo SSI Team, Imaging Jupiter's aurora at visible wavelengths, *Icarus*, *135*, 251–264, 1998.

Ip, A. K., and G. H. Voigt, Plasma-dominated magnetic field configurations for the magnetosphere of Uranus, *J. Geophys. Res*., *90*, 6287–6293, 1985.

Ip, W.-H., Magnetospheric charge exchange effect on the electroglow of Uranus, *Nature*, *326*, 775–777, 1987.

Judge, D. L., F. M. Wu, and R. W. Carlson, Ultraviolet spectrometer observations of the Saturnian system, *Science*, *207*, 431–434, 1980.

Kaiser, M. L., Time-variable magnetospheric radio emissions from Jupiter, *J. Geophys. Res*., *98*, 18,757–18,765, 1993.

Kaiser, M. L., and M. D. Desch, Radio emissions from the planets Earth, Jupiter, and Saturn, *Rev. Geophys*., *22*, 373–384, 1984.

Kaiser, M. L., M. D. Desch, and A. Lecacheux, Saturnian kilometric radiation: Statistical properties and beam geometry, *Nature*, *292*, 731–733, 1981.

Kaiser, M. L., M. D. Desch, W. Kurth, A. Lecacheux, F. Genova, B. M. Pedersen, and D. R. Evans, Saturn as a radio source, in *Saturn*, edited by T. Gehrels and M. S. Matthews, pp. 378–415, Univ. of Ariz. Press, Tucson, 1984.

Kao, L., T. Oka, S. Miller, and J. Tennyson, A table of astronomically important ro-vibrational transitions for the H_3^+ molecular ion, *Astrophys. J. Suppl. Ser*., *77*, 317–329, 1991.

Karkoschka, E., and M. G. Tomasko, Saturn's upper atmospheric hazes observed by the Hubble Space Telescope, *Icarus*, *106*, 428–441, 1993.

Kharchenko, V., W. H. Liu, and A. Dalgarno, X ray and EUV emission spectra of oxygen ions precipitating into the Jovian atmosphere, *J. Geophys. Res*., *103*, 26,687–26,698, 1998.

Kim, S. J., Infrared processes in the Jovian auroral zone, *Icarus*, *75*, 399–408, 1988.

Kim, S. J., and W. Maguire, Two micron quadrupole line emission of H_2 from the Jovian auroral zone, in *The Jovian Atmosphere*, *NASA Conf. Publ*., *2441*, 95–98, 1986.

Kim, S. J., J. Caldwell, A. R. Rivolo, R. Wagener, and G. S. Orton, Infrared polar brightening on Jupiter, 3, Spectrometry from the Voyager 1 IRIS experiment, *Icarus*, *64*, 233–248, 1985.

Kim, S. J., P. Drossart, J. Caldwell, and J.-P. Maillard, Temperatures of the Jovian auroral zone inferred from 2-μm H_2 quadrupole line emissions, *Icarus*, *84*, 54–61, 1990.

Kim, S. J., P. Drossart, J. Caldwell, J.-P. Maillard, T. Herbst, and M. Shure, Images of aurorae on Jupiter from H_3^+ emission at 4 μm, *Nature*, *353*, 536–542, 1991.

Kim, S. J., D. A. Glenar, R. R. Joyce, and T. Kostiuk, Spatial

and spectral characteristics of the near-infrared aurorae of Jupiter, *Icarus*, *102*, 99–106, 1993.

Kim, S. J., Y. H. Kim, J.-P. Maillard, J. Caldwell, and G. Bjoraker, Four-micron polar continuum of Jupiter, *Icarus*, *116*, 423–432, 1995.

Kim, S. J., G. S. Orton, C. Dumas, and Y. H. Kim, Infrared spectroscopy of Jupiter's atmosphere after the A and E impacts of comet Shoemaker-Levy 9, *Icarus*, *120*, 326–331, 1996.

Kim, S. J., D. H. Lee, and Y. H. Kim, Jovian aurorae, *Rep. Prog. Phys*., *61*, 525–568, 1998.

Kim, Y. H., J. L. Fox, and H. S. Porter, Densities and vibrational distribution of H_3^+ in the Jovian auroral ionosphere, *J. Geophys. Res*., *97*, 6093–6101, 1992.

Kim, Y. H., S. J. Kim, J. A. Stuewe, J. Caldwell, and T. M. Herbst, Jovian auroral ovals inferred from infrared H_3^+ images, *Icarus*, *112*, 326–336, 1994.

Kim, Y. H., J. J. Caldwell, and J. L. Fox, High-resolution ultraviolet spectroscopy of Jupiter's aurora with the Hubble Space Telescope, *Astrophys. J*., *447*, 906–914, 1995.

Kim, Y. H., J. L. Fox, and J. J. Caldwell, Temperatures and altitudes of Jupiter's ultraviolet aurora inferred from GHRS observations with the Hubble Space Telescope, *Icarus*, *128*, 189–201, 1997.

Kirsch, E., S. M. Krimigis, J. W. Kohl, and E. P. Keath, Upper limits for X-ray and energetic neutral particle emission from Jupiter: Voyager 1 results, *Geophys. Res. Lett*., *8*, 169–172, 1981a.

Kirsch, E., S. M. Krimigis, W.-H. Ip, and G. Gloeckler, X-ray energetic neutral particle emission from Saturn's magnetosphere: Measurements by Voyager 1, *Nature*, *292*, 718–721, 1981b.

Kostiuk, T., M. J. Mumma, F. Espenak, D. Deming, D. E. Jennings, W. Maguire, and D. Zipoy, Measurements of stratospheric ethane in the Jovian south polar region from infrared heterodyne spectroscopy of the ν_9 band near 12 microns, *Astrophys. J*., *265*, 564–569, 1983.

Kostiuk, T., F. Espenak, M. J. Mumma, D. Deming, and D. Zipoy, Variability of ethane on Jupiter, *Icarus*, *72*, 394–410, 1987.

Kostiuk, T., F. Espenak, M. J. Mumma, D. Deming, and P. Romani, Infrared studies of hydrocarbons on Jupiter, *Infrared Phys*., *29*, 199–204, 1989.

Kostiuk, T., P. Romani, F. Espenak, T. A. Livengood, and J. J. Goldstein, Temperature and abundances in the Jovian auroral stratosphere, 2, Ethylene as a probe of the microbar region, *J. Geophys. Res*., *98*, 18,823–18,830, 1993.

Krimigis, S. M., T. P. Armstrong, W. I. Axford, A. F. Cheng, G. Gloeckler, D. C. Hamilton, E. P. Keath, L. J. Lanzerotti, and B. H. Mauk, The magnetosphere of Uranus: Hot plasma and radiation environment, *Science*, *233*, 97–102, 1986.

Krimigis, S. M., E. P. Keath, B. H. Mauk, A. F. Cheng, L. J. Lanzerotti, R. P. Lepping, and N. F. Ness, Observations of energetic ion enhancements and fast neutrals upstream and downstream of Uranus' bow shock by the Voyager 2 spacecraft, *Planet. Space Sci*., *36*, 311–328, 1988.

Krimigis, S. M., et al., Hot plasma and energetic particles in Neptune's magnetosphere, *Science*, *246*, 1483–1489, 1989.

Kurth, W. S., D. A. Gurnett, F. L. Scarf, and F. V. Coroniti, Wave-particle interactions in the magnetosphere of Uranus: Uranus as a radio source, in *Uranus*, edited by J. T. Bergstralh, E. D. Miner, and M. S. Matthews, pp. 926–958, Univ. of Ariz. Press, Tucson, 1991.

Lam, H. A., N. Achilleos, S. Miller, J. Tennyson, L. M. Trafton, T. R. Geballe, and G. E. Ballester, A baseline spectroscopic study of the infrared auroras of Jupiter, *Icarus*, *127*, 379–393, 1997a.

Lam, H. A., S. Miller, R. D. Joseph, T. R. Geballe, L. M. Trafton, J. Tennyson, and G. E. Ballester, Variation in the H_3^+ emission of Uranus, *Astron. Astrophys*., *474*, L73–L76, 1997b.

Lane, A. L., C. W. Hord, R. A. West, L. W. Esposito, D. L. Coffeen, M. Sato, K. E. Simmons, R. B. Pomphrey, and R. B. Morris, Photopolarimetry from Voyager 2: Preliminary results on Saturn, Titan, and the rings, *Science*, *215*, 537–543, 1982.

Lanzerotti, L. J., T. P. Armstrong, R. E. Gold, K. A. Anderson, S. M. Krimigis, R. P. Lin, M. Pick, E. C. Roelof, E. T. Sarris, and G. M. Simnett, The hot plasma environment at Jupiter—Ulysses results, *Science*, *257*, 1518–1524, 1992.

Lanzerotti, L. J., C. G. MacClennon, and D. M. Feldman, Ulysses measurements of energetic H_3 molecules in Jupiter's magnetosphere, *J. Geophys. Res*., *98*, 21,145–21,149, 1993.

Liu, W., and A. Dalgarno, The ultraviolet spectra of the Jovian aurora, *Astrophys. J*., *467*, 446–453, 1996.

Livengood, T. A., and H. W. Moos, Jupiter's north and south polar aurorae with IUE data, *Geophys. Res. Lett*., *17*, 2265–2268, 1990.

Livengood, T. A., H. W. Moos, and G. E. Ballester, Phenomenological analysis of Jovian north auroral H_2 Lyman band emissions, in *A Decade of UV Astronomy With the IUE Satellite*, vol. 1, pp. 97–100, Eur. Space Agency, Paris, 1988.

Livengood, T. A., D. F. Strobel, and H. W. Moos, Long-term study of longitudinal dependence in primary particle precipitation in the north Jovian aurora, *J. Geophys. Res*., *95*, 10,375–10,388, 1990.

Livengood, T. A., H. W. Moos, G. E. Ballester, and R. M. Prangé, Jovian ultraviolet auroral activity, 1981–1991, *Icarus*, *97*, 26–45, 1992.

Livengood, T. A., T. Kostiuk, F. Espenak, and J. J. Goldstein, Temperature and abundances in the Jovian auroral stratosphere, 1, Ethane as a probe of the millibar region, *J. Geophys. Res*., *98*, 18,813–18,822, 1993.

Mahoney, W. A., Hard X-ray spectra of discrete cosmic sources, Ph.D. thesis, Univ. of Calif., Berkeley, 1973.

Maillard, J.-P., P. Drossart, J. K. G. Watson, S. J. Kim, and J. Caldwell, H_3^+ fundamental band in Jupiter's auroral zones at high resolution from 2400 to 2900 inverse centimeters, *Astrophys. J*., *363*, L37–L41, 1990.

Margon, B. H., Model-fitting in X-ray astronomy, Ph.D. thesis, Univ. of Calif. at Berkeley, 1973.

Mauk, B. H., M. Kane, E. P. Keath, A. F. Cheng, S. M. Krimigis, T. P. Armstrong, and N. F. Ness, Energetic charged particle angular distributions near ($r \leq 2\ R_N$) and over the pole of Neptune, *Geophys. Res. Lett*., *17*, 1701–1704, 1990.

Mauk, B. H., E. P. Keath, M. Kane, S. M. Krimigis, A. F. Cheng, M. H. Acuña, T. P. Armstrong, and N. F. Ness, The magnetosphere of Neptune: Hot plasmas and energetic particles, *J. Geophys. Res*., *96*, 19,061–19,084, 1991.

Mauk, B. H., S. M. Krimigis, and M. H. Acuña, Neptune's inner magnetosphere and aurora: Energetic particle constraints, *J. Geophys. Res*., *99*, 14,781–14,788, 1994.

Mauk, B. H., S. A. Gary, M. Kane, E. P. Keath, S. M. Krimigis, and T. P. Armstrong, Hot plasma parameters of Jupiter's inner magnetosphere, *J. Geophys. Res*., *101*, 7685–7695, 1996.

Maurice, S., E. C. Sittler, J. F. Cooper, B. H. Mauk, M. Blanc, and R. S. Selesnick, Comprehensive analysis of electron observations at Saturn: Voyager 1 and 2, *J. Geophys. Res*., *101*, 15,211–15,232, 1996.

McConnell, J. C., and T. Majeed, H_3^+ in the Jovian ionosphere, *J. Geophys. Res*., *92*, 8570–8578, 1987.

McElroy, M. B., The ionospheres of the major planets, *Space Sci. Rev*., *14*, 460–473, 1973.

McGrath, M. A., and J. T. Clarke, H I Lyman alpha emission

from Saturn (1980–1990), *J. Geophys. Res*., *97*, 13,691–13,703, 1992.

McNutt, R. L., F. Bagenal, and R. M. Thorne, Observation of auroral secondary electrons in the Jovian magnetosphere, *Geophys. Res. Lett*., *17*, 291–294, 1990.

Metzger, A. E., D. A. Gilman, J. L. Luthey, K. C. Hurley, H. W. Schnopper, F. D. Seward, and J. D. Sullivan, The detection of X rays from Jupiter, *J. Geophys. Res*., *88*, 7731–7741, 1983.

Mihalov, J. D., On limits to Jupiter's magnetospheric diffusion rates, *Astrophys. Space Sci*., *20*, 483, 1973.

Miller, S., R. D. Joseph, and J. Tennyson, Infrared emissions of H_3^+ in the atmosphere of Jupiter in the 2.1 and 4.0 micron region, *Astrophys. J*., *360*, L55–L58, 1990.

Miller, S., H. A. Lam, and J. Tennyson, What astronomy has learned from observations of H_3^+, *Can. J. Phys*., *72*, 760–771, 1994.

Miller, S., N. Achilleos, G. E. Ballester, H. A. Lam, J. Tennyson, T. R. Geballe, and L. M. Trafton, Mid-to-low latitude H_3^+ emission from Jupiter, *Icarus*, *130*, 57–67, 1997a.

Miller, S., N. Achilleos, H. A. Lam, B. M. Dinelli, and R. Prangé, The impact of comet Shoemaker-Levy 9 on the Jovian ionosphere and aurorae, *Planet. Space Sci*., *45*, 1237–1250, 1997b.

Morrissey, P. F., P. D. Feldman, J. T. Clarke, B. C. Wolven, D. F. Strobel, S. T. Durrance, and J. T. Trauger, Simultaneous spectroscopy and imaging of the Jovian aurora with the Hopkins Ultraviolet Telescope and the Hubble Space Telescope, *Astrophys. J*., *476*, 918–923, 1997.

Nagy, A. F., W. L. Chameides, R. H. Chen, and S. K. Atreya, Electron temperatures in the Jovian ionosphere, *J. Geophys. Res*., *81*, 5567–5569, 1976.

Ness, N. F., Comment on "Reply to comment on 'Evidence of Saturn's magnetic field anomaly from Saturnian kilometric radiation high-frequency limit' by P. Galopeau and P. Zarka," *J. Geophys. Res*., *98*, 1505, 1993.

Ness, N. F., M. H. Acuña, K. W. Behannon, and F. M. Neubauer, Magnetic fields at Uranus, *Science*, *233*, 85–89, 1986.

Ness, N. F., M. H. Acuña, L. F. Burlaga, J. E. P. Connerney, R. P. Lepping, and F. M. Neubauer, Magnetic fields at Neptune, *Science*, *246*, 1473–1478, 1989.

Ness, N. F., J. E. P. Connerney, R. P. Lepping, M. Schulz, and G.-H. Voigt, The magnetic field and magnetospheric configuration of Uranus, in *Uranus*, edited by J. T. Bergstralh, E. D. Miner, and M. S. Matthews, pp. 739–779, Univ. of Ariz. Press, Tucson, 1991.

Neubauer, F. M., Nonlinear standing Alfvén wave current system at Io: Theory, *J. Geophys. Res*., *85*, 1171–1178, 1980.

Noll, K. S., H. A. Weaver, and P. D. Feldman (Eds.), *The Collision of Comet Shoemaker-Levy 9 and Jupiter*, Cambridge Univ. Press, New York, 1996.

Ogino, T., R. J. Walker, and M. G. Kivelson, A global magnetohydrodynamic simulation of the Jovian magnetosphere, *J. Geophys. Res*., *103*, 225–235, 1998.

Oka, T., The infrared spectrum of H_3^+ in laboratory and space plasmas, *Rev. Mod. Phys*., *64*, 1141–1149, 1992.

Oka, T., and T. R. Geballe, Observations of the 4 micron fundamental band of H_3^+ in Jupiter, *Astrophys. J*., *351*, L53–L56, 1990.

Orton, G. S., The thermal structure of Jupiter, 2, Observations and analysis of 8–14 micron radiation, *Icarus*, *26*, 142–158, 1975.

Orton, G. S., et al., Thermal maps of Jupiter: Spatial organization and time dependence of stratospheric temperatures, 1980 to 1990, *Science*, *252*, 537–542, 1991.

Orton, G. S., et al., Collision of comet Shoemaker-Levy 9 with Jupiter observed by the NASA Infrared Telescope Facility, *Science*, *267*, 1277–1282, 1995.

Paranicas, C., and A. F. Cheng, Drift shells and aurora computed using the O8 magnetic field model for Neptune, *J. Geophys. Res*., *99*, 19,433–19,440, 1994.

Perry, J. J., Y. H. Kim, J. L. Fox, and H. S. Porter, Chemistry of the Jovian auroral ionosphere, *J. Geophys. Res*., *104*, 16,541–16,565, 1999.

Piddington, J. H., and J. F. Drake, Electrodynamic effects of Jupiter's satellite Io, *Nature*, *217*, 935–937, 1968.

Prangé, R., Jovian UV aurorae, IR aurorae, and particle precipitation—A common origin?, *Astron. Astrophys*., *251*, L15–L18, 1991.

Prangé, R., The UV and IR Jovian aurorae, *Adv. Space Res*., *12*(8), 379–389, 1992.

Prangé, R., and M. Elkhamsi, Modeling the precipitation flux in the Jovian auroral zones, 1, The model and its application to the UV auroral emissions, *J. Geophys. Res*., *96*, 21,371–21,389, 1991.

Prangé, R., and T. A. Livengood, Monitoring auroral activity on Jupiter, in *Ultraviolet Astrophysics Beyond the IUE Final Archive*, *Eur. Space Agency Spec. Publ*., *ESA-SP-413*, 29–36, 1998.

Prangé, R., P. Zarka, G. E. Ballester, T. A. Livengood, L. Denis, T. Carr, F. Reyes, S. J. Bame, and H. W. Moos, Correlated variations of UV and radio emissions during an outstanding Jovian auroral event, *J. Geophys. Res*., *98*, 18,779–18,791, 1993.

Prangé, R., D. Rego, and J.-C. Gérard, Auroral Lyman α and H_2 bands from the giant planets, 2, Effect of the anisotropy of the precipitating particles on the interpretation of the "color ratio," *J. Geophys. Res*., *100*, 7513–7521, 1995.

Prangé, R., D. Rego, D. Southwood, P. Zarka, S. Miller, and W. Ip, Rapid energy dissipation and variability of the Io-Jupiter electrodynamic circuit, *Nature*, *379*, 323–325, 1996.

Prangé, R., S. Maurice, W. M. Harris, D. Rego, and T. A. Livengood, Comparison of IUE and HST diagnostics of the Jovian aurorae, *J. Geophys. Res*., *102*, 9289–9301, 1997a.

Prangé, R., D. Rego, L. Pallier, L. Ben Jaffel, C. Emerich, J. Ajello, J. T. Clarke, and G. Ballester, Detection of self-reversed Ly α lines from the Jovian aurorae with the Hubble Space Telescope, *Astrophys. J*., *484*, L169–L173, 1997b.

Prangé, R., D. Rego, L. Pallier, J. E. P. Connerney, P. Zarka, and J. Queinnec, Detailed study of FUV Jovian auroral features with the post-COSTAR HST faint object camera, *J. Geophys. Res*., *103*, 20,195–20,215, 1998.

Pryor, W. R., and C. W. Hord, A study of Photopolarimeter System UV absorption data on Jupiter, Saturn, Uranus, and Neptune: Implications for auroral haze formation, *Icarus*, *91*, 161–172, 1991.

Pryor, W. R., et al., Galileo ultraviolet spectrometer observations of Jupiter's auroral spectrum from 1600 to 3200 Å, *J. Geophys. Res*., *103*, 20,149–20,158, 1998.

Rego, D., R. Prangé, and J.-C. Gérard, Auroral Lyman α and H_2 bands from the giant planets, 1, Excitation by proton precipitation in the Jovian atmosphere, *J. Geophys. Res*., *99*, 17,075–17,094, 1994.

Rego, D., N. Achilleos, T. Stallard, S. Miller, R. Prangé, M. Dougherty, and R. D. Joseph, Supersonic winds in Jupiter's aurorae, *Nature*, *399*, 121–124, 1999.

Rezeau, L., N. Cornilleau-Wehrlin, G. Belmont, P. Canu, R. Prangé, A. Balogh, and R. J. Forsyth, Possible role of electromagnetic low-frequency waves in the Io torus in the production of Jovian aurorae, *Planet. Space Sci*., *45*, 483–493, 1997.

Ridgway, S. T., H. P. Larson, and U. Fink, The infrared spectrum of Jupiter, in *Jupiter*, edited by T. Gehrels, pp. 384–417, Univ. of Ariz. Press, Tucson, 1976.

Rottman, G. J., H. W. Moos, and C. S. Freer, The far-ultraviolet spectrum of Jupiter, *Astrophys. J*., *184*, L89–L92, 1973.

Sandel, B. R., and A. L. Broadfoot, Morphology of Saturn's aurora, *Nature*, *292*, 679–682, 1981.

Sandel, B. R., et al., Extreme ultraviolet observations from Voyager 2 encounter with Jupiter, *Science*, *206*, 962–966, 1979.

Sandel, B. R., et al., Extreme ultraviolet observations from Voyager 2 encounter with Saturn, *Science*, *215*, 548–553, 1982.

Sandel, B. R., F. Herbert, A. J. Dessler, and T. W. Hill, Aurora and airglow on the night side of Neptune, *Geophys. Res. Lett*., *17*, 1693–1696, 1990.

Satoh, T., J. E. P. Connerney, and R. L. Baron, Emission source model of Jupiter's H_3^+ aurorae: A generalized inverse analysis of images, *Icarus*, *122*, 1–23, 1996.

Schwitters, M. T., A search for Jovian limb aurorae, *Icarus*, *9*, 570–573, 1968.

Seidel, R., E. Keppler, N. Krupp, J. Woch, L. J. Lanzerotti, and C. G. MacLennan, Ulysses observations of energetic H_3^+ ions in Jupiter's magnetosphere, *Adv. Space Res*., *20*(2), 229–232, 1997.

Seiff, A., et al., Structure of the atmosphere of Jupiter: Galileo probe measurements, *Science*, *272*, 844–845, 1996.

Seiff, A., et al., Thermal structure of Jupiter upper atmosphere derived from the Galileo Probe, *Science*, *276*, 102–104, 1997.

Shemansky, D. E., Mass-loading and diffusion-loss rates of the Io plasma torus, *Astrophys. J*., *242*, 1266–1277, 1980.

Shemansky, D. E., and J. M. Ajello, The Saturn spectrum in the EUV: Electron excited hydrogen, *J. Geophys. Res*., *88*, 459–464, 1983.

Shemansky, D. E., and G. R. Smith, The implication for the presence of a magnetosphere on Uranus in the relationship of EUV and radio emission, *Geophys. Res. Lett*., *13*, 2–5, 1986.

Shingawa, H., and J. H. Waite Jr., The ionosphere of Neptune, *Geophys. Res. Lett*., *16*, 945–948, 1989.

Singh, V., Proton energy deposition and EUV emission in the Jovian and Saturnian atmospheres, *Indian J. Radio Space Phys*., *20*, 140–149, 1991.

Singhal, R. P., and A. Bhardwaj, Monte Carlo simulation of photoelectron energization in parallel electric fields: Electroglow on Uranus, *J. Geophys. Res*., *96*, 15,963–15,972, 1991.

Singhal, R. P., S. C. Chakravarty, A. Bhardwaj, and B. Prasad, Energetic electron precipitation in Jupiter's upper atmosphere, *J. Geophys. Res*., *97*, 18,245–18,256, 1992.

Sittler, E. C., Jr., K. W. Ogilvie, and J. D. Scudder, Survey of low-energy plasma electrons in Saturn's magnetosphere: Voyager 1 and 2, *J. Geophys. Res*., *88*, 8847–8870, 1983.

Skinner, T. E., and H. W. Moos, Comparison of the Jovian north and south polar aurorae using the IUE observatory, *Geophys. Res. Lett*., *11*, 1107–1110, 1984.

Skinner, T. E., S. T. Durrance, P. D. Feldman, and H. W. Moos, IUE observations of longitudinal and temporal variations in the Jovian auroral emission, *Astrophys. J*., *278*, 441–448, 1984.

Smith, B. A., L. A. Soderblom, R. Beebe, J. Boyce, G. Briggs, M. Carr, S. A. Collins, T. V. Johnson, A. F. Cook II, G. E. Danielson, and D. Morrison, The Galilean satellites and Jupiter—Voyager 2 imaging science results, *Science*, *206*, 927–950, 1979.

Sommeria, J., L. Ben Jaffel, and R. Prangé, On the existence of supersonic jets in the upper atmosphere of Jupiter, *Icarus*, *119*, 2–24, 1995.

Stallard, T., S. Miller, G. E. Ballester, D. Rego, R. D. Joseph, and L. M. Trafton, The H_3^+ latitudinal profile of Saturn, *Astrophys. J*., *521*, L149–L152, 1999.

Stevens, M. H., D. F. Strobel, and F. Herbert, An analysis of the Voyager 2 ultraviolet spectrometer occultation data at Uranus: Inferring heat sources and model atmospheres, *Icarus*, *101*, 45–63, 1993.

Strobel, D. F., and S. K. Atreya, Ionosphere, in *Physics of the Jovian Magnetosphere*, edited by A. J. Dessler, pp. 51–67, Cambridge Univ. Press, New York, 1983.

Strobel, D. F., and D. E. Shemansky, EUV emission from Titan's upper atmosphere: Voyager 1 encounter, *J. Geophys. Res*., *87*, 1361–1368, 1982.

Suess, S. T., and A. J. Dessler, Probing the local interstellar medium, *Nature*, *317*, 702–703, 1985.

Tennyson, J., Spectroscopy of H_3^+: Planets, chaos and the universe, *Rep. Prog. Phys*., *58*, 421–476, 1995.

Thorne, R. M., Jovian auroral secondary electrons and their influence on the Io plasma torus, *Geophys. Res. Lett*., *8*, 509–512, 1981.

Thorne, R. M., Injection and loss mechanisms for energetic ions in the inner Jovian magnetosphere, *J. Geophys. Res*., *87*, 8105–8110, 1982.

Thorne, R. M., Microscopic plasma processes in the Jovian magnetosphere, in *Physics of the Jovian magnetosphere*, edited by A. J. Dessler, pp. 454–458, Cambridge Univ. Press, New York, 1983.

Thorne, R. M., and J. Moses, Electromagnetic ion-cyclotron instability in the multi-ion Jovian magnetosphere, *Geophys. Res. Lett*., *10*, 631–634, 1983.

Thorne, R. M., and B. T. Tsurutani, Diffuse Jovian aurora influenced by plasma injection from Io, *Geophys. Res. Lett*., *6*, 649–652, 1979.

Tomasko, M. G., and L. R. Doose, Polarimetry and photometry of Saturn from Pioneer 11: Observations and constraints on the distribution and properties of cloud and aerosol particles, *Icarus*, *58*, 1–34, 1984.

Trafton, L. M., J. Carr, D. Lester, and P. Harvey, A possible detection of Jupiter's northern auroral $S_1(1)$ H_2 quadrupole line emission, *Icarus*, *74*, 351–356, 1988.

Trafton, L. M., D. F. Lester, and K. L. Thompson, Unidentified emissions lines in Jupiter's northern and southern 2 μm aurorae, *Astrophys. J*., *343*, L73–L76, 1989a.

Trafton, L. M., J. Carr, D. Lester, and P. Harvey, Jupiter's aurora: Detection of quadrupole H_2 emission, in *Time-Variable Phenomena in the Jovian System*, edited by M. J. S. Belton, R. A. West, and J. Rahe, *NASA Spec. Publ*., *SP-494*, 229–234, 1989b.

Trafton, L. M., T. R. Geballe, S. Miller, J. Tennyson, and G. E. Ballester, Detection of H_3^+ from Uranus, *Astrophys. J*., *405*, 761–766, 1993.

Trafton, L. M., J.-C. Gérard, G. Munhoven, and J. H. Waite Jr., High-resolution spectra of Jupiter's northern auroral ultraviolet emission with the Hubble Space Telescope, *Astrophys. J*., *421*, 816–827, 1994.

Trafton, L. M., V. Dols, J.-C. Gérard, J. H. Waite Jr., G. R. Gladstone, and G. Munhoven, HST spectra of the Jovian ultraviolet aurora: Search for heavy ion precipitation, *Astrophys. J*., *507*, 955–967, 1998.

Trafton, L. M., S. Miller, T. R. Geballe, J. Tennyson, and G. E. Ballester, H_2 quadrupole and H_3^+ emission from Uranus: The Uranian thermosphere, ionosphere, and aurora, *Astrophys. J*., *524*, 1059–1083, 1999.

Trauger, J. T., et al., Saturn's hydrogen aurora: Wide field and planetary camera 2 imaging from the Hubble Space Telescope, *J. Geophys. Res*., *103*, 20,237–20,244, 1998.

Vesecky, J. F., J. R. Culhane, and F. J. Hawkins, Upper limits for X-ray emission from Jupiter as measured from the Copernicus satellite, in *The Magnetospheres of the Earth and Jupiter*, edited by V. Formisano, pp. 245–251, D. Reidel, Norwell, Mass., 1975.

Voigt, G. H., and N. F. Ness, The magnetosphere of Neptune: Its response to daily rotation, *Geophys. Res. Lett*., *17*, 1705–1708, 1990.

Waite, J. H., Jr., The ionosphere of Saturn, Ph.D. thesis, Univ. of Mich., Ann Arbor, 1981.
Waite, J. H., Jr., Comment on "Bremsstrahlung X rays from Jovian auroral electrons" by D. D. Barbosa, *J. Geophys. Res*., *96*, 19,529–19,532, 1991.
Waite, J. H., Jr., T. E. Cravens, J. Kozyra, A. F. Nagy, S. K. Atreya, and R. H. Chen, Electron precipitation and related aeronomy of the Jovian thermosphere and ionosphere, *J. Geophys. Res*., *88*, 6143–6163, 1983.
Waite, J. H., Jr., J. T. Clarke, T. E. Cravens, and C. M. Hammond, The Jovian aurora: Electron or ion precipitation?, *J. Geophys. Res*., *93*, 7244–7250, 1988a.
Waite, J. H., Jr., M. O. Chandler, R. V. Yelle, B. R. Sandel, and T. E. Cravens, Superthermal electron processes in the upper atmosphere of Uranus: Aurora and electroglow, *J. Geophys. Res*., *93*, 14,295–14,308, 1988b.
Waite, J. H., Jr., D. C. Boice, K. C. Hurley, S. A. Stern, and M. Sommer, Jovian bremsstrahlung X rays: A Ulysses prediction, *Geophys. Res. Lett*., *19*, 83–86, 1992.
Waite, J. H., Jr., F. Bagenal, F. Seward, C. Na, G. R. Gladstone, T. E. Cravens, K. C. Hurley, J. T. Clarke, R. Elsner, and S. A. Stern, ROSAT observations of the Jupiter aurora, *J. Geophys. Res*., *99*, 14,799–14,809, 1994.
Waite, J. H., Jr., G. R. Gladstone, W. S. Lewis, P. Drossart, T. E. Cravens, A. N. Maurellis, B. H. Mauk, and S. Miller, Equatorial X-ray emissions: Implications for Jupiter's high exospheric temperatures, *Science*, *276*, 104–108, 1997.
Walt, M., L. L. Newkirk, and W. E. Francis, Bremsstrahlung produced by precipitating electrons, *J. Geophys. Res*., *84*, 967–973, 1979.
Warwick, J. W., et al., Voyager planetary radio astronomy at Neptune, *Science*, *246*, 1498–1501, 1989.
West, R., and H. Böhnhardt (Eds.), *Proceedings of the European SL-9/Jupiter Workshop*, Eur. Southern Obs., Garching, Germany, 1995.
West, R. A., M. Sato, H. Hart, A. L. Lane, C. W. Hord, K. E. Simmons, L. W. Esposito, D. L. Coffeen, and R. B. Pomphrey, Photometry and polarimetry of Saturn at 2640 and 7500 Å, *J. Geophys. Res*., *88*, 8679–8697, 1983.
Wolven, B. C., and P. D. Feldman, Self-absorption by vibrationally excited H_2 in the Astro-2 Hopkins Ultraviolet Telescope spectrum of the Jovian aurora, *Geophys. Res. Lett*., *25*, 1537–1540, 1998.
Yelle, R. V., and B. R. Sandel, Uranian H Ly-α emission: The interstellar wind source, *Geophys. Res. Lett*., *13*, 89–92, 1986.
Yung, Y. L., G. R. Gladstone, K. M. Chang, J. M. Ajello, and S. K. Srivastava, H_2 fluorescence spectrum from 1200 to 1700 Å by electron impact: Laboratory study and application to Jovian aurora, *Astrophys. J*., *254*, L65–L69, 1982.
Zarka, P., The auroral radio emissions from planetary magnetospheres: What do we know, what don't we know, what do we learn from them?, *Adv. Space Res*., *12*(8), 99–115, 1992.
Zarka, P., Auroral radio emissions at the outer planets: Observations and theories, *J. Geophys. Res*., *103*, 20,159–20,194, 1998.
Zarka, P., and F. Genova, Solar wind effect on Jovian low-frequency magnetospheric radio emissions from ground-based and spacecraft observations, in *Time-Variable Phenomena in the Jovian System*, edited by M. J. S. Belton, R. A. West, and J. Rahe, pp. 175–178, *NASA Spec. Publ. SP-494*, 1989.
Zarka, P., et al., Radio emissions from Neptune, in *Neptune and Triton*, edited by D. Cruikshank and M. S. Matthews, pp. 341–387, Univ. of Ariz. Press, Tucson, 1995.

A. Bhardwaj, Space Physics Laboratory, Vikram Sarabhai Space Centre, Trivandrum 695 022, India. (spl_vssc@vssc.org)
G. R. Gladstone, Southwest Research Institute, 6220 Culebra Road, San Antonio, TX 78238. (randy@whistler.space.swri.edu)